CORRELATIVE ELECTRON MICROSCOPY STUDIES OF THE INTRACELLULAR LIFESTYLE OF *BRUCELLA*

Inauguraldissertation

zur

Erlangung der Würde eines Doktors der Philosophie

vorgelegt der

Philosophisch-Naturwissenschaftlichen Fakultät

der Universität Basel

von

Jarosław Sędzicki

aus Świdwin, Polen

Basel, 2018

Genehmigt von der Philosophisch-Naturwissenschaftlichen Fakultät

auf Antrag von

Prof. Dr. Christoph Dehio
Prof. Dr. Henning Stahlberg
Prof. Dr. Marek Basler

Basel, den 17.10.2017

Prof. Dr. Martin Spiess
Dekan

STATEMENT TO MY THESIS

This work has been carried out in the groups of Prof. Christoph Dehio in the Focal Area Infection Biology and Prof. Henning Stahlberg in the Focal Area Structural Biology & Biophysics of the University of Basel, Switzerland.

My PhD thesis committee consisted of:

Prof. Dr. Christoph Dehio
Prof. Dr. Henning Stahlberg
Prof. Dr. Marek Basler

My thesis is written as a cumulative dissertation. It consists of a general introduction covering aspects relevant for this work followed by the results section composed of a submitted scientific publication, one article in preparation and unpublished results. Supplementary information can be found on the CD attached to the thesis. Finally, I provide a summary of different aspects of my thesis with suggestions for the future steps in this project.

SUMMARY

A number of pathogens have evolved strategies that allow them to survive and multiply inside eukaryotic cells. This lifestyle requires the ability to interact and influence different processes within the host cell. The bacteria need ways of avoiding detection and clearance. Moreover, the pathogen's survival relies on its ability to establish a replicative niche, which is often a modified host cell compartment. A plethora of interactions between intracellular pathogens and host cell organelles have been described by different means. There is, however, a need to gain more knowledge about this subject.

Our studies focus on *Brucella*, a zoonotic pathogen responsible for 500'000 infections annually. Upon host entry, *Brucella* follows a complex trafficking process that allows the bacterium to avoid lysosome degradation and establish a replicative niche inside the host's endoplasmic reticulum. The molecular mechanisms responsible for this process remain largely unknown. In my work, we employed a combination of light and electron microscopy techniques that allowed the visualization of different stages of the intracellular lifestyle of *Brucella* inside host cells. The goal was to shed new light on the interactions of the bacteria with different host cell organelles and cellular processes.

In *research article I*, we present a more detailed description of the *Brucella* replicative niche by using three-dimensional correlative light and electron microscopy. This approach allowed us to resolve the interactions of the pathogen with the endoplasmic reticulum to a great detail. We provide strong indications that the replicative niche of *Brucella* is in fact integrated with the organelle. Our initial results in HeLa cells were additionally recapitulated using an *in vivo* model.

In *research article II*, we look in more detail at the role of host cell factors in the intermediate trafficking of *Brucella*. We focus on a number of components of the retromer machinery that have been identified in a siRNA screen. We were able to show that knockdown of the protein VPS35 blocks the transition of the *Brucella* vacuole into the endoplasmic reticulum by arresting it at the late endosome stage. This suggests the role of a previously unknown mechanism in the establishment of the *Brucella* replicative niche.

Additionally, I present a series of *unpublished results* that are part of on-going research. They provide exciting new findings regarding the localization of *Brucella* during its intracellular trafficking towards the replicative niche. We have established new cell lines and reporter strains that were used in a combination of different imaging approaches to describe the occurrence of cytosolic *Brucella* at this stage. It remains to be determined if this novel observation represents a crucial step in *Brucella* biology or an off-pathway event.

Together, the results improve our understanding of *Brucella* lifestyle inside host cells. We were able to identify new factors involved in the intermediate trafficking of *Brucella* and indicate previously unknown events that may occur in the process. We also provided a more detailed description of the replicative niche and improved the understanding of its interactions with the endoplasmic reticulum. Additionally, we explored the potential as well as limitations of combining different light and electron microscopy approaches for studying intracellular pathogens.

CONTENTS

1 Introduction

1. INTRODUCTION

1.1. Organelles of mammalian cells and intracellular trafficking

One of the most important evolutionary events responsible for the diversity of life on our planet was the development of organelles. Compartmentalization through the formation of different membranous structures allowed the primitive ancestors of eukaryotes to increase their complexity and explore new evolutionary possibilities. These include new metabolic pathways for energy production, protein synthesis and degradation and more sophisticated structural components. Modern eukaryotic cells are characterized by the presence of different organelles that have unique composition and specialized functions. These include the nucleus, endoplasmic reticulum (ER), Golgi apparatus, mitochondria and the endocytic pathway [1].

One of the main issues arising from the existence of membranous cellular compartments is the need to transport components between them in an efficient and specific manner. Different mechanisms have evolved to accommodate that. These include pores and channels that transport small molecules, nuclear pores that allow diffusion of macromolecular assemblies and vesicles that can sequester and move cargos between membranes. Proper functioning of vesicular transport pathways is essential for maintaining the composition of different organelles. The transport needs to be bidirectional in order to allow adequate distribution of different molecules and preservation of homeostasis within the cell [1].

1.1.1. Trafficking routes and organelles of mammalian cells

Different trafficking routes are responsible for creating links between all organelles of the eukaryotic cell in order to allow transport of components and preservation of homeostasis (Fig. 1). A complex network of interactions connects the endoplasmic reticulum (ER), the site of protein biosynthesis, with the plasma membrane. Trafficking routes can be understood as a means of bidirectional exchange between those two structures, with other organelles representing

intermediate stages that play specific roles. The transport of material is mediated by vesicles that can shuttle between membranes [2, 3].

Vesicular transport is a complex process that requires a carefully orchestrated series of events (Fig. 2). It starts with the recruitment and concentration of cargo by coat proteins followed by budding of the vesicle from the donor membrane. In the end, the vesicle travels to the acceptor membrane and fuses with it. Vesicle formation is mediated by a number of factors that include transmembrane and cytosolic proteins that can affect the overall geometry of the membrane. After vesicle formation, the cargo travels to the target membrane and fuses with it. Molecules responsible for this step include tethering factors responsible for long-distance interactions between the vesicle and acceptor membrane and SNARE (SNAP (Soluble NSF Attachment Protein) REceptor) proteins. SNAREs are short transmembrane proteins that take part in the fusion process. There are sets of both tethering molecules and SNAREs responsible for controlling different steps of the trafficking network, which provides specificity of interactions between cargos and target membranes [4, 5].

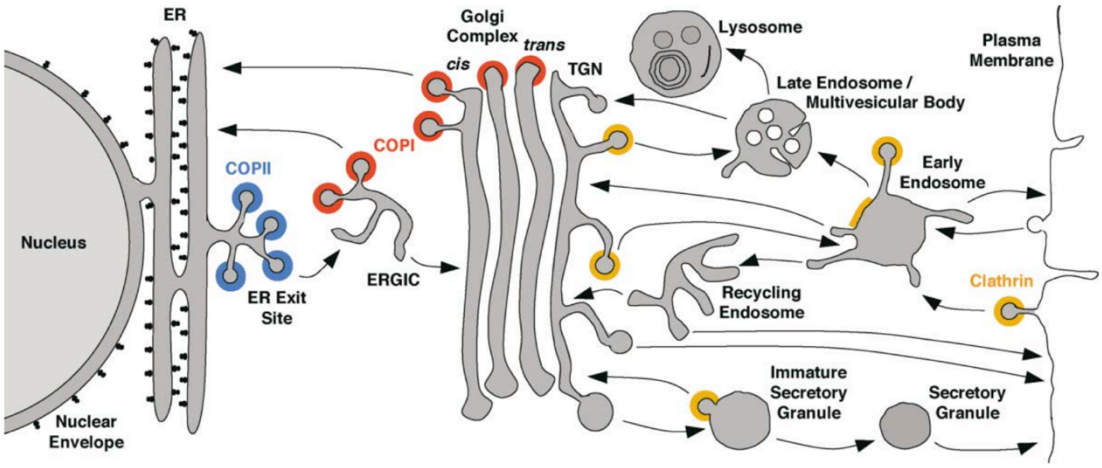

Figure 1. Intracellular trafficking pathways. The scheme illustrates major routes along which vesicular cargo is moved within the cell. The whole network can be divided into four major categories: the endoplasmic reticulum (ER), the Golgi complex, the endosome network the and plasma membrane. Locations of different coat complexes are indicated in color: COPI (red), COPII (blue) and clathrin (yellow). Arrows indicate the directionality of cargo exchange between organelles. Figure taken from [1]

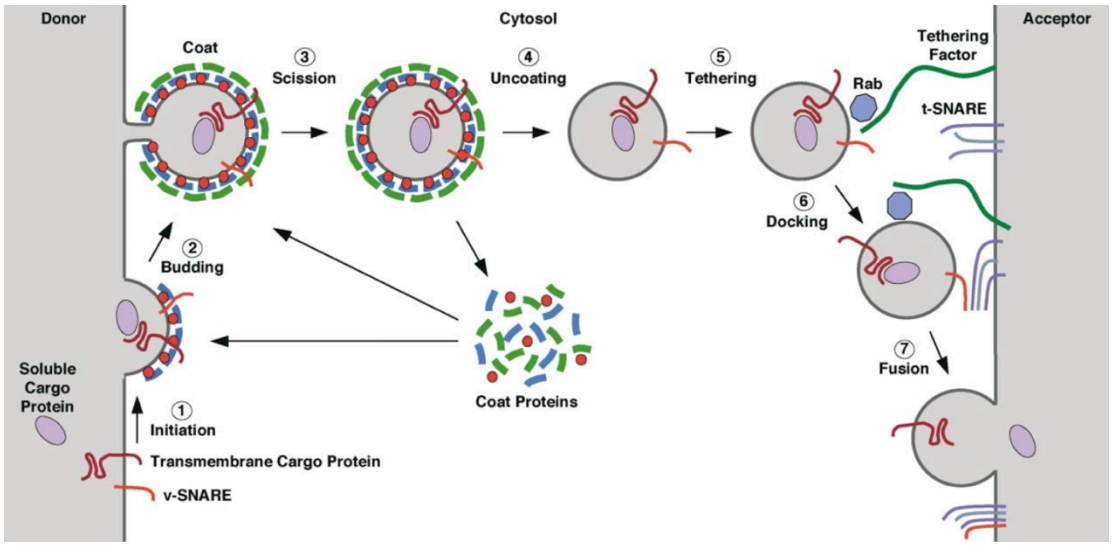

Figure 2. Vesicle budding and fusion. The scheme illustrates stages of vesicle transport. (1) Initiation. Cargo proteins are recognized at donor membrane. The inner coat proteins are recruited to the membrane, inducing initial geometry changes. v-SNARE proteins are included into the future vesicle. (2) Budding. Outer coat proteins assemble and induce further geometry changes, leading to the formation of a spherical vesicle. (3) Scission. The membrane connecting the vesicle to the donor membrane is disrupted. (4) Uncoating. Coat proteins are released from vesicle surface. This requires conformation changes, which can be induced by GTP hydrolysis. Free coat proteins can be recycled to newly forming vesicles. (5) Tethering. The vesicle is recognized at the acceptor membrane through the interaction of specific tethering factors with GTP-bound Rab molecules. (6) Docking. Closer association of the vesicle with the acceptor membrane allows the interaction between the v-SNARE and three t-SNAREs. This leads to the formation of a four-helix bundle between the SNARE molecules. (7) Fusion. The SNARE complex induces fusion between two membranes. Soluble cargo is released into the lumen of the acceptor compartment. Membrane proteins become integrated into the acceptor membrane. Figure taken from [1]

Anterograde pathway (ER to Golgi)

One of the most important and best-studied processes taking place in the ER is protein biosynthesis. Every protein that needs to enter the secretory pathway originates from there. As new polypeptides are generated by the ribosomes, they become translocated into the lumen of the ER or docked in its membrane via the pore of the Sec61 translocon. Nascent proteins that are meant for export are characterized by the presence of a signal recognition sequence [6]. They are recognized by specific receptors at ER exit sites (ERES), which in turn leads to the binding of the COPII coat. The process is initiated by Sec16, which forms a scaffold for the recruitment of

the coat components [7, 8]. This involves binding of the GTP-bound form of Sar1 (Sar1-GTP) and Sec23-Sec24. This is followed by the attachment of the Sec13-Sec31 complex, which drives membrane deformation and vesicle formation (Fig. 3) [9]. After scission from the membrane the COPII coat is disassembled [3] and the vesicles reach the ER-proximal side of the Golgi apparatus (*cis*-Golgi) through a region called the ER-Golgi intermediate compartment (ERGIC) [10, 11]. The recognition of the target membrane is mediated by tethering factors such as p115 and GM130 [12-14], while the fusion is mediated by SNARE proteins syntaxin-6 and Sec22B [13, 15]. The Golgi apparatus can be separated into several subcompartments. It is composed on a series of flattened cisternae. The vesicles delivered from the ER fuse with the Golgi stack at *cis*-Golgi. The cargo proteins are segregated and undergo post-translational modifications. The *cis* cisternae gradually maturate into medial and *trans* cisternae. From there, the cargo can enter the compartment called the trans-Golgi network (TGN), from which they can be exported towards the plasma membrane in secretory granules [16].

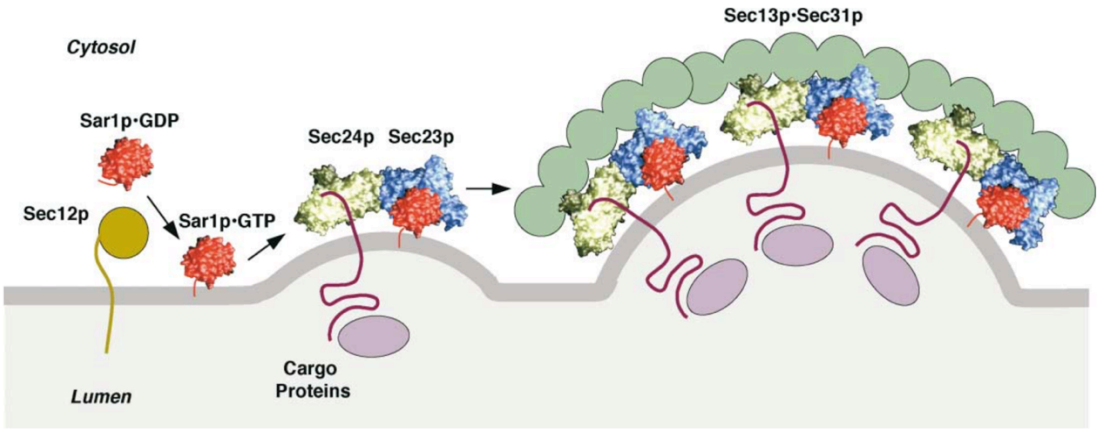

Figure 3. Formation of COPII vesicles. The transmembrane protein Sec12p acts as a guanine nucleotide exchange factor (GEF) and converts cytosolic Sar1p-GDP into membrane-bound Sar1p-GTP. Sar1p-GTP in turn forms the pre-budding complex by recruiting the Sec23p/Sec24p dimer through Sec23p binding. Proteins destined for export from the ER bind to Sec24p directly or through specific transmembrane receptors. The Sec13p/Sec31p subcomplex polymerizes onto the pre-budding complex, which leads to cargo concentration and further deformation of vesicle membrane. Picture taken from [1]

Retrograde trafficking

There are different mechanisms that allow the transport of cargos in the direction opposite to the anterograde pathway. Retrograde trafficking is required in order for some cargos to be recycled from *cis*-Golgi back to the ER. In this case, the components of the COPI complex are responsible for the generation of vesicles. Although the process is orchestrated by a different set of proteins, there are many analogies with the anterograde pathway. It starts with the activation of a small GTPase Arf1, which binds to the membrane in its GTP-bound form and recruits the inner coat (β-COP, γ-COP, δ-COP, and ζ-COP) and outer coat (α-COP, β'-COP, and ε-COP) components. Similar to Sec23p/Sec24p and Sec13p/Sec31p complexes, these proteins orchestrate binding of cargo and membrane deformation that results in vesicle formation [17, 18].

Trafficking between the Golgi apparatus and plasma membrane

Apart from the exchange of cargo vesicles between ER and Golgi, there is a rich set of interactions at the interface between the Golgi apparatus (notably the TGN) and the plasma membrane. Cargos that enter the cell through endocytosis (see section 1.1.2) are initially located in an early endosome, from where then can be sorted in different ways. One possibility is that the endosome content gets directed to the degradative pathway, which results in endosome maturation followed by lysosome fusion. Certain cargos follow an alternative route. Some proteins, such as the transferrin receptor (TfR), avoid degradation and are redirected to the plasma membrane upon internalization [19]. This may occur directly from the early endosome through a Rab4-dependent mechanism or indirectly through recycling endosomes in a Rab11-dependent process [20]. Another alternative pathway allows trafficking from the plasma membrane via sorting endosomes to the TGN. This is mediated by the retromer complex, which consists of two subcomplexes: the Vps26-Vps29-Vps35 trimer (cargo selective trimer or CTS), and a set of sorting nexins (SNX) (see section 3.2. for details about the retromer complex) [21-23].

1.1.2. Endocytic pathway

Cargo uptake mechanisms

There are several known mechanisms responsible for taking up different kinds of cargos from the outside environment. These include phagocytosis, macropinocytosis, clathrin-dependent endocytosis and different clathrin-independent pathways (Fig. 4).

Clathrin-mediated endocytosis (CME) is the best-studied pathway among endocytic processes. It involves recruitment of clathrin on the inner side of the plasma membrane, which causes increased membrane curvature and formation of a vesicle around the cargo [24]. The scission of the fully formed vesicle requires the polymerization of dynamin around the neck of the vesicle, which leads to membrane fission [25]. Receptors responsible for the recruitment of clathrin include the low-density lipoprotein receptor (LDLR), epidermal growth factor receptor (EGFR) and transferrin receptor (TfR) [26-28].

Macropinocytosis is a clathrin- and dynamin-independent process that enables the uptake of liquid phase in a non-selective manner. It is characterized by the formation of large membrane ruffles on the surface of the plasma membrane that then fold back and fuse with the membrane. The ruffling is caused by actin remodeling and the activity of PI3 kinase and CDC42 [29, 30].

One of the better-studied clathrin-independent endocytosis pathways is the caveolin-mediated endocytosis [31, 32]. It involves the formation of structures termed caveolae through the assembly of caveolins, which are integral membrane proteins that induce membrane curvature [32-34]. Similar to CME, the formation of vesicles is dynamin-dependent [35].

Phagocytosis is a receptor-mediated process that allows internalization of large particles. These include viruses, bacteria and cell debris. The process requires the involvement of different receptors and downstream signaling. The receptors can recognize various factors, such as pathogen-associated molecular patterns (PAMPs) or opsonized particles. Phagocytosis is characterized by actin polymerization leading to the formation of pseudopodia, which then engulf the particle. Since this process requires remodeling of the actin network, it requires the activation of Rac1 and CDC42 [36, 37].

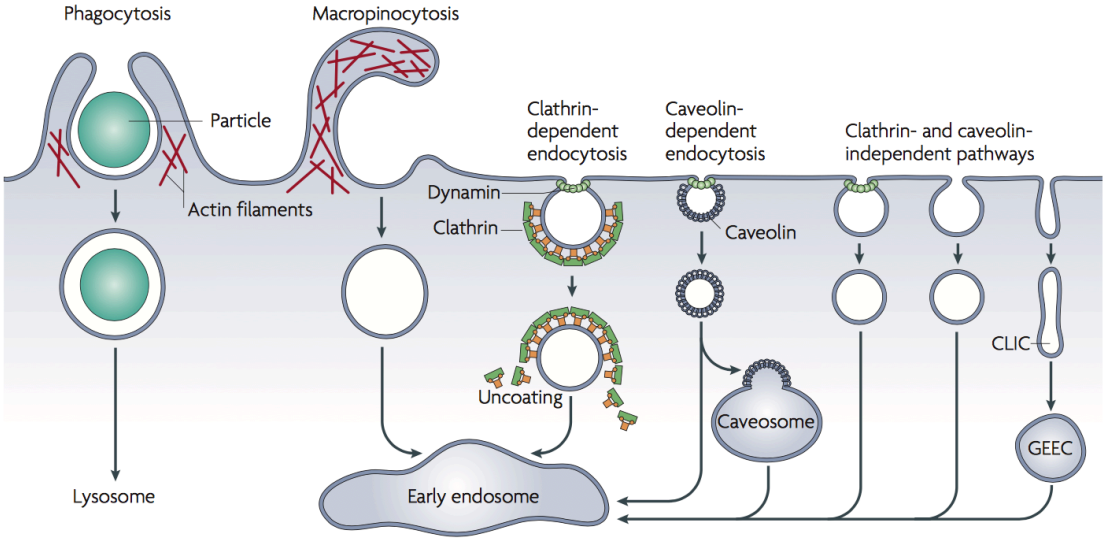

Figure 4. Mechanisms of uptake in eukaryotic cells. Phagocytosis is a process of internalizing large particles, including entire bacteria. It results in the formation of the phagosome, which is directed towards endosome fusion. Macropinocytosis is needed for the uptake of liquid phase. Both phagocytosis and macropinocytosis are involved in the uptake of relatively large volumes and require actin remodeling. Clathrin-dependent endocytosis requires the formation of clathrin pits at the plasma membrane, which leads to the budding of clathrin vesicles. There are also clathrin-independent (CI) processes that can be both orchestrated by caveolin or caveolin-independent. Most of the cargo taken up from the plasma membrane is directed towards the endosome. In some cases this occurs through intermediate compartments, such as the caveosome or glycosyl phosphatidylinositol-anchored protein enriched early endosomal compartments (GEEC). Dynamin is essential for clathrin- and caveolin-dependent endocytosis as well as in some of the independent processes. Figure taken from [38].

Endosome maturation

Engulfment of different cargos by membranes through endocytosis results in the formation of an early endosome (EE). Cargos that are directed for degradation enter the lysis pathway. It is characterized the replacement of the EE marker Rab5, a GTPase, by late endosome (LE) markers such as Rab7 and LAMP1 [39]. The pH of the organelle is gradually lowered by the activity of the proton pump v-ATPase [39, 40]. In parallel, the phosphate composition of the endosome membrane changes. Notably, phosphatidylinositol-3-phosphate (PtdIns(3)P) is converted to phosphatidylinositol-3,5-bisphosphate (PtdIns(3,5)P2) [41]. Proteins from the EE surface that need to be degraded are sequestered into luminal invaginations that are eventually separated from the membrane and form intraluminal vesicles (ILVs). The process requires the action of the endosomal sorting complexes required for transport (ESCRT) [42, 43]. Endosomes containing ILVs form multivesicular bodies (MVBs).

The process ends with lysosome fusion and lysis of the endosome content by hydrolases [41, 44]. Alternatively, the cargo taken up at the plasma membrane can avoid degradation and be sent to different organelles, such as the TGN.

1.1.3. The endoplasmic reticulum (ER)

Structural and functional characteristics of the ER

The ER constitutes around half of the total membrane surface and around 10% of volume in a typical eukaryotic cell [45]. It fulfills a number of key functions. One of the main roles of the ER is the synthesis, modification and quality control of proteins. Other functions include synthesis of sterols and lipids, calcium homeostasis, carbohydrate metabolism and neutralization of harmful substances [46]. The morphology of the ER is extremely complex compared to other organelles. It is a continuous system of membranes that includes the nuclear envelope and a meshwork of sheets and tubules [47-49]. The organelle can be divided into a number of subcompartments that play different roles, such as rough ER (RER) and smooth ER (SER) (Fig. 5). The former has mostly sheet-like architecture. It is decorated with ribosomes and is responsible for synthesizing proteins for export. SER is more tubular and plays different roles, such as lipid synthesis and conferring contacts of ER with other organelles [50].

The appearance of the ER can differ substantially across cell types. Cells involved in extensive secretion of proteins (pancreatic acinar cells or plasma cells) are characterized by the abundance of ribosome-studded sheets. Hepatocytes are in turn equipped with a rich SER network responsible for the metabolism of carbohydrates and detoxification. In muscle cells, a specialized form of SER called the sarcoplasmic reticulum is responsible for highly regulated release of Ca^{2+} that controls contraction. Lastly, the nuclear envelope is rich in complex nuclear pore complexes (NPCs) that orchestrate the exchange of molecules between the cytosol and nucleoplasm [45, 51]. The ER is closely associated with other cellular structures. These include cytoskeleton components, the plasma membrane and different organelles, such as mitochondria and endosomes [52-55]. The structures comprising the ER are highly dynamic, i.e. they are constantly forming and collapsing. The organelle constantly undergoes shape changes mediated by membrane fission and

fusion events between different components of the network. Some of the morphology changes are very dramatic, the best example is the collapse of the nuclear envelope during cell division [56-58].

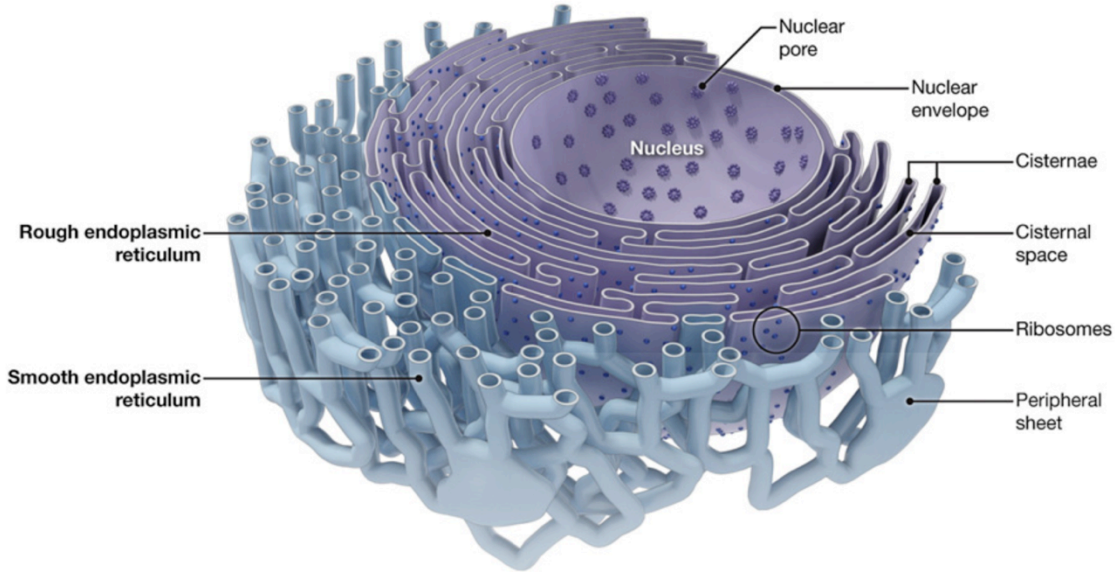

Figure 5. The ER network. The diagram shows different subcompartments of the ER. These include the nuclear envelope, RER and SER. The nuclear envelope is perforated by NPCs, which allows the diffusion of macromolecular complexes. The RER is studded with ribosomes and consists mostly of flattened cisternae. The SER does not host ribosomes and is predominantly built by ER tubes. Picture taken from [59]

In order to accommodate the large variety of shapes, there has to be a range of membrane curvatures within the organelle. Structural proteins of the ER are mostly responsible for introducing different membrane geometries. Other mechanisms, such as asymmetric lipid distribution between membrane leaflets, are believed to play a limited role [48, 52, 60]. Proteins introduce membrane curvature in many ways, including membrane deformation by force-generating proteins, highly-curved protein scaffolds and hydrophobic wedging (insertion of proteins into the outer membrane leaflet) [48, 61, 62]. In some cases the forces extending the ER tubules are generated by assembling microtubules or motor proteins sliding along the cytoskeleton [63, 64]. Curvature-stabilizing proteins can be divided into two families, the DP1/ REEP/Yop1p proteins and the reticulons. Both groups are characterized by long hydrophobic hairpin motifs (or wedge domains) that partially span the membrane

[65-68]. Overexpression or depletion of those proteins leads to changes in the ER sheet-to-tube ratio [48, 65, 69, 70] and recombinant Yop1p and Rtn1p are sufficient to convert proteoliposomes into tubules *in vitro* [71].

ER sheets do not require stabilization and can form spontaneously. The degree of curvature at the edges of sheets resembles the one of ER tubes, which has been linked to local enrichment of reticulons [71, 72]. The constant thickness of ER sheets is maintained in different ways. Proteins such as CLIMP-63, p180, and kinectin are enriched in those structures and are believed to accommodate even spacing between membranes through their coiled-coil domains [73]. Their overexpression has been linked to proliferation of sheet structures, while depletion leads to a decrease of luminal width [45, 72].

The nuclear envelope consists of two membranes that build sheet-like structures. Both membranes remain mostly separated, but come into contact at nuclear pore complexes (NPCs) [51, 74]. The spacing between the inner and outer membranes is around 40-50 nm, which is less than in a typical ER sheet. Membrane proteins interact with chromatin and nuclear lamina, stabilizing the flat areas of the nuclear envelope [51]. The best-described interactions are between transmembrane complexes of SUN proteins (Sun 1 and Sun 2) and nesprins, which constitute a linker between the envelope and cytoskeleton elements such as actin and intermediate filaments [45, 75, 76].

One of the key elements of the ER is the three-way junction, which constitutes an intersection of tubules and is responsible for the network-like structure of the organelle. Creation of this kind of assembly requires fusion of tubules. Atlastins, a family of dynamin-related GTPases, are believed to play a pivotal role in this process. These integral membrane proteins can be found mainly at spots of high curvature, such as ends of tubules and edges of sheets [77, 78]. Atlastins interact with both the DP1/REEP/Yop1p and reticulon families and orchestrate formation of three-way junctions through homotypic fusion [79-83]. The mechanism is believed to involve in trans tethering between GTP-bound atlastin oligomers form opposing membranes, followed by GTP hydrolysis and conformation changes that pull the membranes closer. The curvature generated during this process destabilizes the membrane and leads to fusion [45, 84-86]. It is unknown whether atlastins are responsible for all fusion events occurring between ER tubules, as there are reports of other factors being involved [83].

The overall shape of the ER is also stabilized through interactions with the cytoskeleton, plasma membrane and other organelles. The association with cytoskeleton varies across different kingdoms of life. In animal cells, the interactions between ER and microtubules are particularly important and occur through a number of mechanisms [63, 64, 87]. Examples of interactions include the association of the microtubule-severing protein spastin with atlastin and DRP1 [88-90]. CLIMP-63 has been shown to mediate the attachment of ER sheets to microtubules [91]. Interactions with the plasma membrane also play a crucial role in ER integrity. In yeast, the depletion of ER-plasma membrane tethering proteins Ist2, tricalbins, Scs2 and Scs22 lead to detachment and accumulation of ER membranes in the cytoplasm [54].

ER stress and the unfolded protein response (UPR)

A large proportion of the eukaryotic proteome is synthesized and processed at the ER. The ER lumen provides an environment for protein folding and glycosylation. A number of protein chaperones, such as binding immunoglobulin protein (BiP), calnexin and calreticulin, are responsible for those processes [92]. When the amount of proteins that require folding exceeds the processing capacity of the ER, unfolded proteins start to accumulate. This can be caused by different stress conditions, including elevated biosynthesis, perturbations in calcium homeostasis and redox balance [93]. Accumulation of unfolded proteins induces ER stress and activates the unfolded protein response (UPR). This evolutionarily conserved mechanism inhibits translation, increases the protein folding capacity of the ER and induces ER-associated degradation (ERAD). This reduces cellular stress and helps preserving homeostasis. In cases where balance cannot be restored, UPR leads to programmed cell death [94]. Additionally, the UPR activates pathways associated with innate immunity, which links it to detection of intracellular pathogens [95].

There are three sensors that are responsible for the activation of UPR: the inositol-requiring enzyme 1 (IRE1), double-stranded RNA-dependent protein kinase R (PERK) and activating transcription factor 6 (ATF6). All of them are located in the ER membrane and have a cytosolic effector domain linked to an ER-luminal domain through a transmembrane helix [92, 94, 96]. All three proteins can independently detect different inputs indicating ER stress [97, 98]. This results in the activation of

signaling pathways of the UPR, which leads to an increase in chaperone production, arrest in translation (apart from proteins involved in UPR) and degradation of misfolded proteins though ERAD [99]. UPR activation also results in ER expansion though the induction of autophagy and increased lipid biogenesis. The combination of selective autophagy with elevated lipid production increases ER volume and capacity to resolve stress [100-102].

1.1.4. Interactions of pathogen with host organelles and trafficking pathways

Intracellular pathogens

There are several bacterial pathogens that thrive inside host cells (Fig. 6). Intracellular lifestyle has many advantages for the bacteria. Inside eukaryotic cells, the bacteria are shielded from immune recognition and competing microbes. They may also benefit from host cell nutrients and use them for growth. There are, however, several risks associated with choosing such a strategy. Most bacteria enter the host cell through the phagosome, which is specialized in detecting and neutralizing threats. In more advanced hosts, like vertebrates, the endolysosomal compartments and the host cytosol have factors that may lead to the activation of the immune system [103]. Intracellular pathogens have evolved numerous mechanisms of manipulating the host cells. These involve structural modifications of the surface of the bacterial cells and usage of effector proteins that affect different aspects of the host cell's trafficking processes [104-106].

Internalization of bacterial pathogens

Due to their size, bacterial pathogens need to be internalized by the host cell through engulfment in a large portion of the plasma membrane. Dependent on the species, this process may involve different mechanisms. Most bacteria fall into one of two major categories of entry type, which are the zipper and trigger mechanisms (Fig. 6).

The zipper mechanism requires clathrin structures. It occurs although bacteria are much larger than the usual cargo limit for clathrin-coated vesicles, which is around 100 nm [107]. Clathrin is involved at early steps of the process. *Listeria*

monocytogenes, a gram-positive bacterium, is the best-known pathogen using the zipper mechanism. The bacterium expresses proteins Internalin A (InlA) and Internalin B (InlB) that bind to host cell surface molecules (E-cadherin and c-Met, respectively), which in turn leads to Arp2/3-dependent actin remodeling [108-110].

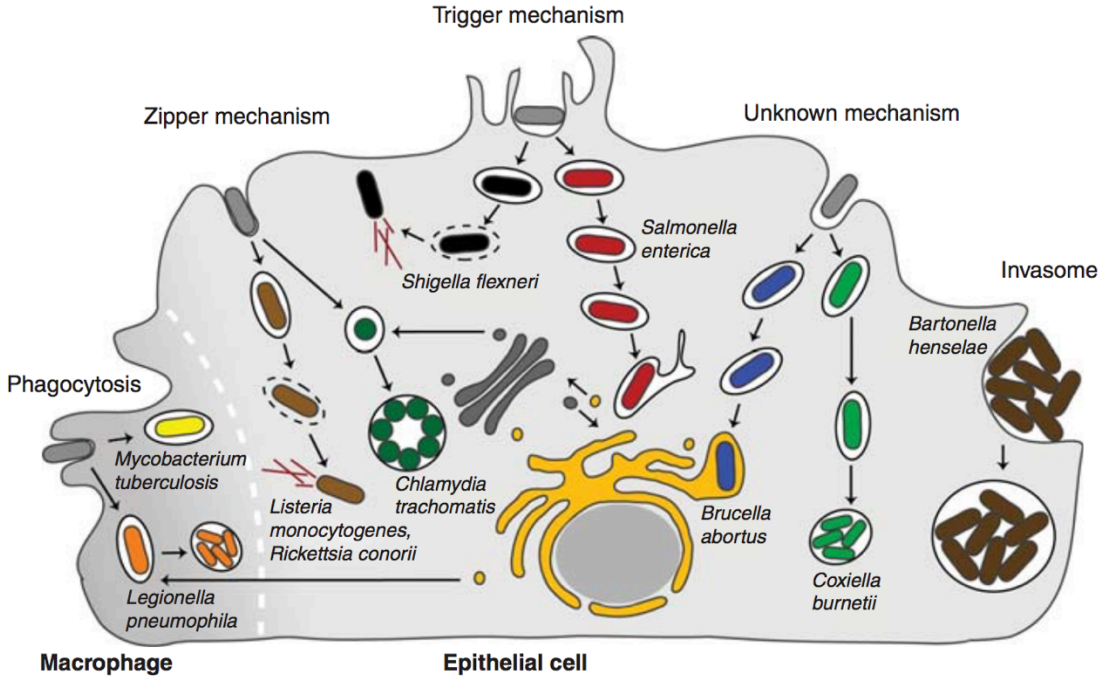

Figure 6. Intracellular pathogens. The illustration depicts strategies of entry and survival of intracellular pathogens. *Listeria monocytogenes* uses two internalins to induce entry through zipper mechanism. This is followed by vacuole lysis and actin-based motility. *Chlamydia trachomatis* intercepts sphingomyelin-rich cargos trafficking from the Golgi apparatus. *Shigella* injects type III secretion system (T3SS) effectors that induce entry through the trigger mechanism, vacuole formation and subsequent escape into the cytosol. The bacteria also induce actin comet tails for movement and cell-to-cell spread. *Salmonella* uses T3SS-1 to induce entry into the host cell and formation of its vacuole. The activity of T3SS-2 is required for the maintenance of the *Salmonella* intracellular niche. Alternatively, the bacteria can escape into the cytosol in a process that is T3SS-2-independent. *Brucella* uses its T4SS to change the nature of the phagosome from endosome-like to an ER-associated replicative niche. *Coxiella burnetii* is the only known pathogen that replicates inside a lysosome-derived vacuole. *Bartonella henselae* can enter host epithelial cells in a large cluster termed the "invasome". *Mycobacterium* and *Legionella* are taken up by macrophages and end up enclosed in phagosomes. *Legionella* induces acquisition of ER markers by its vacuole, while *Mycobacterium* blocks phagosome maturation and lysosome fusion. Picture taken form [111].

Similarly, *Yersinia pseudotuberculosis* uses Invasin that interacts with β1-integrins, leading to the activation of Arp2/3. The local changes in actin structure result in deformations of the plasma membrane that gradually engulf the bacteria [112, 113].

In the trigger mechanism, the plasma membrane forms large ruffles that surround the bacterium. The process is similar to macropinocytosis. *Salmonella*, for example, uses T3SS-1 effectors SopE and SopE2 to induce this process. Both proteins are guanine nucleotide exchange factors (GEFs) that activate Cdc42 and Rac1 [114]. Effectors SipC and SipA lead to polymerization and bundling of actin [115, 116], which causes the formation of large structures on the host cell surface that eventually engulf the bacteria.

The pathogen *Bartonella henselae* uses an unusual strategy of host entry. The bacteria can enter the host cell as large aggregates termed *invasomes* that are taken up in bulk by endothelial cells [117, 118]. The process is triggered by T4SS effectors and involves large-scale actin rearrangements [119, 120].

Nature of the intracellular niche

Once inside the host cell, the bacteria may form a replicative niche inside a membrane-bound compartment. This requires inhibiting the fusion of the phagosome with lysosomes or modifying the physiological conditions of the vacuole. In many cases the compartment gains characteristics of some host organelles [121]. There is a group of pathogens that follow an alternative approach and escape from the phagosome into the cytosol. The phagosome lumen and the cytosol represent two drastically different environments in terms of nutrient access, pathogen recognition and possibilities for cell-to-cell spreading [121].

Vacuolar bacteria

Bacteria that thrive inside membranous compartments have established ways of preventing the fusion of the phagosome with lysosomes. Each species has developed its own unique strategy for survival. The goal is achieved by introducing effectors that interfere with trafficking processes. One approach is causing an arrest in endosome maturation. Species like *Mycobacterium tuberculosis* and *Salmonella* achieve that by secreting phosphoinositide phosphatases that keep the lipid composition of their vacuoles in an EE-like state [122, 123].

Salmonella enterica serovar Typhimurium (S. Typhimurium) is equipped with two type III secretion systems (T3SS-1 and T3SS-2). The T3SS-1 plays a role in entry into host cells. One of its effectors, SopB, plays multiple roles in the formation of the *Salmonella*-containing vacuole (SCV) [124]. Following entry, the SCV localizes to the perinuclear region, close to the Golgi apparatus. The T3SS-2 is important later during infection. Its effector SifA induces formation of tubules from the surface of the SCV, which helps in the maintenance of the organelle [125]. Lack of T3SS-2 has been linked to vacuole rapture (see below) [125, 126].

Other species allow limited interactions of their vacuoles with late endosomes. In case of *Brucella*, the initial acidification of the vacuole triggers the expression of a VirB type IV secretion system (T4SS) that introduces effector proteins [127]. These induce interactions of the *Brucella*-containing vacuole (BCV) with ERES, which results in the formation of an ER-associated replicative niche (rBCV) [128]. *Legionella* employs a repertoire of over 200 effector proteins to establish a niche with ER-like characteristics. In this case, however, this is achieved by interactions of the *Legionella*-containing vacuole (LCV) with ARF1-dependent trafficking [129].

Cytosolic bacteria and phagosomal escape

Some pathogens have evolved ways to disrupt the endosome membrane and escape into the cytosol, which allows them to avoid lysosome fusion upon entry (Fig. 7) [130, 131]. The mechanism of escape from the phagosome has been well studied for a number of bacteria, e.g. *Listeria*, *Francisella* and *Shigella flexneri*. In case of *Listeria*, molecules secreted by the bacterium induce escape. These include proteins listeriolysine O (LLO) and phospholipases PI-PLC and PC-PLC [132, 133]. The process requires additional factors, such as Ca2+ flux across LLO pores that slows down endosome maturation and delays lysosome fusion [134]. *Francisella tularensis* is believed to follow a similar trafficking route. Factors IglC, MglA and FF1103 have been linked to cytosol access. More recently, the role of the type VI secretion system (T6SS) effectors PdpC and PdpD has been identified as factors responsible for vacuole rapture [135]. Upon release, the pathogen divides rapidly and eventually breaks free to infect neighboring cells [136]. *Shigella flexneri* entry into host cells involves introduction of effector proteins through the mxi-spa T3SS [137]. The effectors IpaB and IpaC have been linked to destabilization of eukaryotic membranes

[138-140]. Additionally, there are indications that the escape requires the assembly of autophagy machinery in the proximity of the vacuole, indicating that some host factors need to be recruited [141, 142]. Once in the cytosol, *Shigella* employs actin-based motility. The process occurs through massive recruitment of actin and the assembly of "comet tails", which in turn pushes the bacterium across the cell body. It is induced by the protein IcsA, which recruits actin at one pole of the bacterium. This allows avoiding detection and even results in cell-to-cell spreading [143, 144].

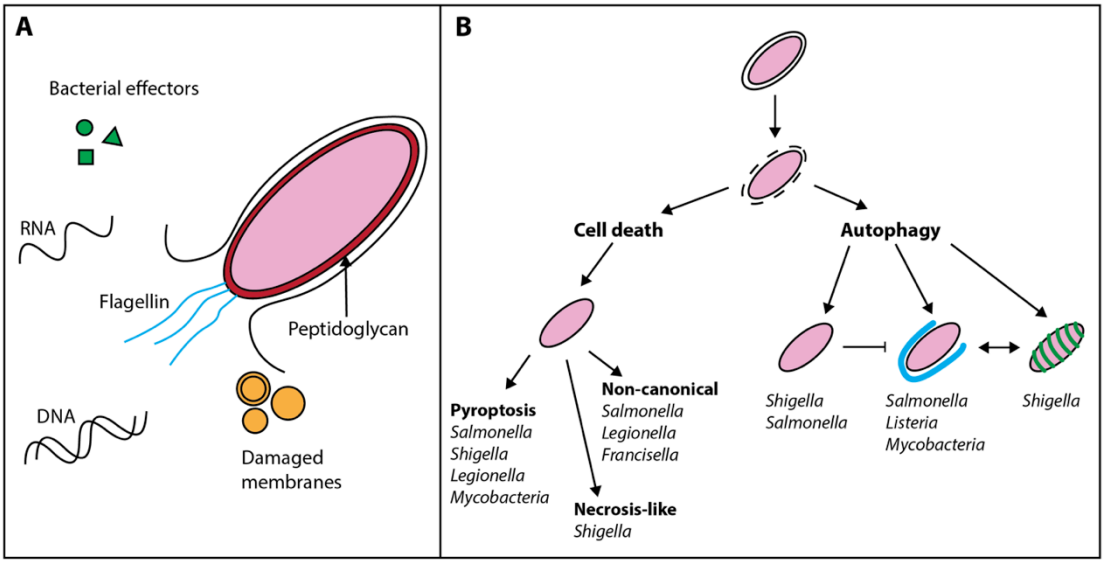

Figure 7. The impact of phagosome escape of pathogens. (A) Different factors can trigger host signaling pathways during phagosome rapture. These include damaged membranes and different molecules associated with the bacteria, such as secreted effector proteins, flagellin, peptidoglycan and bacterial nucleic acids. **(B)** Phagosome rapture may have different outcomes depending on bacteria species and host cell type. Host cell death may occur through pyroptosis, necrosis or different, non-canonical mechanisms. Autophagy (blue line) plays an important role in pathogen recognition and control. Some bacteria inhibit autophagy (left). In the case of *Shigella*, the formation of a septin cage (green lines) is interdependent with autophagy. Figure was adapted from [121].

Until recently, there had been a clear separation of intracellular pathogens into either *vacuolar* or *cytosolic*. However, there is a number of recent reports that challenge this categorization [121]. It seems that at least some pathogens may belong to both groups, with different intracellular localizations playing distinct roles. In case of *Salmonella*, a small subpopulation can be found directly in the cytosol at an early stage of infection. These bacteria were shown to enter a hyper-replicative stage that

results in a large number of cytosolic bacteria [126]. The vacuole escape of *Salmonella* seems to be connected with lack of T3SS-2 expression and the absence of SifA [125], suggesting that some of the bacteria are programmed to enter this path. Recent evidence suggests that the fate of intracellular *Salmonella* depends on the interactions of the SCV with host cell factors such as VAMP7 and COPII [145]. For *M. tuberculosis*, there is a series of reports that seem to contradict the traditional dogma of vacuolar localization [146-148]. One study indicated that the majority of *M. tuberculosis* could be found directly in the cytosol of dendritic cells (DCs) 96 h post infection [146]. The localization in the cytoplasm is dependent on the type VII secretion system (T7SS) ESX-1, which was additionally shown to be important for the recognition of *M. tuberculosis* by autophagy machinery [146, 149, 150]. This suggests that the vacuole escape might be an active process that is required for intracellular survival of *Mycobacteriae*.

Interactions of cytosolic bacteria with host defenses

The cytosol of eukaryotes contains several factors that pose a threat to bacteria. These include antimicrobial peptides [151] and immune receptors that recognize PAMPs and can activate the immune system or autophagy [152, 153]. In some cases, however, those responses may be beneficial for the pathogen.

Activation of cell death is often triggered by the detection of cytosolic bacteria. It can occur through different mechanisms. *Shigella* has been shown to activate pyroptosis through endosome damage [139]. *Shigella* vacuole rapture has also been linked to a caspase-independent pathway that involves loss of mitochondria membrane potential [141]. At the same time, the bacterium seems to activate pro-survival signaling that inhibits cell death until later infection stages [154]. The escape of *Salmonella* into the cytosol induces cell death in the population of infected cells carrying hyper-replicating bacteria. There is evidence suggesting that these bacteria express flagellum components and the T3SS-1 genes. This leads to caspase-1-mediated pyroptosis and release of interleukin-18 [126]. It is speculated that this process is responsible for massive inflammation occurring during *Salmonella* infection.

Autophagy has been originally described as a catabolic process activated by nutrient starvation, which allows the cell to recycle material [155]. The mechanism is

triggered by the presence of ubiquitin that is covalently linked to proteins or membranes destined for autophagy. Ubiquitin is recognized by a series of adaptors that eventually link it physically to LC3 (Atg8 in yeast), which in turn recruits a double membrane that engulfs and isolates the cargo from the rest of the cell volume, forming an autophagosome. The process eventually leads to lysosome fusion and degradation of the autolysosome content [156]. In healthy cells, the process is used to recycle nutrients and entire organelles, including damaged mitochondria in a process called mitophagy [157].

Escape of pathogens into the cytosol often triggers autophagy and in many cases this has been linked to bacteria clearance. The factors responsible for the recruitment of autophagy proteins include different components of bacterial cells, such as DNA, peptidoglycan and flagellar motor elements [158, 159]. In case of *Shigella*, autophagy is connected to septin binding [160]. Septins are a conserved group of GTP-binding proteins that form oligomeric complexes and play various roles in different cellular processes [161]. They have been identified as a factor restricting cytosolic *Shigella* by assembling into *cages* on bacterial surface. siRNA experiments suggest that both septins and autophagy components are required for either of the processes to take place, suggesting that they are strongly interconnected [160]. Other pathogens, such as *Listeria* and group A *Streptococcus* (GAS), are marked with LC3 and engulfed by autophagy membranes following phagosome escape. This process does not, however, involve septin caging [162]. Cytosolic *Francisella* has a strategy of delaying detection by autophagy for more than ten hours [136, 163]. The O-antigen on the bacteria's surface is responsible for evasion of autophagy through the Atg5 pathway [163, 164].

Interactions of pathogens with the ER

As mentioned above, intracellular bacteria are typically enclosed inside phagosomes upon entry. Many of the survival strategies involve modifications of this compartment, which introduce properties of other, less bactericidal compartments. Some pathogen species manage to induce the interaction of the phagosome with the ER (Fig. 8). The ER lies at the crossroads of key metabolic processes and is rich in nutrients. In addition, the ER has presumably limited antimicrobial capacity, which reduces the risk of neutralization by the host [93].

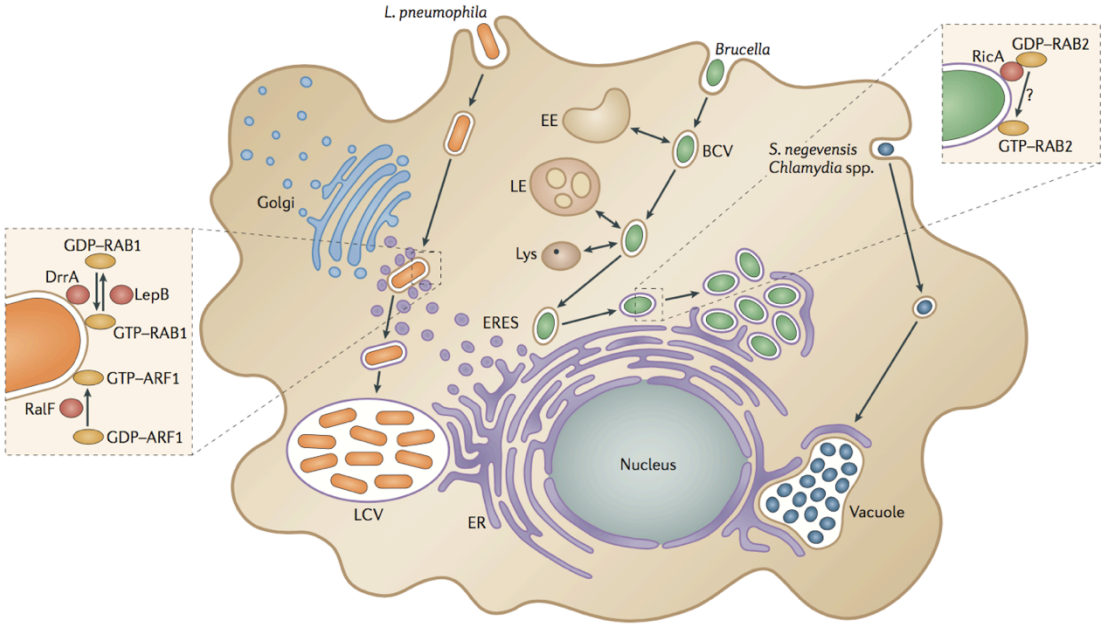

Figure 8. Intracellular pathogens interacting with the ER. *Legionella pneumophila* uses Dot/ICM T4SS effectors DrrA, LepB and RalF to intercept early secretory vesicles to its phagosome. These effectors modify the activities of host GTPases RAB1 and ARF1 on the surface of the phagosome, which leads to a bypass of the endocytic pathway and eventual fusion with the ER. This leads to the formation of an ER-derived *Legionella*-containing vacuole (LCV). *Brucella* spp. resides in a vacuole termed the *Brucella*-containing vacuole (BCV), which initially travels along the endocytic pathway. The BCV localizes to the ER exit sites (ERESs) and fuses with the ER. The process induced by the effectors secreted by a VirB T4SS and small GTPases SAR1 and RAB2. Another effector, RicA, is required for the accumulation of GTP-bound form of RAB2 on the BCV. *Chlamydia* uses its type III secretion system (T3SS) to control host trafficking and transform its vacuole into a large inclusion that interacts with the ER at specific contact sites. Figure taken from [93]

Despite ER being and advantageous environment for bacterial proliferation and persistence, there are only few examples of bacteria species that have evolved to colonize it. The first known examples of pathogens interacting with the ER were *Legionella pneumophila* and *Brucella* spp. It was demonstrated that the replicative vacuoles of those species are decorated with ribosomes and derived from the ER both ultrastructurally and functionally [128, 165-171]. Later, other species such as *Legionella longbeachae* [172], *Chlamydia trachomatis* [173, 174] and *Simkania negevensis* [175] have been shown replicate in organelles that closely interact with the ER.

In case of *L. pneumophila* and *Brucella* spp., the trafficking to the ER involves the activity of a T4SS (*Legionella* Dot/Icm and *Brucella* VirB T4SS), which introduces effector proteins that alter trafficking pathways of the host [128, 176, 177].

This results in subversion of early secretory vesicles. Each of the pathogens, however, uses a distinct mechanism. Phagocytosis of *L. pneumophila* leads to the formation of the *Legionella*-containing vacuole (LCV). Instead of following the phagocytic pathway, the LCV intercepts secretory vesicles trafficking between ER and Golgi. The vesicles are tethered to the LCV and eventually fuse with it. The vacuole changes its characteristics to an ER-like compartment that becomes replication-permissive [170, 171, 178-180]. The whole process is tightly orchestrated by a set of T4SS effectors, which induce recruiting of vesicles to the LCV and unusual pairing of SNARE proteins [176, 177, 181-184].

Chlamydia spp. resides in a spacious vacuole called the *Chlamydia* inclusion. The organelle intercepts vesicles trafficking from the Golgi to the plasma membrane. This allows the acquisition of sphingolipids, which are necessary for the biogenesis of the vacuole and growth of the bacteria [185, 186]. The inclusion has been shown to form contact points, or *synapses*, with the ER. Those structures are believed to deliver material to the inclusion and are important for intracellular for bacterial growth [173, 174].

Brucella uses its VirB T4SS effectors to induce the interaction of the *Brucella*-containing vacuole with ERES [128, 187]. The details of the mechanism used by *Brucella* spp. will be discussed below in Section 1.2 of the Introduction.

1.2. Interactions of *Brucella* with host cells

1.2.1. The genus *Brucella* and brucellosis

The bacteria belonging to the genus *Brucella* are gram-negative, facultative intracellular pathogens, classified as α-Proteobacteria. There have been 11 species described so far. Brucellae are the causative agents of brucellosis, a zoonosis that has major health and economic impact around the world. The disease can be transmitted to humans, which occurs mostly through contaminated milk products. With around 500'000 new cases reported annually worldwide, brucellosis is the most important zoonotic infection. The bacteria can colonize different organs and reproduce in various cell types, including macrophages, dendritic cells and placenta trophoblasts. This leads to a debilitating condition, which is hard to diagnose and eliminate [188-190].

1.2.2. *Brucella* entry

Brucella is capable of invading both phagocytic and non-phagocytic cells (Fig. 9). Attachment of *Brucella* to macrophages and epithelial cells is mediated by several factors, such as surface protein 41 (SP41), fibronectin and vironectin [191, 192]. Interaction with fibronectin is mediated by the autotransporter BmaC [193]. Entry into non-phagocytic cells occurs through unknown receptors. It requires the activity of Rac, Rho and Cdc42 and involves actin polymerization [194]. Entry into trophoblast giant cells depends on Hsc70 and ezrin [195].

During macrophage entry, non-opsonized *Brucellae* need to associate with lipid rafts. There are two receptors that have been proposed to play a role. The class A scavenger receptor (SR-A) is believed to interact with *Brucella* lipopolysaccharide (LPS), while the cellular prion receptor PrPc was proposed to bind Hsp60 [196, 197]. The process occurs through phosphoinositide-3-kinase (PI3K)-dependent membrane ruffling [196, 198-200]. There is no data suggesting that *Brucella* actively induces its own internalization. The T4SS remains inactive during entry and is induced only upon the acidification of the phagosome [127].

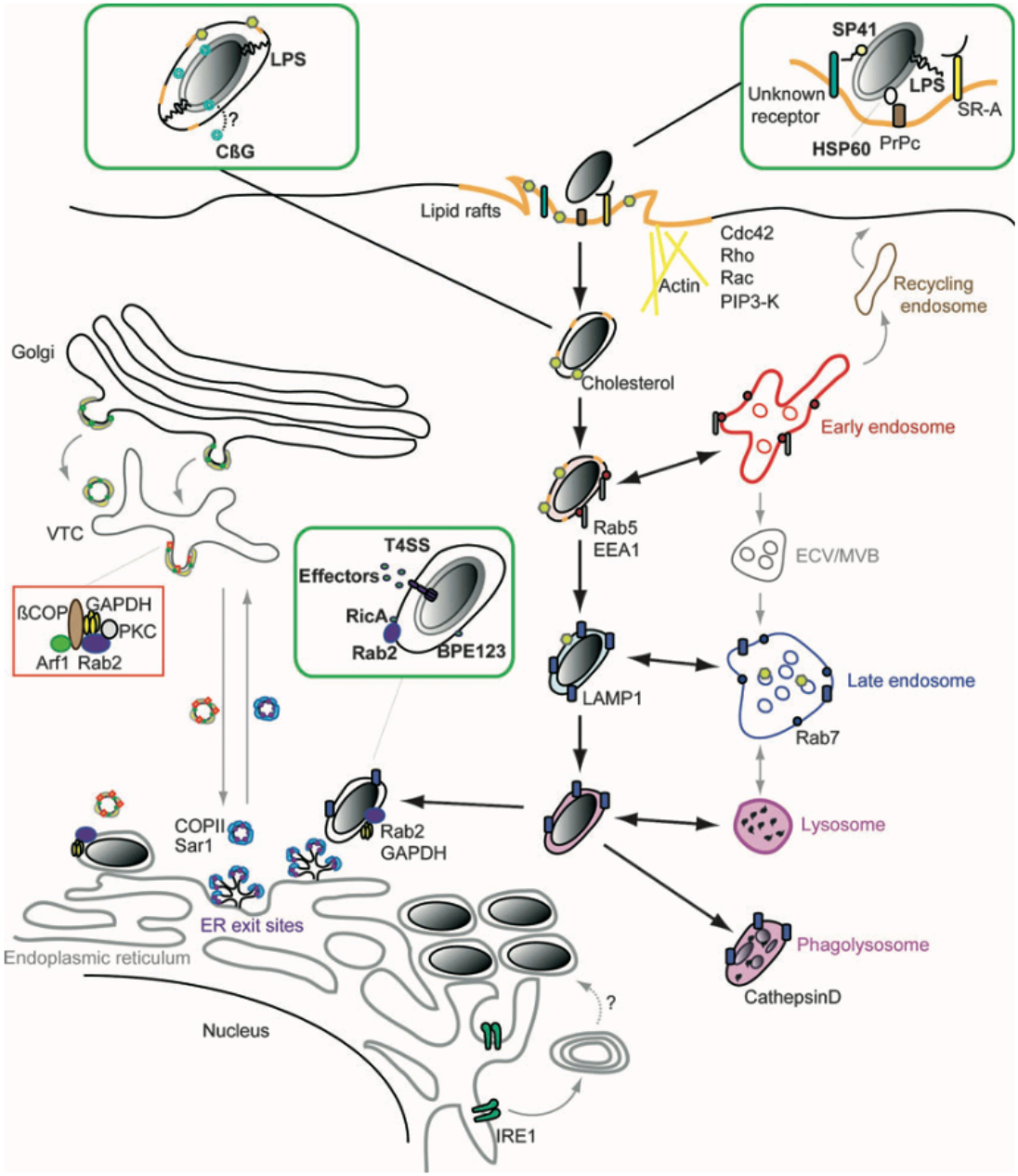

Figure 9. Intracellular lifestyle of *Brucella*. The scheme summarizes the findings concerning the entry, trafficking and replication of *Brucella*. Green boxes indicate factors involved in chosen trafficking steps in detail. *Brucella* entry occurs at lipid rafts (orange). Cyclic β-1,2-glucan (CβB) produced by the bacterium is believed to deplete the cholesterol from phagosome membrane. The *Brucella*-containing vacuole (BCV) traffics along the endocytic pathway, interacting with early and late endosomes. Acidification of the vacuole induces the expression of a T4SS that delivers effector proteins into the host. This results in interaction of the BCV with early secretory vesicles at ER exit sites (ERES), which in turn leads to the establishment of an ER-derived replicative BCV (rBCV). After several rounds of replication, the bacteria interact with autophagy in a non-canonical manner. Picture taken from [201].

1.2.3. Intracellular trafficking of *Brucella*

Internalization of *Brucella* leads to the formation of an EE-like compartment called the *Brucella*-containing vacuole (BCV), which remains non-replicative (nrBCV) during the first stages of trafficking. EE markers, such as Rab5 and EEA1 have been found on the surface. As the vacuole maturates, EE markers are gradually replaced by LE markers Rab7 and LAMP1 [128, 168, 169, 202, 203]. Lowering of the pH induces the expression of T4SS, which translocates a number of effector proteins into the host cell [127, 187, 204]. This leads to changes in the trafficking of the BCV that only allow limited interactions of the organelle with lysosomes, preventing degradation of the bacteria [128, 169, 202, 205]. Instead, the bacteria establish a replicative niche (replicative BCV or rBCV), which is associated with the host ER [202, 206]. Although the exact mechanism remains unknown, it is believed that interactions of the BCV with vesicles originating from ERES gradually change the nature of the vacuole. This was demonstrated by showing the colocalization of Sar1 and the COPII complex colocalizing with the BCV [128, 168, 169, 207]. Despite clear evidence that the T4SS plays a key role in this transition, there is limited data on the exact mechanism by which the effectors orchestrate it.

The effector protein RicA was shown to interact with the inactive form of GTPase Rab2, which is found mostly in ERGIC and orchestrates Golgi-to-ER trafficking [208]. The *ricA* deletion did not lower the ability of *Brucella* for intracellular survival and replication. In fact, the mutant displayed faster LE escape and enhanced proliferation, indicating that the effector has a regulatory effect on bacteria replication [209, 210]. There are reports suggesting that the importance of *Brucella* effectors stretches beyond orchestrating intermediate trafficking stages. In a recent study, BspB has been shown to affect Golgi-to-ER trafficking through interacting with the COG tethering complex [211]. This function of BspB seems to play a role not only in the establishment of the rBCV, but is also required for efficient bacterial growth. At the same time, the deletion of *bspB* does not completely prevent intracellular replication of the bacteria, which suggest a more modulatory role of the protein. There are also indications that a functional T4SS is required during post-replication stages of *Brucella* life cycle, possibly orchestrating egress from the host cell [212]. Despite those finding, our knowledge about the role of T4SS effectors in

Brucella infection remains limited. Further research needs to indicate the actual mechanism of action of those effectors.

1.2.4. The replicative niche of *Brucella*

Upon establishing the replicative niche, *Brucella* undergoes several rounds of division, with a doubling rate of around 3 hours. The process lasts until the host cell volume is completely overwhelmed with bacteria [213].

The rBCV has been described as 'ER-derived' or 'ER-associated'. Several ER markers, such as calnexin, calreticulin, Sec61β, PDI and surface ribosomes were shown to colocalize with dividing Brucellae. A characteristic feature of the rBCV is the relative isolation of the bacteria – most of the vacuoles are compact and contain from one up to a few bacteria when visualized by transmission electron microscopy (TEM) [128, 165, 169]. This distinguishes *Brucella* from many other intracellular pathogens, notably *Legionella*, another ER-dwelling pathogen that occupies spacious vacuoles during replication [170, 178]. Several reports have indicated continuity between the rBCVs and ER, including the presence of bacteria in the perinuclear space. This suggests at least partial fusion of the vacuoles with the endoplasmic reticulum [128, 165, 214].

There are reports of UPR induction in macrophages and epithelial cells infected with both *B. melitensis* and *B. abortus* [215, 216]. IRE1 has been identified as a necessary factor for the intracellular growth of *B. abortus* [217], which indicates that the UPR is somehow beneficial for the bacteria. Depletion of either ATF6 or PERK did not influence *B. abortus* replication, which suggests that the role of IRE1 may be non-canonical [217]. Infection of mouse macrophages in vitro and in vivo leads to ER stress and the activation of all three UPR pathways. This effect was also observed in case of a VirB-deficient mutant, suggesting that it is induced independently of the replicative-niche formation [216].

The final stages of *Brucella* intracellular lifestyle are poorly understood. One study made a connection between cell-to-cell spread and the activity of autophagy initiation factors [218]. Proteins ULK1, Beclin1, ATG14L and PI3K were shown to play a role in the process. Interestingly, proteins involved in later autophagy stages were not indicated. This suggests that the cycle is completed by a process that may represent non-canonical autophagy.

1.3. Correlative focused ion beam scanning electron microscopy (FIB/SEM)

Electron microscopy has been used for exploring subcellular structures for over half a century. The main method of choice has traditionally been imaging of thin slices of resin embedded samples with transmission electron microscopy (TEM). The thickness of the sample in this approach is usually kept below 100 nm.

The development of three-dimensional (3D) approaches allowed increasing sample thickness. Electron tomography (ET) can resolve sections up to 500 nm. The sample is imaged at many different angles and the images are later used to compute a model of the sample [219, 220]. Despite the possibility of resolving 3D structures, the sample thickness limit for TEM-based methods still remains low. Even flat cell monolayers are usually several micrometers thick, which makes them impossible to resolve. One of the solutions to this problem has been the development of imaging techniques where consecutive serial sections are imaged using TEM [221, 222] or scanning electron microscopy (SEM) [223]. These techniques require complex sample handling and image manipulation.

The introduction of block face scanning electron microscopy has largely improved the speed and reliability of acquiring image series of thick samples [224-226]. The method uses a scanning electron beam to image the surface of the sample block. Each acquisition is followed by the removal of a thin layer of the sample's face. This is achieved either by a built-in ultramicrotome [224] (serial block face scanning electron microscopy, SBEM) or milling with a focused beam of gallium ions (FIB/SEM) [226]. Several rounds of imaging and sample removal result in an image stack that represents the 3D structure of the sample.

Both block face approaches have different advantages and limitations. SBEM allows imaging of large volumes (up to 6,000,000 μm^3), but the voxel size does not go below 16.5 nm × 16.5 nm × 25 nm. In case of FIB/SEM the achievable resolution is higher due to both decreased voxel size (as low as 4 nm × 4 nm × 4nm) and improved precision of the ion beam. However, the sample size is limited to around 10,000 μm^3 [225]. This results in SBEM being usually applied in studies that require an overview of entire tissue fragments, such as imaging of entire neuron networks in brain fragments [227]. FIB/SEM, on the other hand, has been successfully used to reveal subcellular structures of smaller fragments with greater detail [228-230].

The most commonly used approach of sample preparation for block face microscopy involves infusion with a number of heavy metal compounds. These include osmium tetroxide, uranyl acetate and lead aspartate [231]. Compared to traditional TEM approaches, the treatment provides increased contrast and also improves the conductivity of the sample, which prevents excessive charging [232].

Block face methods have been successfully combined with different microscopy approaches, notably fluorescence microscopy. This allows targeting of specific cell types, structures or events within the sample. The labeling can be achieved either by antibody staining or expression of fluorescently tagged proteins [233, 234].

References

1. Bonifacino JS, Glick BS. The mechanisms of vesicle budding and fusion. Cell. 2004;116(2):153-66. PubMed PMID: 14744428.
2. Barlowe C. COPII: a membrane coat that forms endoplasmic reticulum-derived vesicles. FEBS Lett. 1995;369(1):93-6. PubMed PMID: 7641893.
3. Oka T, Nakano A. Inhibition of GTP hydrolysis by Sar1p causes accumulation of vesicles that are a functional intermediate of the ER-to-Golgi transport in yeast. J Cell Biol. 1994;124(4):425-34. PubMed PMID: 8106544; PubMed Central PMCID: PMC2119918.
4. Sutton RB, Fasshauer D, Jahn R, Brunger AT. Crystal structure of a SNARE complex involved in synaptic exocytosis at 2.4 A resolution. Nature. 1998;395(6700):347-53. doi: 10.1038/26412. PubMed PMID: 9759724.
5. Deborde S, Perret E, Gravotta D, Deora A, Salvarezza S, Schreiner R, et al. Clathrin is a key regulator of basolateral polarity. Nature. 2008;452(7188):719-23. doi: 10.1038/nature06828. PubMed PMID: 18401403; PubMed Central PMCID: PMC4078870.
6. Sanders SL, Whitfield KM, Vogel JP, Rose MD, Schekman RW. Sec61p and BiP directly facilitate polypeptide translocation into the ER. Cell. 1992;69(2):353-65. PubMed PMID: 1568250.
7. Bannykh SI, Rowe T, Balch WE. The organization of endoplasmic reticulum export complexes. J Cell Biol. 1996;135(1):19-35. PubMed PMID: 8858160; PubMed Central PMCID: PMC2121027.
8. Miller EA, Barlowe C. Regulation of coat assembly--sorting things out at the ER. Curr Opin Cell Biol. 2010;22(4):447-53. doi: 10.1016/j.ceb.2010.04.003. PubMed PMID: 20439155; PubMed Central PMCID: PMC2910129.
9. Brandizzi F, Barlowe C. Organization of the ER-Golgi interface for membrane traffic control. Nat Rev Mol Cell Biol. 2013;14(6):382-92. doi: 10.1038/nrm3588. PubMed PMID: 23698585; PubMed Central PMCID: PMC4064004.
10. Schweizer A, Fransen JA, Matter K, Kreis TE, Ginsel L, Hauri HP. Identification of an intermediate compartment involved in protein transport from endoplasmic reticulum to Golgi apparatus. Eur J Cell Biol. 1990;53(2):185-96. PubMed PMID: 1964413.
11. Spang A. On vesicle formation and tethering in the ER-Golgi shuttle. Curr Opin Cell Biol. 2009;21(4):531-6. doi: 10.1016/j.ceb.2009.03.003. PubMed PMID: 19394211.
12. Moyer BD, Allan BB, Balch WE. Rab1 interaction with a GM130 effector complex regulates COPII vesicle cis--Golgi tethering. Traffic. 2001;2(4):268-76. PubMed PMID: 11285137.

13. Rowe T, Dascher C, Bannykh S, Plutner H, Balch WE. Role of vesicle-associated syntaxin 5 in the assembly of pre-Golgi intermediates. Science. 1998;279(5351):696-700. PubMed PMID: 9445473.
14. Shorter J, Beard MB, Seemann J, Dirac-Svejstrup AB, Warren G. Sequential tethering of Golgins and catalysis of SNAREpin assembly by the vesicle-tethering protein p115. J Cell Biol. 2002;157(1):45-62. doi: 10.1083/jcb.200112127. PubMed PMID: 11927603; PubMed Central PMCID: PMC2173270.
15. Hay JC, Chao DS, Kuo CS, Scheller RH. Protein interactions regulating vesicle transport between the endoplasmic reticulum and Golgi apparatus in mammalian cells. Cell. 1997;89(1):149-58. PubMed PMID: 9094723.
16. De Matteis MA, Rega LR. Endoplasmic reticulum-Golgi complex membrane contact sites. Curr Opin Cell Biol. 2015;35:43-50. doi: 10.1016/j.ceb.2015.04.001. PubMed PMID: 25950841.
17. Hara-Kuge S, Kuge O, Orci L, Amherdt M, Ravazzola M, Wieland FT, et al. En bloc incorporation of coatomer subunits during the assembly of COP-coated vesicles. J Cell Biol. 1994;124(6):883-92. PubMed PMID: 8132710; PubMed Central PMCID: PMC2119964.
18. Cosson P, Letourneur F. Coatomer interaction with di-lysine endoplasmic reticulum retention motifs. Science. 1994;263(5153):1629-31. PubMed PMID: 8128252.
19. Bleil JD, Bretscher MS. Transferrin receptor and its recycling in HeLa cells. EMBO J. 1982;1(3):351-5. PubMed PMID: 6325161; PubMed Central PMCID: PMC553048.
20. Galvez T, Gilleron J, Zerial M, O'Sullivan GA. SnapShot: Mammalian Rab proteins in endocytic trafficking. Cell. 2012;151(1):234- e2. doi: 10.1016/j.cell.2012.09.013. PubMed PMID: 23021225.
21. Wassmer T, Attar N, Harterink M, van Weering JR, Traer CJ, Oakley J, et al. The retromer coat complex coordinates endosomal sorting and dynein-mediated transport, with carrier recognition by the trans-Golgi network. Dev Cell. 2009;17(1):110-22. doi: 10.1016/j.devcel.2009.04.016. PubMed PMID: 19619496; PubMed Central PMCID: PMC2714578.
22. Nothwehr SF, Ha SA, Bruinsma P. Sorting of yeast membrane proteins into an endosome-to-Golgi pathway involves direct interaction of their cytosolic domains with Vps35p. J Cell Biol. 2000;151(2):297-310. PubMed PMID: 11038177; PubMed Central PMCID: PMC2192648.
23. Arighi CN, Hartnell LM, Aguilar RC, Haft CR, Bonifacino JS. Role of the mammalian retromer in sorting of the cation-independent mannose 6-phosphate receptor. J Cell Biol. 2004;165(1):123-33. doi: 10.1083/jcb.200312055. PubMed PMID: 15078903; PubMed Central PMCID: PMC2172094.
24. Pearse BM. Clathrin: a unique protein associated with intracellular transfer of membrane by coated vesicles. Proc Natl Acad Sci U S A. 1976;73(4):1255-9. PubMed PMID: 1063406; PubMed Central PMCID: PMC430241.
25. Kosaka T, Ikeda K. Reversible blockage of membrane retrieval and endocytosis in the garland cell of the temperature-sensitive mutant of *Drosophila melanogaster*, shibirets1. J Cell Biol. 1983;97(2):499-507. PubMed PMID: 6411734; PubMed Central PMCID: PMC2112522.
26. Hopkins CR, Miller K, Beardmore JM. Receptor-mediated endocytosis of transferrin and epidermal growth factor receptors: a comparison of constitutive and ligand-induced uptake. J Cell Sci Suppl. 1985;3:173-86. PubMed PMID: 3011821.
27. Maxfield FR, Schlessinger J, Shechter Y, Pastan I, Willingham MC. Collection of insulin, EGF and alpha2-macroglobulin in the same patches on the surface of cultured fibroblasts and common internalization. Cell. 1978;14(4):805-10. PubMed PMID: 80283.
28. Di Guglielmo GM, Le Roy C, Goodfellow AF, Wrana JL. Distinct endocytic pathways regulate TGF-beta receptor signalling and turnover. Nat Cell Biol. 2003;5(5):410-21. doi: 10.1038/ncb975. PubMed PMID: 12717440.

29. Clague MJ, Thorpe C, Jones AT. Phosphatidylinositol 3-kinase regulation of fluid phase endocytosis. FEBS Lett. 1995;367(3):272-4. PubMed PMID: 7607321.
30. Sabharanjak S, Sharma P, Parton RG, Mayor S. GPI-anchored proteins are delivered to recycling endosomes via a distinct cdc42-regulated, clathrin-independent pinocytic pathway. Dev Cell. 2002;2(4):411-23. PubMed PMID: 11970892.
31. Parton RG, Simons K. The multiple faces of caveolae. Nat Rev Mol Cell Biol. 2007;8(3):185-94. doi: 10.1038/nrm2122. PubMed PMID: 17318224.
32. Drab M, Verkade P, Elger M, Kasper M, Lohn M, Lauterbach B, et al. Loss of caveolae, vascular dysfunction, and pulmonary defects in caveolin-1 gene-disrupted mice. Science. 2001;293(5539):2449-52. doi: 10.1126/science.1062688. PubMed PMID: 11498544.
33. Walser PJ, Ariotti N, Howes M, Ferguson C, Webb R, Schwudke D, et al. Constitutive formation of caveolae in a bacterium. Cell. 2012;150(4):752-63. doi: 10.1016/j.cell.2012.06.042. PubMed PMID: 22901807.
34. Hill MM, Bastiani M, Luetterforst R, Kirkham M, Kirkham A, Nixon SJ, et al. PTRF-Cavin, a conserved cytoplasmic protein required for caveola formation and function. Cell. 2008;132(1):113-24. doi: 10.1016/j.cell.2007.11.042. PubMed PMID: 18191225; PubMed Central PMCID: PMC2265257.
35. Henley JR, Krueger EW, Oswald BJ, McNiven MA. Dynamin-mediated internalization of caveolae. J Cell Biol. 1998;141(1):85-99. PubMed PMID: 9531550; PubMed Central PMCID: PMC2132718.
36. Hoppe AD, Swanson JA. Cdc42, Rac1, and Rac2 display distinct patterns of activation during phagocytosis. Mol Biol Cell. 2004;15(8):3509-19. doi: 10.1091/mbc.E03-11-0847. PubMed PMID: 15169870; PubMed Central PMCID: PMC491814.
37. Levin R, Grinstein S, Schlam D. Phosphoinositides in phagocytosis and macropinocytosis. Biochim Biophys Acta. 2015;1851(6):805-23. doi: 10.1016/j.bbalip.2014.09.005. PubMed PMID: 25238964.
38. Mayor S, Pagano RE. Pathways of clathrin-independent endocytosis. Nat Rev Mol Cell Biol. 2007;8(8):603-12. doi: 10.1038/nrm2216. PubMed PMID: 17609668.
39. Rink J, Ghigo E, Kalaidzidis Y, Zerial M. Rab conversion as a mechanism of progression from early to late endosomes. Cell. 2005;122(5):735-49. doi: 10.1016/j.cell.2005.06.043. PubMed PMID: 16143105.
40. Poteryaev D, Datta S, Ackema K, Zerial M, Spang A. Identification of the switch in early-to-late endosome transition. Cell. 2010;141(3):497-508. doi: 10.1016/j.cell.2010.03.011. PubMed PMID: 20434987.
41. Huotari J, Helenius A. Endosome maturation. EMBO J. 2011;30(17):3481-500. doi: 10.1038/emboj.2011.286. PubMed PMID: 21878991; PubMed Central PMCID: PMC3181477.
42. Hurley JH, Stenmark H. Molecular mechanisms of ubiquitin-dependent membrane traffic. Annu Rev Biophys. 2011;40:119-42. doi: 10.1146/annurev-biophys-042910-155404. PubMed PMID: 21332354; PubMed Central PMCID: PMC3272705.
43. Henne WM, Buchkovich NJ, Emr SD. The ESCRT pathway. Dev Cell. 2011;21(1):77-91. doi: 10.1016/j.devcel.2011.05.015. PubMed PMID: 21763610.
44. Marshansky V, Futai M. The V-type H+-ATPase in vesicular trafficking: targeting, regulation and function. Curr Opin Cell Biol. 2008;20(4):415-26. doi: 10.1016/j.ceb.2008.03.015. PubMed PMID: 18511251.
45. Lin S, Sun S, Hu J. Molecular basis for sculpting the endoplasmic reticulum membrane. Int J Biochem Cell Biol. 2012;44(9):1436-43. doi: 10.1016/j.biocel.2012.05.013. PubMed PMID: 22640864.
46. Lynes EM, Simmen T. Urban planning of the endoplasmic reticulum (ER): how diverse mechanisms segregate the many functions of the ER. Biochim Biophys Acta. 2011;1813(10):1893-905. doi: 10.1016/j.bbamcr.2011.06.011. PubMed PMID: 21756943.

47. Baumann O, Walz B. Endoplasmic reticulum of animal cells and its organization into structural and functional domains. Int Rev Cytol. 2001;205:149-214. PubMed PMID: 11336391.
48. Shibata Y, Hu J, Kozlov MM, Rapoport TA. Mechanisms shaping the membranes of cellular organelles. Annu Rev Cell Dev Biol. 2009;25:329-54. doi: 10.1146/annurev.cellbio.042308.113324. PubMed PMID: 19575675.
49. Voeltz GK, Ongkasuwan J, Standart N, Steitz JA. A novel embryonic poly(A) binding protein, ePAB, regulates mRNA deadenylation in Xenopus egg extracts. Genes Dev. 2001;15(6):774-88. doi: 10.1101/gad.872201. PubMed PMID: 11274061; PubMed Central PMCID: PMC312653.
50. Park SH, Blackstone C. Further assembly required: construction and dynamics of the endoplasmic reticulum network. EMBO Rep. 2010;11(7):515-21. doi: 10.1038/embor.2010.92. PubMed PMID: 20559323; PubMed Central PMCID: PMC2897125.
51. Walters AD, Bommakanti A, Cohen-Fix O. Shaping the nucleus: factors and forces. J Cell Biochem. 2012;113(9):2813-21. doi: 10.1002/jcb.24178. PubMed PMID: 22566057; PubMed Central PMCID: PMC3471212.
52. English AR, Voeltz GK. Endoplasmic reticulum structure and interconnections with other organelles. Cold Spring Harb Perspect Biol. 2013;5(4):a013227. doi: 10.1101/cshperspect.a013227. PubMed PMID: 23545422; PubMed Central PMCID: PMC3683900.
53. de Brito OM, Scorrano L. An intimate liaison: spatial organization of the endoplasmic reticulum-mitochondria relationship. EMBO J. 2010;29(16):2715-23. doi: 10.1038/emboj.2010.177. PubMed PMID: 20717141; PubMed Central PMCID: PMC2924651.
54. Manford AG, Stefan CJ, Yuan HL, Macgurn JA, Emr SD. ER-to-plasma membrane tethering proteins regulate cell signaling and ER morphology. Dev Cell. 2012;23(6):1129-40. doi: 10.1016/j.devcel.2012.11.004. PubMed PMID: 23237950.
55. Rowland AA, Voeltz GK. Endoplasmic reticulum-mitochondria contacts: function of the junction. Nat Rev Mol Cell Biol. 2012;13(10):607-25. doi: 10.1038/nrm3440. PubMed PMID: 22992592; PubMed Central PMCID: PMC5111635.
56. Prinz WA, Grzyb L, Veenhuis M, Kahana JA, Silver PA, Rapoport TA. Mutants affecting the structure of the cortical endoplasmic reticulum in Saccharomyces cerevisiae. J Cell Biol. 2000;150(3):461-74. PubMed PMID: 10931860; PubMed Central PMCID: PMC2175198.
57. Puhka M, Joensuu M, Vihinen H, Belevich I, Jokitalo E. Progressive sheet-to-tubule transformation is a general mechanism for endoplasmic reticulum partitioning in dividing mammalian cells. Mol Biol Cell. 2012;23(13):2424-32. doi: 10.1091/mbc.E10-12-0950. PubMed PMID: 22573885; PubMed Central PMCID: PMC3386207.
58. English AR, Voeltz GK. Rab10 GTPase regulates ER dynamics and morphology. Nat Cell Biol. 2013;15(2):169-78. doi: 10.1038/ncb2647. PubMed PMID: 23263280; PubMed Central PMCID: PMC3582403.
59. Goyal U, Blackstone C. Untangling the web: mechanisms underlying ER network formation. Biochim Biophys Acta. 2013;1833(11):2492-8. doi: 10.1016/j.bbamcr.2013.04.009. PubMed PMID: 23602970; PubMed Central PMCID: PMC3729797.
60. Zimmerberg J, Kozlov MM. How proteins produce cellular membrane curvature. Nat Rev Mol Cell Biol. 2006;7(1):9-19. doi: 10.1038/nrm1784. PubMed PMID: 16365634.
61. Dannhauser PN, Ungewickell EJ. Reconstitution of clathrin-coated bud and vesicle formation with minimal components. Nat Cell Biol. 2012;14(6):634-9. doi: 10.1038/ncb2478. PubMed PMID: 22522172.
62. Stachowiak JC, Schmid EM, Ryan CJ, Ann HS, Sasaki DY, Sherman MB, et al. Membrane bending by protein-protein crowding. Nat Cell Biol. 2012;14(9):944-9. doi: 10.1038/ncb2561. PubMed PMID: 22902598.

63. Waterman-Storer CM, Salmon ED. Endoplasmic reticulum membrane tubules are distributed by microtubules in living cells using three distinct mechanisms. Curr Biol. 1998;8(14):798-806. PubMed PMID: 9663388.
64. Grigoriev I, Gouveia SM, van der Vaart B, Demmers J, Smyth JT, Honnappa S, et al. STIM1 is a MT-plus-end-tracking protein involved in remodeling of the ER. Curr Biol. 2008;18(3):177-82. doi: 10.1016/j.cub.2007.12.050. PubMed PMID: 18249114; PubMed Central PMCID: PMC2600655.
65. Voeltz GK, Prinz WA, Shibata Y, Rist JM, Rapoport TA. A class of membrane proteins shaping the tubular endoplasmic reticulum. Cell. 2006;124(3):573-86. doi: 10.1016/j.cell.2005.11.047. PubMed PMID: 16469703.
66. Sparkes I, Tolley N, Aller I, Svozil J, Osterrieder A, Botchway S, et al. Five *Arabidopsis* reticulon isoforms share endoplasmic reticulum location, topology, and membrane-shaping properties. Plant Cell. 2010;22(4):1333-43. doi: 10.1105/tpc.110.074385. PubMed PMID: 20424177; PubMed Central PMCID: PMC2879755.
67. Tolley N, Sparkes I, Craddock CP, Eastmond PJ, Runions J, Hawes C, et al. Transmembrane domain length is responsible for the ability of a plant reticulon to shape endoplasmic reticulum tubules in vivo. Plant J. 2010;64(3):411-8. doi: 10.1111/j.1365-313X.2010.04337.x. PubMed PMID: 20969742.
68. Ronchi P, Colombo S, Francolini M, Borgese N. Transmembrane domain-dependent partitioning of membrane proteins within the endoplasmic reticulum. J Cell Biol. 2008;181(1):105-18. doi: 10.1083/jcb.200710093. PubMed PMID: 18391072; PubMed Central PMCID: PMC2287291.
69. Tolley N, Sparkes IA, Hunter PR, Craddock CP, Nuttall J, Roberts LM, et al. Overexpression of a plant reticulon remodels the lumen of the cortical endoplasmic reticulum but does not perturb protein transport. Traffic. 2008;9(1):94-102. doi: 10.1111/j.1600-0854.2007.00670.x. PubMed PMID: 17980018.
70. Anderson DJ, Hetzer MW. Reshaping of the endoplasmic reticulum limits the rate for nuclear envelope formation. J Cell Biol. 2008;182(5):911-24. doi: 10.1083/jcb.200805140. PubMed PMID: 18779370; PubMed Central PMCID: PMC2528577.
71. Hu J, Shibata Y, Voss C, Shemesh T, Li Z, Coughlin M, et al. Membrane proteins of the endoplasmic reticulum induce high-curvature tubules. Science. 2008;319(5867):1247-50. doi: 10.1126/science.1153634. PubMed PMID: 18309084.
72. Shibata Y, Shemesh T, Prinz WA, Palazzo AF, Kozlov MM, Rapoport TA. Mechanisms determining the morphology of the peripheral ER. Cell. 2010;143(5):774-88. doi: 10.1016/j.cell.2010.11.007. PubMed PMID: 21111237; PubMed Central PMCID: PMC3008339.
73. Klopfenstein DR, Klumperman J, Lustig A, Kammerer RA, Oorschot V, Hauri HP. Subdomain-specific localization of CLIMP-63 (p63) in the endoplasmic reticulum is mediated by its luminal alpha-helical segment. J Cell Biol. 2001;153(6):1287-300. PubMed PMID: 11402071; PubMed Central PMCID: PMC2192027.
74. Raices M, D'Angelo MA. Nuclear pore complex composition: a new regulator of tissue-specific and developmental functions. Nat Rev Mol Cell Biol. 2012;13(11):687-99. doi: 10.1038/nrm3461. PubMed PMID: 23090414.
75. Sosa BA, Rothballer A, Kutay U, Schwartz TU. LINC complexes form by binding of three KASH peptides to domain interfaces of trimeric SUN proteins. Cell. 2012;149(5):1035-47. doi: 10.1016/j.cell.2012.03.046. PubMed PMID: 22632968; PubMed Central PMCID: PMC3383001.
76. Sosa BA, Kutay U, Schwartz TU. Structural insights into LINC complexes. Curr Opin Struct Biol. 2013;23(2):285-91. doi: 10.1016/j.sbi.2013.03.005. PubMed PMID: 23597672; PubMed Central PMCID: PMC4077334.
77. Zhu PP, Patterson A, Lavoie B, Stadler J, Shoeb M, Patel R, et al. Cellular localization, oligomerization, and membrane association of the hereditary spastic paraplegia 3A

(SPG3A) protein atlastin. J Biol Chem. 2003;278(49):49063-71. doi: 10.1074/jbc.M306702200. PubMed PMID: 14506257.
78. Zhu PP, Soderblom C, Tao-Cheng JH, Stadler J, Blackstone C. SPG3A protein atlastin-1 is enriched in growth cones and promotes axon elongation during neuronal development. Hum Mol Genet. 2006;15(8):1343-53. doi: 10.1093/hmg/ddl054. PubMed PMID: 16537571.
79. Rismanchi N, Soderblom C, Stadler J, Zhu PP, Blackstone C. Atlastin GTPases are required for Golgi apparatus and ER morphogenesis. Hum Mol Genet. 2008;17(11):1591-604. doi: 10.1093/hmg/ddn046. PubMed PMID: 18270207; PubMed Central PMCID: PMC2902292.
80. Hu J, Shibata Y, Zhu PP, Voss C, Rismanchi N, Prinz WA, et al. A class of dynamin-like GTPases involved in the generation of the tubular ER network. Cell. 2009;138(3):549-61. doi: 10.1016/j.cell.2009.05.025. PubMed PMID: 19665976; PubMed Central PMCID: PMC2746359.
81. Orso G, Pendin D, Liu S, Tosetto J, Moss TJ, Faust JE, et al. Homotypic fusion of ER membranes requires the dynamin-like GTPase atlastin. Nature. 2009;460(7258):978-83. doi: 10.1038/nature08280. PubMed PMID: 19633650.
82. Lee H, Sparkes I, Gattolin S, Dzimitrowicz N, Roberts LM, Hawes C, et al. An Arabidopsis reticulon and the atlastin homologue RHD3-like2 act together in shaping the tubular endoplasmic reticulum. New Phytol. 2013;197(2):481-9. doi: 10.1111/nph.12038. PubMed PMID: 23163512.
83. Anwar K, Klemm RW, Condon A, Severin KN, Zhang M, Ghirlando R, et al. The dynamin-like GTPase Sey1p mediates homotypic ER fusion in S. cerevisiae. J Cell Biol. 2012;197(2):209-17. doi: 10.1083/jcb.201111115. PubMed PMID: 22508509; PubMed Central PMCID: PMC3328390.
84. Moss TJ, Andreazza C, Verma A, Daga A, McNew JA. Membrane fusion by the GTPase atlastin requires a conserved C-terminal cytoplasmic tail and dimerization through the middle domain. Proc Natl Acad Sci U S A. 2011;108(27):11133-8. doi: 10.1073/pnas.1105056108. PubMed PMID: 21690399; PubMed Central PMCID: PMC3131361.
85. Liu TY, Bian X, Sun S, Hu X, Klemm RW, Prinz WA, et al. Lipid interaction of the C terminus and association of the transmembrane segments facilitate atlastin-mediated homotypic endoplasmic reticulum fusion. Proc Natl Acad Sci U S A. 2012;109(32):E2146-54. doi: 10.1073/pnas.1208385109. PubMed PMID: 22802620; PubMed Central PMCID: PMC3420179.
86. Byrnes LJ, Singh A, Szeto K, Benvin NM, O'Donnell JP, Zipfel WR, et al. Structural basis for conformational switching and GTP loading of the large G protein atlastin. EMBO J. 2013;32(3):369-84. doi: 10.1038/emboj.2012.353. PubMed PMID: 23334294; PubMed Central PMCID: PMC3567502.
87. Terasaki M, Chen LB, Fujiwara K. Microtubules and the endoplasmic reticulum are highly interdependent structures. J Cell Biol. 1986;103(4):1557-68. PubMed PMID: 3533956; PubMed Central PMCID: PMC2114338.
88. Evans K, Keller C, Pavur K, Glasgow K, Conn B, Lauring B. Interaction of two hereditary spastic paraplegia gene products, spastin and atlastin, suggests a common pathway for axonal maintenance. Proc Natl Acad Sci U S A. 2006;103(28):10666-71. doi: 10.1073/pnas.0510863103. PubMed PMID: 16815977; PubMed Central PMCID: PMC1502289.
89. Sanderson CM, Connell JW, Edwards TL, Bright NA, Duley S, Thompson A, et al. Spastin and atlastin, two proteins mutated in autosomal-dominant hereditary spastic paraplegia, are binding partners. Hum Mol Genet. 2006;15(2):307-18. doi: 10.1093/hmg/ddi447. PubMed PMID: 16339213; PubMed Central PMCID: PMC2443951.
90. Park SH, Zhu PP, Parker RL, Blackstone C. Hereditary spastic paraplegia proteins REEP1, spastin, and atlastin-1 coordinate microtubule interactions with the tubular ER

network. J Clin Invest. 2010;120(4):1097-110. doi: 10.1172/JCI40979. PubMed PMID: 20200447; PubMed Central PMCID: PMC2846052.
91. Klopfenstein DR, Kappeler F, Hauri HP. A novel direct interaction of endoplasmic reticulum with microtubules. EMBO J. 1998;17(21):6168-77. doi: 10.1093/emboj/17.21.6168. PubMed PMID: 9799226; PubMed Central PMCID: PMC1170943.
92. Schroder M, Kaufman RJ. The mammalian unfolded protein response. Annu Rev Biochem. 2005;74:739-89. doi: 10.1146/annurev.biochem.73.011303.074134. PubMed PMID: 15952902.
93. Celli J, Tsolis RM. Bacteria, the endoplasmic reticulum and the unfolded protein response: friends or foes? Nat Rev Microbiol. 2015;13(2):71-82. doi: 10.1038/nrmicro3393. PubMed PMID: 25534809; PubMed Central PMCID: PMC4447104.
94. Walter P, Ron D. The unfolded protein response: from stress pathway to homeostatic regulation. Science. 2011;334(6059):1081-6. doi: 10.1126/science.1209038. PubMed PMID: 22116877.
95. Cho JA, Lee AH, Platzer B, Cross BC, Gardner BM, De Luca H, et al. The unfolded protein response element IRE1alpha senses bacterial proteins invading the ER to activate RIG-I and innate immune signaling. Cell Host Microbe. 2013;13(5):558-69. doi: 10.1016/j.chom.2013.03.011. PubMed PMID: 23684307; PubMed Central PMCID: PMC3766372.
96. Zhang K, Kaufman RJ. From endoplasmic-reticulum stress to the inflammatory response. Nature. 2008;454(7203):455-62. doi: 10.1038/nature07203. PubMed PMID: 18650916; PubMed Central PMCID: PMC2727659.
97. Gardner BM, Walter P. Unfolded proteins are Ire1-activating ligands that directly induce the unfolded protein response. Science. 2011;333(6051):1891-4. doi: 10.1126/science.1209126. PubMed PMID: 21852455; PubMed Central PMCID: PMC3202989.
98. Pincus D, Chevalier MW, Aragon T, van Anken E, Vidal SE, El-Samad H, et al. BiP binding to the ER-stress sensor Ire1 tunes the homeostatic behavior of the unfolded protein response. PLoS Biol. 2010;8(7):e1000415. doi: 10.1371/journal.pbio.1000415. PubMed PMID: 20625545; PubMed Central PMCID: PMC2897766.
99. Olzmann JA, Kopito RR, Christianson JC. The mammalian endoplasmic reticulum-associated degradation system. Cold Spring Harb Perspect Biol. 2013;5(9). doi: 10.1101/cshperspect.a013185. PubMed PMID: 23232094; PubMed Central PMCID: PMC3753711.
100. Bernales S, McDonald KL, Walter P. Autophagy counterbalances endoplasmic reticulum expansion during the unfolded protein response. PLoS Biol. 2006;4(12):e423. doi: 10.1371/journal.pbio.0040423. PubMed PMID: 17132049; PubMed Central PMCID: PMC1661684.
101. Bommiasamy H, Back SH, Fagone P, Lee K, Meshinchi S, Vink E, et al. ATF6alpha induces XBP1-independent expansion of the endoplasmic reticulum. J Cell Sci. 2009;122(Pt 10):1626-36. doi: 10.1242/jcs.045625. PubMed PMID: 19420237; PubMed Central PMCID: PMC2680102.
102. Schuck S, Prinz WA, Thorn KS, Voss C, Walter P. Membrane expansion alleviates endoplasmic reticulum stress independently of the unfolded protein response. J Cell Biol. 2009;187(4):525-36. doi: 10.1083/jcb.200907074. PubMed PMID: 19948500; PubMed Central PMCID: PMC2779237.
103. Savina A, Amigorena S. Phagocytosis and antigen presentation in dendritic cells. Immunol Rev. 2007;219:143-56. doi: 10.1111/j.1600-065X.2007.00552.x. PubMed PMID: 17850487.
104. Byndloss MX, Rivera-Chavez F, Tsolis RM, Baumler AJ. How bacterial pathogens use type III and type IV secretion systems to facilitate their transmission. Curr Opin Microbiol. 2017;35:1-7. doi: 10.1016/j.mib.2016.08.007. PubMed PMID: 27621139.

105. Stradal TE, Costa SC. Type III Secreted Virulence Factors Manipulating Signaling to Actin Dynamics. Curr Top Microbiol Immunol. 2017;399:175-99. doi: 10.1007/82_2016_35. PubMed PMID: 27744505.
106. Alvarez-Martinez CE, Christie PJ. Biological diversity of prokaryotic type IV secretion systems. Microbiol Mol Biol Rev. 2009;73(4):775-808. doi: 10.1128/MMBR.00023-09. PubMed PMID: 19946141; PubMed Central PMCID: PMC2786583.
107. McMahon HT, Boucrot E. Molecular mechanism and physiological functions of clathrin-mediated endocytosis. Nat Rev Mol Cell Biol. 2011;12(8):517-33. doi: 10.1038/nrm3151. PubMed PMID: 21779028.
108. Mengaud J, Ohayon H, Gounon P, Mege RM, Cossart P. E-cadherin is the receptor for internalin, a surface protein required for entry of *L. monocytogenes* into epithelial cells. Cell. 1996;84(6):923-32. PubMed PMID: 8601315.
109. Shen Y, Naujokas M, Park M, Ireton K. InIB-dependent internalization of *Listeria* is mediated by the Met receptor tyrosine kinase. Cell. 2000;103(3):501-10. PubMed PMID: 11081636.
110. Cossart P, Pizarro-Cerda J, Lecuit M. Invasion of mammalian cells by Listeria monocytogenes: functional mimicry to subvert cellular functions. Trends Cell Biol. 2003;13(1):23-31. PubMed PMID: 12480337.
111. Cossart P, Helenius A. Endocytosis of viruses and bacteria. Cold Spring Harb Perspect Biol. 2014;6(8). doi: 10.1101/cshperspect.a016972. PubMed PMID: 25085912; PubMed Central PMCID: PMC4107984.
112. Harburger DS, Calderwood DA. Integrin signalling at a glance. J Cell Sci. 2009;122(Pt 2):159-63. doi: 10.1242/jcs.018093. PubMed PMID: 19118207; PubMed Central PMCID: PMC2714413.
113. Isberg RR, Hamburger Z, Dersch P. Signaling and invasin-promoted uptake via integrin receptors. Microbes Infect. 2000;2(7):793-801. PubMed PMID: 10955960.
114. Hardt WD, Chen LM, Schuebel KE, Bustelo XR, Galan JE. *S. typhimurium* encodes an activator of Rho GTPases that induces membrane ruffling and nuclear responses in host cells. Cell. 1998;93(5):815-26. PubMed PMID: 9630225.
115. Hayward RD, Koronakis V. Direct nucleation and bundling of actin by the SipC protein of invasive *Salmonella*. EMBO J. 1999;18(18):4926-34. doi: 10.1093/emboj/18.18.4926. PubMed PMID: 10487745; PubMed Central PMCID: PMC1171564.
116. McGhie EJ, Hayward RD, Koronakis V. Control of actin turnover by a *Salmonella* invasion protein. Mol Cell. 2004;13(4):497-510. PubMed PMID: 14992720.
117. Dehio C. Molecular and cellular basis of *Bartonella* pathogenesis. Annu Rev Microbiol. 2004;58:365-90. doi: 10.1146/annurev.micro.58.030603.123700. PubMed PMID: 15487942.
118. Dehio C, Meyer M, Berger J, Schwarz H, Lanz C. Interaction of *Bartonella henselae* with endothelial cells results in bacterial aggregation on the cell surface and the subsequent engulfment and internalisation of the bacterial aggregate by a unique structure, the invasome. J Cell Sci. 1997;110 (Pt 18):2141-54. PubMed PMID: 9378764.
119. Rhomberg TA, Truttmann MC, Guye P, Ellner Y, Dehio C. A translocated protein of *Bartonella henselae* interferes with endocytic uptake of individual bacteria and triggers uptake of large bacterial aggregates via the invasome. Cell Microbiol. 2009;11(6):927-45. doi: 10.1111/j.1462-5822.2009.01302.x. PubMed PMID: 19302579.
120. Truttmann MC, Rhomberg TA, Dehio C. Combined action of the type IV secretion effector proteins BepC and BepF promotes invasome formation of *Bartonella henselae* on endothelial and epithelial cells. Cell Microbiol. 2011;13(2):284-99. doi: 10.1111/j.1462-5822.2010.01535.x. PubMed PMID: 20964799.
121. Fredlund J, Enninga J. Cytoplasmic access by intracellular bacterial pathogens. Trends Microbiol. 2014;22(3):128-37. doi: 10.1016/j.tim.2014.01.003. PubMed PMID: 24530174.

122. Vergne I, Chua J, Lee HH, Lucas M, Belisle J, Deretic V. Mechanism of phagolysosome biogenesis block by viable *Mycobacterium tuberculosis*. Proc Natl Acad Sci U S A. 2005;102(11):4033-8. doi: 10.1073/pnas.0409716102. PubMed PMID: 15753315; PubMed Central PMCID: PMC554822.
123. Bakowski MA, Braun V, Lam GY, Yeung T, Heo WD, Meyer T, et al. The phosphoinositide phosphatase SopB manipulates membrane surface charge and trafficking of the *Salmonella*-containing vacuole. Cell Host Microbe. 2010;7(6):453-62. doi: 10.1016/j.chom.2010.05.011. PubMed PMID: 20542249.
124. Hernandez LD, Hueffer K, Wenk MR, Galan JE. *Salmonella* modulates vesicular traffic by altering phosphoinositide metabolism. Science. 2004;304(5678):1805-7. doi: 10.1126/science.1098188. PubMed PMID: 15205533.
125. Beuzon CR, Meresse S, Unsworth KE, Ruiz-Albert J, Garvis S, Waterman SR, et al. *Salmonella* maintains the integrity of its intracellular vacuole through the action of SifA. EMBO J. 2000;19(13):3235-49. doi: 10.1093/emboj/19.13.3235. PubMed PMID: 10880437; PubMed Central PMCID: PMC313946.
126. Knodler LA, Vallance BA, Celli J, Winfree S, Hansen B, Montero M, et al. Dissemination of invasive *Salmonella* via bacterial-induced extrusion of mucosal epithelia. Proc Natl Acad Sci U S A. 2010;107(41):17733-8. doi: 10.1073/pnas.1006098107. PubMed PMID: 20876119; PubMed Central PMCID: PMC2955089.
127. Boschiroli ML, Ouahrani-Bettache S, Foulongne V, Michaux-Charachon S, Bourg G, Allardet-Servent A, et al. The *Brucella suis* virB operon is induced intracellularly in macrophages. Proc Natl Acad Sci U S A. 2002;99(3):1544-9. doi: 10.1073/pnas.032514299. PubMed PMID: 11830669; PubMed Central PMCID: PMC122227.
128. Celli J, de Chastellier C, Franchini DM, Pizarro-Cerda J, Moreno E, Gorvel JP. *Brucella* evades macrophage killing via VirB-dependent sustained interactions with the endoplasmic reticulum. J Exp Med. 2003;198(4):545-56. doi: 10.1084/jem.20030088. PubMed PMID: 12925673; PubMed Central PMCID: PMC2194179.
129. Hubber A, Roy CR. Modulation of host cell function by *Legionella pneumophila* type IV effectors. Annu Rev Cell Dev Biol. 2010;26:261-83. doi: 10.1146/annurev-cellbio-100109-104034. PubMed PMID: 20929312.
130. Sansonetti PJ, Ryter A, Clerc P, Maurelli AT, Mounier J. Multiplication of *Shigella flexneri* within HeLa cells: lysis of the phagocytic vacuole and plasmid-mediated contact hemolysis. Infect Immun. 1986;51(2):461-9. PubMed PMID: 3510976; PubMed Central PMCID: PMC262354.
131. Myers JT, Tsang AW, Swanson JA. Localized reactive oxygen and nitrogen intermediates inhibit escape of *Listeria monocytogenes* from vacuoles in activated macrophages. J Immunol. 2003;171(10):5447-53. PubMed PMID: 14607950; PubMed Central PMCID: PMC2972186.
132. Portnoy DA, Jacks PS, Hinrichs DJ. Role of hemolysin for the intracellular growth of *Listeria monocytogenes*. J Exp Med. 1988;167(4):1459-71. PubMed PMID: 2833557; PubMed Central PMCID: PMC2188911.
133. Smith GA, Marquis H, Jones S, Johnston NC, Portnoy DA, Goldfine H. The two distinct phospholipases C of *Listeria monocytogenes* have overlapping roles in escape from a vacuole and cell-to-cell spread. Infect Immun. 1995;63(11):4231-7. PubMed PMID: 7591052; PubMed Central PMCID: PMC173601.
134. Shaughnessy LM, Hoppe AD, Christensen KA, Swanson JA. Membrane perforations inhibit lysosome fusion by altering pH and calcium in *Listeria monocytogenes* vacuoles. Cell Microbiol. 2006;8(5):781-92. doi: 10.1111/j.1462-5822.2005.00665.x. PubMed PMID: 16611227; PubMed Central PMCID: PMC1435990.
135. Brodmann M, Dreier RF, Broz P, Basler M. *Francisella* requires dynamic type VI secretion system and ClpB to deliver effectors for phagosomal escape. Nat Commun. 2017;8:15853. doi: 10.1038/ncomms15853. PubMed PMID: 28621333; PubMed Central PMCID: PMC5481754.

136. Barker JR, Chong A, Wehrly TD, Yu JJ, Rodriguez SA, Liu J, et al. The *Francisella tularensis* pathogenicity island encodes a secretion system that is required for phagosome escape and virulence. Mol Microbiol. 2009;74(6):1459-70. PubMed PMID: 20054881; PubMed Central PMCID: PMC2814410.
137. Hale TL, Bonventre PF. *Shigella* infection of Henle intestinal epithelial cells: role of the bacterium. Infect Immun. 1979;24(3):879-86. PubMed PMID: 381204; PubMed Central PMCID: PMC414389.
138. Blocker A, Gounon P, Larquet E, Niebuhr K, Cabiaux V, Parsot C, et al. The tripartite type III secreton of *Shigella flexneri* inserts IpaB and IpaC into host membranes. J Cell Biol. 1999;147(3):683-93. PubMed PMID: 10545510; PubMed Central PMCID: PMC2151192.
139. Senerovic L, Tsunoda SP, Goosmann C, Brinkmann V, Zychlinsky A, Meissner F, et al. Spontaneous formation of IpaB ion channels in host cell membranes reveals how *Shigella* induces pyroptosis in macrophages. Cell Death Dis. 2012;3:e384. doi: 10.1038/cddis.2012.124. PubMed PMID: 22951981; PubMed Central PMCID: PMC3461361.
140. Dickenson NE, Choudhari SP, Adam PR, Kramer RM, Joshi SB, Middaugh CR, et al. Oligomeric states of the *Shigella* translocator protein IpaB provide structural insights into formation of the type III secretion translocon. Protein Sci. 2013;22(5):614-27. doi: 10.1002/pro.2245. PubMed PMID: 23456854; PubMed Central PMCID: PMC3649263.
141. Dupont N, Lacas-Gervais S, Bertout J, Paz I, Freche B, Van Nhieu GT, et al. *Shigella* phagocytic vacuolar membrane remnants participate in the cellular response to pathogen invasion and are regulated by autophagy. Cell Host Microbe. 2009;6(2):137-49. doi: 10.1016/j.chom.2009.07.005. PubMed PMID: 19683680.
142. Ehsani S, Santos JC, Rodrigues CD, Henriques R, Audry L, Zimmer C, et al. Hierarchies of host factor dynamics at the entry site of *Shigella flexneri* during host cell invasion. Infect Immun. 2012;80(7):2548-57. doi: 10.1128/IAI.06391-11. PubMed PMID: 22526677; PubMed Central PMCID: PMC3416480.
143. Stevens JM, Galyov EE, Stevens MP. Actin-dependent movement of bacterial pathogens. Nat Rev Microbiol. 2006;4(2):91-101. doi: 10.1038/nrmicro1320. PubMed PMID: 16415925.
144. Perrin AJ, Jiang X, Birmingham CL, So NS, Brumell JH. Recognition of bacteria in the cytosol of mammalian cells by the ubiquitin system. Curr Biol. 2004;14(9):806-11. doi: 10.1016/j.cub.2004.04.033. PubMed PMID: 15120074.
145. Santos JC, Duchateau M, Fredlund J, Weiner A, Mallet A, Schmitt C, et al. The COPII complex and lysosomal VAMP7 determine intracellular *Salmonella* localization and growth. Cell Microbiol. 2015;17(12):1699-720. doi: 10.1111/cmi.12475. PubMed PMID: 26084942.
146. van der Wel N, Hava D, Houben D, Fluitsma D, van Zon M, Pierson J, et al. *M. tuberculosis* and *M. leprae* translocate from the phagolysosome to the cytosol in myeloid cells. Cell. 2007;129(7):1287-98. doi: 10.1016/j.cell.2007.05.059. PubMed PMID: 17604718.
147. Myrvik QN, Leake ES, Wright MJ. Disruption of phagosomal membranes of normal alveolar macrophages by the H37Rv strain of *Mycobacterium tuberculosis*. A correlate of virulence. Am Rev Respir Dis. 1984;129(2):322-8. PubMed PMID: 6421212.
148. McDonough KA, Kress Y, Bloom BR. Pathogenesis of tuberculosis: interaction of *Mycobacterium tuberculosis* with macrophages. Infect Immun. 1993;61(7):2763-73. PubMed PMID: 8514378; PubMed Central PMCID: PMC280919.
149. Simeone R, Bobard A, Lippmann J, Bitter W, Majlessi L, Brosch R, et al. Phagosomal rupture by *Mycobacterium tuberculosis* results in toxicity and host cell death. PLoS Pathog. 2012;8(2):e1002507. doi: 10.1371/journal.ppat.1002507. PubMed PMID: 22319448; PubMed Central PMCID: PMC3271072.
150. Smith J, Manoranjan J, Pan M, Bohsali A, Xu J, Liu J, et al. Evidence for pore formation in host cell membranes by ESX-1-secreted ESAT-6 and its role in

Mycobacterium marinum escape from the vacuole. Infect Immun. 2008;76(12):5478-87. doi: 10.1128/IAI.00614-08. PubMed PMID: 18852239; PubMed Central PMCID: PMC2583575.

151. Hiemstra PS, van den Barselaar MT, Roest M, Nibbering PH, van Furth R. Ubiquicidin, a novel murine microbicidal protein present in the cytosolic fraction of macrophages. J Leukoc Biol. 1999;66(3):423-8. PubMed PMID: 10496312.
152. Delbridge LM, O'Riordan MX. Innate recognition of intracellular bacteria. Curr Opin Immunol. 2007;19(1):10-6. doi: 10.1016/j.coi.2006.11.005. PubMed PMID: 17126540.
153. Koizumi Y, Toma C, Higa N, Nohara T, Nakasone N, Suzuki T. Inflammasome activation via intracellular NLRs triggered by bacterial infection. Cell Microbiol. 2012;14(2):149-54. doi: 10.1111/j.1462-5822.2011.01707.x. PubMed PMID: 21995284.
154. Carneiro LA, Travassos LH, Soares F, Tattoli I, Magalhaes JG, Bozza MT, et al. Shigella induces mitochondrial dysfunction and cell death in nonmyleoid cells. Cell Host Microbe. 2009;5(2):123-36. doi: 10.1016/j.chom.2008.12.011. PubMed PMID: 19218084.
155. Kroemer G, Marino G, Levine B. Autophagy and the integrated stress response. Mol Cell. 2010;40(2):280-93. doi: 10.1016/j.molcel.2010.09.023. PubMed PMID: 20965422; PubMed Central PMCID: PMC3127250.
156. Boya P, Reggiori F, Codogno P. Emerging regulation and functions of autophagy. Nat Cell Biol. 2013;15(7):713-20. doi: 10.1038/ncb2788. PubMed PMID: 23817233.
157. Palikaras K, Lionaki E, Tavernarakis N. Mitophagy: In sickness and in health. Mol Cell Oncol. 2016;3(1):e1056332. doi: 10.1080/23723556.2015.1056332. PubMed PMID: 27308569; PubMed Central PMCID: PMC4845207.
158. Watson RO, Manzanillo PS, Cox JS. Extracellular *M. tuberculosis* DNA targets bacteria for autophagy by activating the host DNA-sensing pathway. Cell. 2012;150(4):803-15. doi: 10.1016/j.cell.2012.06.040. PubMed PMID: 22901810; PubMed Central PMCID: PMC3708656.
159. Yano T, Mita S, Ohmori H, Oshima Y, Fujimoto Y, Ueda R, et al. Autophagic control of listeria through intracellular innate immune recognition in *Drosophila*. Nat Immunol. 2008;9(8):908-16. doi: 10.1038/ni.1634. PubMed PMID: 18604211; PubMed Central PMCID: PMC2562576.
160. Mostowy S, Bonazzi M, Hamon MA, Tham TN, Mallet A, Lelek M, et al. Entrapment of intracytosolic bacteria by septin cage-like structures. Cell Host Microbe. 2010;8(5):433-44. doi: 10.1016/j.chom.2010.10.009. PubMed PMID: 21075354.
161. Hall PA, Russell SE. The pathobiology of the septin gene family. J Pathol. 2004;204(4):489-505. doi: 10.1002/path.1654. PubMed PMID: 15495264.
162. Nakagawa I, Amano A, Mizushima N, Yamamoto A, Yamaguchi H, Kamimoto T, et al. Autophagy defends cells against invading group A *Streptococcus*. Science. 2004;306(5698):1037-40. doi: 10.1126/science.1103966. PubMed PMID: 15528445.
163. Checroun C, Wehrly TD, Fischer ER, Hayes SF, Celli J. Autophagy-mediated reentry of *Francisella tularensis* into the endocytic compartment after cytoplasmic replication. Proc Natl Acad Sci U S A. 2006;103(39):14578-83. doi: 10.1073/pnas.0601838103. PubMed PMID: 16983090; PubMed Central PMCID: PMC1600002.
164. Case ED, Chong A, Wehrly TD, Hansen B, Child R, Hwang S, et al. The *Francisella* O-antigen mediates survival in the macrophage cytosol via autophagy avoidance. Cell Microbiol. 2014;16(6):862-77. doi: 10.1111/cmi.12246. PubMed PMID: 24286610; PubMed Central PMCID: PMC4028363.
165. Detilleux PG, Deyoe BL, Cheville NF. Entry and intracellular localization of *Brucella* spp. in Vero cells: fluorescence and electron microscopy. Vet Pathol. 1990;27(5):317-28. doi: 10.1177/030098589002700503. PubMed PMID: 2122572.
166. Detilleux PG, Deyoe BL, Cheville NF. Penetration and intracellular growth of *Brucella abortus* in nonphagocytic cells in vitro. Infect Immun. 1990;58(7):2320-8. PubMed PMID: 2114362; PubMed Central PMCID: PMC258815.

167. Horwitz MA. Formation of a novel phagosome by the Legionnaires' disease bacterium (*Legionella pneumophila*) in human monocytes. J Exp Med. 1983;158(4):1319-31. PubMed PMID: 6619736; PubMed Central PMCID: PMC2187375.
168. Pizarro-Cerda J, Meresse S, Parton RG, van der Goot G, Sola-Landa A, Lopez-Goni I, et al. *Brucella abortus* transits through the autophagic pathway and replicates in the endoplasmic reticulum of nonprofessional phagocytes. Infect Immun. 1998;66(12):5711-24. PubMed PMID: 9826346; PubMed Central PMCID: PMC108722.
169. Pizarro-Cerda J, Moreno E, Sanguedolce V, Mege JL, Gorvel JP. Virulent *Brucella abortus* prevents lysosome fusion and is distributed within autophagosome-like compartments. Infect Immun. 1998;66(5):2387-92. PubMed PMID: 9573138; PubMed Central PMCID: PMC108212.
170. Tilney LG, Harb OS, Connelly PS, Robinson CG, Roy CR. How the parasitic bacterium *Legionella pneumophila* modifies its phagosome and transforms it into rough ER: implications for conversion of plasma membrane to the ER membrane. J Cell Sci. 2001;114(Pt 24):4637-50. PubMed PMID: 11792828.
171. Robinson CG, Roy CR. Attachment and fusion of endoplasmic reticulum with vacuoles containing *Legionella pneumophila*. Cell Microbiol. 2006;8(5):793-805. doi: 10.1111/j.1462-5822.2005.00666.x. PubMed PMID: 16611228.
172. Asare R, Abu Kwaik Y. Early trafficking and intracellular replication of *Legionella longbeachaea* within an ER-derived late endosome-like phagosome. Cell Microbiol. 2007;9(6):1571-87. doi: 10.1111/j.1462-5822.2007.00894.x. PubMed PMID: 17309675.
173. Derre I, Swiss R, Agaisse H. The lipid transfer protein CERT interacts with the *Chlamydia* inclusion protein IncD and participates to ER-Chlamydia inclusion membrane contact sites. PLoS Pathog. 2011;7(6):e1002092. doi: 10.1371/journal.ppat.1002092. PubMed PMID: 21731489; PubMed Central PMCID: PMC3121800.
174. Dumoux M, Clare DK, Saibil HR, Hayward RD. Chlamydiae assemble a pathogen synapse to hijack the host endoplasmic reticulum. Traffic. 2012;13(12):1612-27. doi: 10.1111/tra.12002. PubMed PMID: 22901061; PubMed Central PMCID: PMC3533787.
175. Mehlitz A, Karunakaran K, Herweg JA, Krohne G, van de Linde S, Rieck E, et al. The chlamydial organism *Simkania negevensis* forms ER vacuole contact sites and inhibits ER-stress. Cell Microbiol. 2014;16(8):1224-43. doi: 10.1111/cmi.12278. PubMed PMID: 24528559.
176. Arasaki K, Roy CR. *Legionella pneumophila* promotes functional interactions between plasma membrane syntaxins and Sec22b. Traffic. 2010;11(5):587-600. doi: 10.1111/j.1600-0854.2010.01050.x. PubMed PMID: 20163564; PubMed Central PMCID: PMC3164831.
177. Ingmundson A, Delprato A, Lambright DG, Roy CR. *Legionella pneumophila* proteins that regulate Rab1 membrane cycling. Nature. 2007;450(7168):365-9. doi: 10.1038/nature06336. PubMed PMID: 17952054.
178. Kagan JC, Roy CR. *Legionella* phagosomes intercept vesicular traffic from endoplasmic reticulum exit sites. Nat Cell Biol. 2002;4(12):945-54. doi: 10.1038/ncb883. PubMed PMID: 12447391.
179. Hubber A, Arasaki K, Nakatsu F, Hardiman C, Lambright D, De Camilli P, et al. The machinery at endoplasmic reticulum-plasma membrane contact sites contributes to spatial regulation of multiple *Legionella* effector proteins. PLoS Pathog. 2014;10(7):e1004222. doi: 10.1371/journal.ppat.1004222. PubMed PMID: 24992562; PubMed Central PMCID: PMC4081824.
180. Horenkamp FA, Mukherjee S, Alix E, Schauder CM, Hubber AM, Roy CR, et al. *Legionella pneumophila* subversion of host vesicular transport by SidC effector proteins. Traffic. 2014;15(5):488-99. doi: 10.1111/tra.12158. PubMed PMID: 24483784; PubMed Central PMCID: PMC4041529.

181. Machner MP, Isberg RR. Targeting of host Rab GTPase function by the intravacuolar pathogen *Legionella pneumophila.* Dev Cell. 2006;11(1):47-56. doi: 10.1016/j.devcel.2006.05.013. PubMed PMID: 16824952.
182. Murata T, Delprato A, Ingmundson A, Toomre DK, Lambright DG, Roy CR. The *Legionella pneumophila* effector protein DrrA is a Rab1 guanine nucleotide-exchange factor. Nat Cell Biol. 2006;8(9):971-7. doi: 10.1038/ncb1463. PubMed PMID: 16906144.
183. Hubber A, Kubori T, Coban C, Matsuzawa T, Ogawa M, Kawabata T, et al. Bacterial secretion system skews the fate of *Legionella*-containing vacuoles towards LC3-associated phagocytosis. Sci Rep. 2017;7:44795. doi: 10.1038/srep44795. PubMed PMID: 28317932; PubMed Central PMCID: PMC5357938.
184. Arasaki K, Toomre DK, Roy CR. The *Legionella pneumophila* effector DrrA is sufficient to stimulate SNARE-dependent membrane fusion. Cell Host Microbe. 2012;11(1):46-57. doi: 10.1016/j.chom.2011.11.009. PubMed PMID: 22264512; PubMed Central PMCID: PMC3266541.
185. Robertson DK, Gu L, Rowe RK, Beatty WL. Inclusion biogenesis and reactivation of persistent *Chlamydia trachomatis* requires host cell sphingolipid biosynthesis. PLoS Pathog. 2009;5(11):e1000664. doi: 10.1371/journal.ppat.1000664. PubMed PMID: 19936056; PubMed Central PMCID: PMC2774160.
186. van Ooij C, Kalman L, van I, Nishijima M, Hanada K, Mostov K, et al. Host cell-derived sphingolipids are required for the intracellular growth of *Chlamydia trachomatis*. Cell Microbiol. 2000;2(6):627-37. PubMed PMID: 11207614.
187. Myeni S, Child R, Ng TW, Kupko JJ, 3rd, Wehrly TD, Porcella SF, et al. *Brucella* modulates secretory trafficking via multiple type IV secretion effector proteins. PLoS Pathog. 2013;9(8):e1003556. doi: 10.1371/journal.ppat.1003556. PubMed PMID: 23950720; PubMed Central PMCID: PMC3738490.
188. Pappas G, Akritidis N, Bosilkovski M, Tsianos E. Brucellosis. N Engl J Med. 2005;352(22):2325-36. doi: 10.1056/NEJMra050570. PubMed PMID: 15930423.
189. Atluri VL, Xavier MN, de Jong MF, den Hartigh AB, Tsolis RM. Interactions of the human pathogenic *Brucella* species with their hosts. Annu Rev Microbiol. 2011;65:523-41. doi: 10.1146/annurev-micro-090110-102905. PubMed PMID: 21939378.
190. Archambaud C, Salcedo SP, Lelouard H, Devilard E, de Bovis B, Van Rooijen N, et al. Contrasting roles of macrophages and dendritic cells in controlling initial pulmonary *Brucella* infection. Eur J Immunol. 2010;40(12):3458-71. doi: 10.1002/eji.201040497. PubMed PMID: 21108467.
191. Castaneda-Roldan EI, Ouahrani-Bettache S, Saldana Z, Avelino F, Rendon MA, Dornand J, et al. Characterization of SP41, a surface protein of *Brucella* associated with adherence and invasion of host epithelial cells. Cell Microbiol. 2006;8(12):1877-87. doi: 10.1111/j.1462-5822.2006.00754.x. PubMed PMID: 16817909.
192. Castaneda-Roldan EI, Avelino-Flores F, Dall'Agnol M, Freer E, Cedillo L, Dornand J, et al. Adherence of *Brucella* to human epithelial cells and macrophages is mediated by sialic acid residues. Cell Microbiol. 2004;6(5):435-45. doi: 10.1111/j.1462-5822.2004.00372.x. PubMed PMID: 15056214.
193. Posadas DM, Ruiz-Ranwez V, Bonomi HR, Martin FA, Zorreguieta A. BmaC, a novel autotransporter of *Brucella suis*, is involved in bacterial adhesion to host cells. Cell Microbiol. 2012;14(6):965-82. doi: 10.1111/j.1462-5822.2012.01771.x. PubMed PMID: 22321605.
194. Guzman-Verri C, Chaves-Olarte E, von Eichel-Streiber C, Lopez-Goni I, Thelestam M, Arvidson S, et al. GTPases of the Rho subfamily are required for Brucella abortus internalization in nonprofessional phagocytes: direct activation of Cdc42. J Biol Chem. 2001;276(48):44435-43. doi: 10.1074/jbc.M105606200. PubMed PMID: 11579087.
195. Watanabe K, Tachibana M, Kim S, Watarai M. EEVD motif of heat shock cognate protein 70 contributes to bacterial uptake by trophoblast giant cells. J Biomed Sci.

2009;16:113. doi: 10.1186/1423-0127-16-113. PubMed PMID: 20003465; PubMed Central PMCID: PMC2800845.
196. Kim S, Watarai M, Suzuki H, Makino S, Kodama T, Shirahata T. Lipid raft microdomains mediate class A scavenger receptor-dependent infection of *Brucella abortus*. Microb Pathog. 2004;37(1):11-9. doi: 10.1016/j.micpath.2004.04.002. PubMed PMID: 15194155.
197. Watarai M. Interaction between *Brucella abortus* and cellular prion protein in lipid raft microdomains. Microbes Infect. 2004;6(1):93-100. PubMed PMID: 14738898.
198. Watarai M, Makino S, Fujii Y, Okamoto K, Shirahata T. Modulation of *Brucella*-induced macropinocytosis by lipid rafts mediates intracellular replication. Cell Microbiol. 2002;4(6):341-55. PubMed PMID: 12067319.
199. Naroeni A, Porte F. Role of cholesterol and the ganglioside GM(1) in entry and short-term survival of *Brucella suis* in murine macrophages. Infect Immun. 2002;70(3):1640-4. PubMed PMID: 11854258; PubMed Central PMCID: PMC127813.
200. Pei J, Turse JE, Ficht TA. Evidence of *Brucella abortus* OPS dictating uptake and restricting NF-kappaB activation in murine macrophages. Microbes Infect. 2008;10(6):582-90. doi: 10.1016/j.micinf.2008.01.005. PubMed PMID: 18457975; PubMed Central PMCID: PMC2752336.
201. von Bargen K, Gorvel JP, Salcedo SP. Internal affairs: investigating the *Brucella* intracellular lifestyle. FEMS Microbiol Rev. 2012;36(3):533-62. doi: 10.1111/j.1574-6976.2012.00334.x. PubMed PMID: 22373010.
202. Comerci DJ, Martinez-Lorenzo MJ, Sieira R, Gorvel JP, Ugalde RA. Essential role of the VirB machinery in the maturation of the *Brucella abortus*-containing vacuole. Cell Microbiol. 2001;3(3):159-68. PubMed PMID: 11260139.
203. Bellaire BH, Roop RM, 2nd, Cardelli JA. Opsonized virulent *Brucella abortus* replicates within nonacidic, endoplasmic reticulum-negative, LAMP-1-positive phagosomes in human monocytes. Infect Immun. 2005;73(6):3702-13. doi: 10.1128/IAI.73.6.3702-3713.2005. PubMed PMID: 15908400; PubMed Central PMCID: PMC1111828.
204. Porte F, Liautard JP, Kohler S. Early acidification of phagosomes containing *Brucella suis* is essential for intracellular survival in murine macrophages. Infect Immun. 1999;67(8):4041-7. PubMed PMID: 10417172; PubMed Central PMCID: PMC96697.
205. Starr T, Ng TW, Wehrly TD, Knodler LA, Celli J. *Brucella* intracellular replication requires trafficking through the late endosomal/lysosomal compartment. Traffic. 2008;9(5):678-94. doi: 10.1111/j.1600-0854.2008.00718.x. PubMed PMID: 18266913.
206. Lestrate P, Delrue RM, Danese I, Didembourg C, Taminiau B, Mertens P, et al. Identification and characterization of in vivo attenuated mutants of *Brucella melitensis*. Mol Microbiol. 2000;38(3):543-51. PubMed PMID: 11069678.
207. Taguchi Y, Imaoka K, Kataoka M, Uda A, Nakatsu D, Horii-Okazaki S, et al. Yip1A, a novel host factor for the activation of the IRE1 pathway of the unfolded protein response during *Brucella* infection. PLoS Pathog. 2015;11(3):e1004747. doi: 10.1371/journal.ppat.1004747. PubMed PMID: 25742138; PubMed Central PMCID: PMC4350842.
208. Herrou J, Crosson S. Molecular structure of the *Brucella abortus* metalloprotein RicA, a Rab2-binding virulence effector. Biochemistry. 2013;52(50):9020-8. doi: 10.1021/bi401373r. PubMed PMID: 24251537; PubMed Central PMCID: PMC3902126.
209. Fugier E, Salcedo SP, de Chastellier C, Pophillat M, Muller A, Arce-Gorvel V, et al. The glyceraldehyde-3-phosphate dehydrogenase and the small GTPase Rab 2 are crucial for *Brucella* replication. PLoS Pathog. 2009;5(6):e1000487. doi: 10.1371/journal.ppat.1000487. PubMed PMID: 19557163; PubMed Central PMCID: PMC2695806.
210. de Barsy M, Jamet A, Filopon D, Nicolas C, Laloux G, Rual JF, et al. Identification of a *Brucella* spp. secreted effector specifically interacting with human small GTPase

Rab2. Cell Microbiol. 2011;13(7):1044-58. doi: 10.1111/j.1462-5822.2011.01601.x. PubMed PMID: 21501366.
211. Miller CN, Smith EP, Cundiff JA, Knodler LA, Bailey Blackburn J, Lupashin V, et al. A *Brucella* Type IV Effector Targets the COG Tethering Complex to Remodel Host Secretory Traffic and Promote Intracellular Replication. Cell Host Microbe. 2017. doi: 10.1016/j.chom.2017.07.017. PubMed PMID: 28844886.
212. Smith EP, Miller CN, Child R, Cundiff JA, Celli J. Postreplication Roles of the *Brucella* VirB Type IV Secretion System Uncovered via Conditional Expression of the VirB11 ATPase. MBio. 2016;7(6). doi: 10.1128/mBio.01730-16. PubMed PMID: 27899503; PubMed Central PMCID: PMC5137499.
213. Gamazo C, Vitas AI, Lopez-Goni I, Diaz R, Moriyon I. Factors affecting detection of *Brucella melitensis* by BACTEC NR730, a nonradiometric system for hemocultures. J Clin Microbiol. 1993;31(12):3200-3. PubMed PMID: 8308111; PubMed Central PMCID: PMC266375.
214. Anderson TD, Cheville NF, Meador VP. Pathogenesis of placentitis in the goat inoculated with Brucella abortus. II. Ultrastructural studies. Vet Pathol. 1986;23(3):227-39. doi: 10.1177/030098588602300302. PubMed PMID: 3088810.
215. de Jong MF, Starr T, Winter MG, den Hartigh AB, Child R, Knodler LA, et al. Sensing of bacterial type IV secretion via the unfolded protein response. MBio. 2013;4(1):e00418-12. doi: 10.1128/mBio.00418-12. PubMed PMID: 23422410; PubMed Central PMCID: PMC3624511.
216. Smith JA, Khan M, Magnani DD, Harms JS, Durward M, Radhakrishnan GK, et al. *Brucella* induces an unfolded protein response via TcpB that supports intracellular replication in macrophages. PLoS Pathog. 2013;9(12):e1003785. doi: 10.1371/journal.ppat.1003785. PubMed PMID: 24339776; PubMed Central PMCID: PMC3855547.
217. Qin QM, Pei J, Ancona V, Shaw BD, Ficht TA, de Figueiredo P. RNAi screen of endoplasmic reticulum-associated host factors reveals a role for IRE1alpha in supporting *Brucella* replication. PLoS Pathog. 2008;4(7):e1000110. doi: 10.1371/journal.ppat.1000110. PubMed PMID: 18654626; PubMed Central PMCID: PMC2453327.
218. Starr T, Child R, Wehrly TD, Hansen B, Hwang S, Lopez-Otin C, et al. Selective subversion of autophagy complexes facilitates completion of the *Brucella* intracellular cycle. Cell Host Microbe. 2012;11(1):33-45. doi: 10.1016/j.chom.2011.12.002. PubMed PMID: 22264511; PubMed Central PMCID: PMC3266535.
219. Soto GE, Young SJ, Martone ME, Deerinck TJ, Lamont S, Carragher BO, et al. Serial section electron tomography: a method for three-dimensional reconstruction of large structures. Neuroimage. 1994;1(3):230-43. doi: 10.1006/nimg.1994.1008. PubMed PMID: 9343574.
220. Chen X, Nelson CD, Li X, Winters CA, Azzam R, Sousa AA, et al. PSD-95 is required to sustain the molecular organization of the postsynaptic density. J Neurosci. 2011;31(17):6329-38. doi: 10.1523/JNEUROSCI.5968-10.2011. PubMed PMID: 21525273; PubMed Central PMCID: PMC3099547.
221. da Costa NM, Martin KA. The proportion of synapses formed by the axons of the lateral geniculate nucleus in layer 4 of area 17 of the cat. J Comp Neurol. 2009;516(4):264-76. doi: 10.1002/cne.22133. PubMed PMID: 19634180.
222. Bock DD, Lee WC, Kerlin AM, Andermann ML, Hood G, Wetzel AW, et al. Network anatomy and in vivo physiology of visual cortical neurons. Nature. 2011;471(7337):177-82. doi: 10.1038/nature09802. PubMed PMID: 21390124; PubMed Central PMCID: PMC3095821.
223. Tapia JC, Kasthuri N, Hayworth KJ, Schalek R, Lichtman JW, Smith SJ, et al. High-contrast en bloc staining of neuronal tissue for field emission scanning electron microscopy. Nat Protoc. 2012;7(2):193-206. doi: 10.1038/nprot.2011.439. PubMed PMID: 22240582; PubMed Central PMCID: PMC3701260.

224. Denk W, Horstmann H. Serial block-face scanning electron microscopy to reconstruct three-dimensional tissue nanostructure. PLoS Biol. 2004;2(11):e329. doi: 10.1371/journal.pbio.0020329. PubMed PMID: 15514700; PubMed Central PMCID: PMC524270.
225. Briggman KL, Helmstaedter M, Denk W. Wiring specificity in the direction-selectivity circuit of the retina. Nature. 2011;471(7337):183-8. doi: 10.1038/nature09818. PubMed PMID: 21390125.
226. Knott G, Marchman H, Wall D, Lich B. Serial section scanning electron microscopy of adult brain tissue using focused ion beam milling. J Neurosci. 2008;28(12):2959-64. doi: 10.1523/JNEUROSCI.3189-07.2008. PubMed PMID: 18353998.
227. Wanner AA, Genoud C, Friedrich RW. 3-dimensional electron microscopic imaging of the zebrafish olfactory bulb and dense reconstruction of neurons. Sci Data. 2016;3:160100. doi: 10.1038/sdata.2016.100. PubMed PMID: 27824337; PubMed Central PMCID: PMC5100684 application EP14736451 and US patent application US14897514. A.A.W. is the founder and owner of ariadne-service.
228. Alcantara CL, Vidal JC, de Souza W, Cunha ESNL. The cytostome-cytopharynx complex of *Trypanosoma cruzi* epimastigotes disassembles during cell division. J Cell Sci. 2017;130(1):164-76. doi: 10.1242/jcs.187419. PubMed PMID: 27363990.
229. Mellouk N, Weiner A, Aulner N, Schmitt C, Elbaum M, Shorte SL, et al. *Shigella* subverts the host recycling compartment to rupture its vacuole. Cell Host Microbe. 2014;16(4):517-30. doi: 10.1016/j.chom.2014.09.005. PubMed PMID: 25299335.
230. Knott G, Rosset S, Cantoni M. Focussed ion beam milling and scanning electron microscopy of brain tissue. J Vis Exp. 2011;(53):e2588. doi: 10.3791/2588. PubMed PMID: 21775953; PubMed Central PMCID: PMC3196160.
231. Walton J. Lead aspartate, an en bloc contrast stain particularly useful for ultrastructural enzymology. J Histochem Cytochem. 1979;27(10):1337-42. doi: 10.1177/27.10.512319. PubMed PMID: 512319.
232. Maco B, Holtmaat A, Jorstad A, Fua P, Knott GW. Correlative in vivo 2-photon imaging and focused ion beam scanning electron microscopy: 3D analysis of neuronal ultrastructure. Methods Cell Biol. 2014;124:339-61. doi: 10.1016/B978-0-12-801075-4.00016-1. PubMed PMID: 25287849.
233. Knott GW, Holtmaat A, Trachtenberg JT, Svoboda K, Welker E. A protocol for preparing GFP-labeled neurons previously imaged in vivo and in slice preparations for light and electron microscopic analysis. Nat Protoc. 2009;4(8):1145-56. doi: 10.1038/nprot.2009.114. PubMed PMID: 19617886.
234. Nagerl UV, Kostinger G, Anderson JC, Martin KA, Bonhoeffer T. Protracted synaptogenesis after activity-dependent spinogenesis in hippocampal neurons. J Neurosci. 2007;27(30):8149-56. doi: 10.1523/JNEUROSCI.0511-07.2007. PubMed PMID: 17652605.

2 Aim of the thesis

2. AIM OF THE THESIS

Started in September 2013, the aim of my thesis was to use a combination of light and electron microscopy techniques to gain new insight into the intracellular lifestyle of *Brucella*. I was able to establish an imaging approach that involves high-resolution light microscopy followed by focused ion beam scanning electron microscopy (FIB/SEM). This approach was successfully applied in the imaging of risk group 3 samples of both *Brucella*-infected cell monolayers and mouse organs. Moreover, I was responsible for the development of new tools such as stable cell lines expressing fluorescently labeled markers. This allowed targeting of specific cellular processes that occur during the trafficking of *Brucella*.

The first part of my work was aimed at visualizing the structure of the replicative niche of *Brucella*. To achieve this, I applied correlative FIB/SEM to image infected cells at late infection stages. The starting point was the imaging of infected HeLa cell monolayers. The approach was later extended to trophoblasts of mice infected with *Brucella*, which allowed the visualization of the replicative niche inside an in vivo infection model.

The second aspect of my work focused on trafficking of *Brucella* inside host cells and the events that lead to the establishment of the replicative niche. In this case a combination of different imaging approaches was used, including immunofluorescence confocal microscopy, correlative FIB/SEM and live-cell imaging. This allowed studying the dynamics of *Brucella* vacuoles and the observation of rare events that occur during intermediate trafficking stages.

3 Results

3. RESULTS

3.1. Research article I (submitted)

3D correlative electron microscopy reveals continuity of replicative *Brucella*-containing vacuoles with the endoplasmic reticulum

Jaroslaw Sedzicki, Therese Tschon, Shyan Huey-Low, Kevin Willemart, Kenneth N. Goldie, Jean-Jacques Letesson, Henning Stahlberg and Christoph Dehio

Manuscript submitted to Journal of Cell Science

3.1.1 Statement of own contribution

I was responsible for developing the CLEM approach used in this study, sample preparation and generation of the microscopic data. Dr. Therese Tschon and Dr. Shyan H. Low were responsible for preparing Brucella-infected cell monolayer samples. Kevin Willemart was responsible for providing the animal samples. The manuscript was written by me.

3.1.2. Manuscript

3D correlative electron microscopy reveals continuity of replicative *Brucella*-containing vacuoles with the endoplasmic reticulum

Jaroslaw Sedzicki[1,2], Therese Tschon[1], Shyan Huey-Low[3], Kevin Willemart[4], Kenneth N. Goldie[2], Jean-Jacques Letesson[4], Henning Stahlberg[2] and Christoph Dehio[1]

[1] Focal Area Infection Biology, Biozentrum, University of Basel, 4056 Basel, Switzerland; [2] Center for Cellular Imaging and Nanoanalytics (C-CINA), Biozentrum, University of Basel, 4056 Basel, Switzerland; [3] Present address: Lee Kong Chian School of Medicine, Nanyang Technological University (NTU), Singapore 639798, Singapore; [4] Microorganisms Biology Research Unit (URBM, Unité de Recherche en Biologie des Microorganismes), University of Namur, 5000 Namur, Belgium

Corresponding author e-mail: christoph.dehio@unibas.ch

Summary statement: 3D correlative light and electron microscopy (3D-CLEM) reveals that replicative *Brucella*-containing vacuoles (rBCVs) are continuous with the endoplasmic reticulum (ER)

Running title: *Brucella* replicates in ER

Keywords: Endoplasmic reticulum (ER), replicative *Brucella*-containing vacuole (rBCV), FIB/SEM tomography, correlative light and electron microscopy (CLEM), Sec61

List of Abbreviations

2D: two-dimensional

3D: three-dimensional

aBCV: autophagic *Brucella*-containing vacuole

BCV: *Brucella*-containing vacuole

CLEM: correlative light and electron microscopy

eBCV: endosomal *Brucella*-containing vacuole

EM: electron microscopy

ER: endoplasmic reticulum

FIB/SEM: focused ion beam/scanning electron microscopy

NPC: nuclear pore complex

rBCV: replicative *Brucella*-containing vacuole

SIM: structured illumination microscopy

T4SS: Type IV secretion system

TEM: transmission electron microscopy

ABSTRACT

Entry of the facultative intracellular pathogen *Brucella* into host cells results in the formation of endosomal *Brucella*-containing vacuoles (eBCVs) that initially traffic along the endocytic pathway. eBCV acidification triggers the expression of a type IV secretion system that translocates bacterial effector proteins into host cells. This interferes with lysosomal fusion of eBCVs and supports their maturation to replicative *Brucella*-containing vacuoles (rBCVs). Bacteria replicate in rBCVs to large numbers, eventually occupying most of the cytoplasmic volume. As rBCV membranes tightly wrap each individual bacterium, they are constantly being expanded and remodeled during exponential bacterial growth. rBCVs are known to carry endoplasmic reticulum (ER) markers, however, the relationship of the vacuole to the genuine ER has remained elusive. We have reconstructed the 3-dimensional ultrastructure of rBCVs and associated ER by correlative structured illumination microscopy (SIM) and focused ion beam/scanning electron microscopic tomography (FIB/SEM). Studying *B. abortus*-infected HeLa cells and trophoblasts derived from *B. melitensis*-infected mice, we demonstrate that rBCVs are complex and interconnected compartments that are continuous with neighboring ER cisternae, thus supporting a model that rBCVs are extensions of genuine ER.

INTRODUCTION

Several bacterial pathogens have adapted to an intracellular lifestyle. Eukaryotic host cells provide an environment for replication and persistence that is rich in nutrients and shields the pathogens from different hostile factors, such as immunity mechanisms or competition with other microbes. An intracellular lifestyle has, however, many challenges of its own. Bacteria internalization by either phagocytic or non-phagocytic cells generates a vacuole equipped with various bactericidal mechanisms. Intracellular bacteria have developed various strategies that allow them to avoid these defenses and create conditions for their successful replication [1]. The establishment and maintenance of an intracellular replicative niche suitable for efficient growth, is a key feature of pathogens that decisively contributes to both their survival in the host and success in transmission to new hosts. Many bacteria have been shown to thrive inside specialized vacuoles that display at least some characteristics of host organelles. The nature of these compartments varies greatly, depending on the pathogen. In some cases, growth occurs inside arrested early endosomes, *Mycobacterium tuberculosis* is one example [2, 3]. *Coxiella* forms a compartment characterized by the presence of autophagy markers [4], while *Chlamydia* thrives in a modified vacuole derived from Golgi membranes [5]. Finally, pathogens such as *Legionella* and *Brucella* replicate inside vacuoles that display characteristics of the endoplasmic reticulum (ER) [6].

Bacteria from the genus *Brucella* are facultative intracellular pathogens. They are the causative agents of brucellosis, a worldwide zoonosis that has serious health and economic impact. In the animal host, the bacteria target the reproductive organs, causing spontaneous abortions or weakening of offspring. Both lead to major losses in livestock husbandry. The pathogen is transmitted from animals to humans mostly through contaminated dairy products. During chronic infection the bacteria get disseminated across different organs and cell types, including macrophages, dendritic cells and placental trophoblasts. This results in a progressive debilitating disease that is difficult to diagnose and treat, often leading to persistence and relapses [7-9].

Following internalization by host cells by a poorly described mechanism, bacteria are enclosed in a membranous compartment called the *Brucella*-containing vacuole (BCV), which initially displays endosome characteristics (eBCV). It acquires early endosome markers, such as Rab5 and EEA1, followed by the emergence of late endosome markers such as LAMP1 and Rab7 later in the maturation process [10-14].

The gradual acidification of the compartment triggers the expression of the VirB type IV secretion system (T4SS), which enables the translocation of a repertoire of effector proteins into the host cell cytoplasm [15-17]. This prevents fusion of the eBCV with lysosomes and eventually leads to the formation of a replicative niche (replicative BCV or rBCV) that has certain characteristics of the ER [12, 18]. This process is thought to occur through interactions of rBCVs with ER exit sites, but the details remain elusive [10, 11, 13, 19]. Once the replicative niche is established, *Brucella* undergoes numerous rounds of division until most of the host cell's cytoplasmic volume is occupied by bacteria, each tightly wrapped by rBCV membranes. It has been suggested that the intracellular life cycle is completed by the formation of autophagic BCVs (aBCVs), a process that may represent non-canonical action of autophagy initiation factors [20].

Despite numerous contributions regarding the nature and characteristics of the replicative niche of *Brucella*, many questions remain open. Not only do we lack knowledge of how the rBCV is established, but also a detailed description of its structure in relation to ER and other cellular organelles. The rBCV, which is often described as 'ER-derived' or 'ER-associated', has many interesting features [6, 21]. It is widely accepted that its membrane is characterized by the presence of different ER markers, such as calnexin, calreticulin, Sec61β and associated ribosomes [10, 13]. Dividing bacteria have been shown to sit in individual, single membrane compartments that are limited in space [10, 11, 13, 22]. There have been several reports indicating fusion between rBCVs and the ER and the presence of the bacteria in the perinuclear space [13, 23, 24], which suggests at least partial continuity between rBCVs and the ER network. The conclusions drawn in these examples are typically based on transmission electron microscopy (TEM) micrographs of ultrathin sections, which provide useful two-dimensional (2D) information on the nature of the rBCV, but do not reflect the complex three-dimensional (3D) structure of the ER [25].

Here, we employed correlative structured illumination microscopy (SIM) and focused ion beam scanning electron microscopy (FIB/SEM) [26] to study the ultrastructural details of rBCVs and their relation to the ER. FIB/SEM allows 3D imaging of biological samples at intermediate electron microscopy resolutions and has proved useful for the detailed description of subcellular structures. In

combination with high-resolution light microscopy this technique can resolve ultrastructure details of the interactions between organelles inside eukaryotic cells [27, 28]. Our unprecedented 3D reconstructions of membrane compartments in *Brucella*-infected cells visualize a network of luminal connections between rBCVs and the ER, supporting the hypothesis that the rBCV is an integral part of this organelle.

RESULTS

3D-CLEM reveals the 3-dimensional ultrastructure of the rBCV

In order to resolve the 3D ultrastructure of rBCVs in relation to other cellular organelles by a correlative light and electron microscopy (CLEM) approach, we used HeLa cells infected with *B. abortus* as a simple infection model. HeLa cells have been extensively used to study *Brucella* interaction with eukaryotic cells, are easy to manipulate and relatively flat, which makes them well suited for microscopy. In order to specifically label ER membranes, we used HeLa cells expressing the ER markers Calnexin-GFP [29] and Emerald-Sec61β [25], both of which have previously been shown to colocalize with the rBCV [10].

SIM of HeLa cells infected with *B. abortus* for 24 hours indicated that the majority of the bacteria were residing, individually, inside compartments that stained positively for the ER markers (Figs 1A, S1A). FIB/SEM tomography images of the corresponding cells revealed the arrangement of membranous organelles enclosing the bacteria. In HeLa cells expressing Calnexin-GFP, we discovered the presence of multi-layered membrane artifacts that often formed around the BCVs (Fig. S1B). These structures probably represent previously reported multilayered ER assemblies induced by Calnexin-GFP overexpression [30]. While the data indirectly support a residency of the pathogen in the ER lumen, the artefactual changes of ER morphology precluded the use of this marker for detailed characterization of the rBCV.

FIB/SEM tomograms of cells expressing Emerald-Sec61β indicated that bacteria reside within single-membrane vacuoles (Fig. 1). The rBCVs were distributed across a large volume of the host cell cytoplasm, with different organelles interspersed between them. Most rBCVs contained apparently a single bacterium, which was described as a characteristic trait of pathogens belonging to the genus

Brucella [21]. Some of the bacteria visualized were undergoing division (Fig. 1A,B). Occasionally, more than one bacterium was present inside the same rBCV (Fig. 1B). Our EM data indicate that rBCV membranes are tightly associated with the surface of the bacteria. During bacterial division, when the daughter cells become separated, rBCV membranes were found to tighten around the invaginations of the central septum, keeping the volume of the rBCV lumen to the minimum (Fig. 1C). To verify the relevance of our findings, we used the 3D FIB/SEM tomography approach to image trophoblasts extracted from pregnant mice infected with *B. melitensis*. The data indicate that, similar to infection of HeLa cells by *B. abortus*, *B. melitensis* are contained in rBCVs, mostly as single bacteria. rBCVs are apparently expanded and remodeled rapidly to cover the surface of the individual bacteria present in the exponentially growing intracellular microcolony (Fig. 1D, E).

FIB/SEM tomography reveals extensive interactions between rBCVs and other host cell membranes

The ultimate advantage of FIB/SEM tomography compared to traditional EM approaches is the ability to image many consecutive layers at a resolution that allows membrane compartments of large 3D-volumes to be reconstructed. Using the tomograms, we could trace the interactions between BCVs and other organelles across the entire cytoplasmic volume of the infected host cell. Single tomogram frames indicated that the membrane of some BCVs form narrow protrusions that vary in shape and length. We were able to follow these protrusions across the consecutive tomogram slices, revealing their arrangement and connections with membranes located in their proximity (Fig. 2). 3D reconstructions demonstrated that some of the protrusions extend into ER cisternae. These structures were continuous with the rest of the ER, indicating that at least some of the bacteria are located directly in the ER lumen (Fig. 2A, B; Movie 1). We also detected extensions of rBCVs that formed vesicle-rich interfaces in the proximity of Golgi structures (Fig. 2C, D). This arrangement of membranes is reminiscent of previously described ER-exit sites, which suggests that the vacuoles are continuous with functional ER [31].

When rBCVs were located in the proximity of the nucleus, some of the extensions were continuous with membranes originating from the outer nuclear membrane (Fig. 2E, F). In some cases, the bacteria were found growing directly in the perinuclear space, with the outer nuclear membrane stretching to accommodate

them (Fig. 2G, H). This phenomenon seemed to coincide with advanced stages of intracellular growth, when a large fraction of intracellular membranes had already been recruited to rBCVs.

We also detected non-continuous contact sites between rBCVs and other membranous compartments. Interestingly, in some cases we noticed slight deformations of the rBCV surface at sites where the membranes were touching (Fig. 2I), which could indicate the engagement of tethering factors that keep the two bilayers in close proximity. When visualized in 3D, the membranes were found to be parts of ER cisternae (Fig. 2J). The apparent prevalence of such contacts found within the host cell indicates that they might represent fusion and fission intermediates of the continuous connections discussed earlier.

The 3D information also allowed us to look at the level of continuity between rBCVs. Closer analysis of the tomograms revealed several sites where the membranes of neighboring rBCVs appeared to be continuous, resulting in assemblies of bacteria sharing the same organelle. These connections, however, were often only at certain points, with most of bacterial surface being surrounded by separated rBCV membranes (Fig 2K, L).

3D-CLEM demonstrates that rBCVs are continuous with genuine ER

In order to unmistakably demonstrate the ER nature of membranes that were continuous with the rBCVs, we explored the full detail of our 3D-CLEM approach in 3D reconstructions of large parts of the host cell (Fig. 3A, B). Flat cisternae identified across the host cell volume (Fig. 3B) were found to be part of a network of interconnected membranes that originate from the outer nuclear membrane (Fig. 3C, bottom). An overlay of the two 3D volumes generated from the SIM and FIB/SEM data, respectively, indicated that the membranous cisternae colocalize with the signal from Emerald-Sec61β, which confirms that they are a part of the ER mesh spanning across the host cell (Fig. 3C, middle). Many rBCVs in a given area were connected to both each other and ER structures, constituting a part of this network (Fig. 3C). We were also able to resolve the fluorescence signal for some of the ER structures that formed direct connection with the rBCVs in the tomograms (Fig. 3D).

The replicative niche of *Brucella* constitutes a complex 3D mesh with numerous connections to other host membranous compartments

After applying 3D-CLEM to explicitly demonstrate the continuity of rBCV membranes with the ER, our next aim was to quantify the level of networking by analyzing larger volumes of non-correlative FIB/SEM datasets (Fig. 4). In HeLa cells infected with *B. abortus,* we observed that many rBCVs were connected to ER cisternae that stretched across large distances (Fig. 4A, B). When the continuity between neighboring rBCVs was also taken into account, we found that a large part of the vacuoles was integrated into the ER network. However, the exact level of connectivity between the rBCVs and the ER was difficult to quantify as there are many sites in the tomograms where the continuity of the membranes is questionable due to the resolution of the FIB/SEM tomograms (Fig. S2). In particular, the ER structures of HeLa cells display great variability in diameter and it was particularly difficult to judge the continuity of some fine cisternae (Fig. S2A). In mouse trophoblasts the ER cisternae are in general more spacious and thus better suited to identify sites of continuity with rBCVs (Fig. S2B). Nevertheless, the following quantifications probably systematically underestimate the level of inter-connectivity. In HeLa cells, 57% of bacteria were found to be located inside rBCVs that were continuous with the ER. In case of mouse trophoblasts infected with *B. melitensis*, around 71% of BCVs were found connected to the ER (Fig. 4C, D). The results suggest that in both cases most bacteria reside inside BCVs that are integrated in the ER meshwork.

After post-division separation of bacteria, continuity between BCVs is limited to small surface areas

As shown above, bacteria residing in rBCVs are not only connected to the ER lumen, but often also straight to neighboring rBCVs. We wondered whether these direct connections between rBCVs are the result of incomplete post-division separation or whether they, at least in part, reflect fusion events between distinct rBCVs. In search for the latter, we examined the structure of the replicative niche in HeLa cells that were co-infected with two strains of *B. abortus*, each expressing a different fluorescent marker (Fig. 5). Confocal analysis of HeLa cells expressing Emerald-Sec61β showed that occasionally cells are infected by both strains, resulting

in mixed microcolonies (Fig. 5A). The level of spatial overlap between bacteria of the two strains varied from cell to cell, suggesting that it might simply depend on the random distribution of bacteria relative to each other at the point when the replicative niche is established.

Our correlative approach allowed us to distinguish both strains in FIB/SEM tomograms (Fig. 5B). We were able to find cases of continuity between rBCVs occupied by bacteria belonging to different lineages, suggesting fusion between the vacuoles. Such connections, however, were always limited to small surface areas. The presence of two bacteria inside the bulk volume of the same rBCV was only observed for bacteria from the same lineage, thus likely representing post-division cells (Fig. 5C). As expected, rBCVs containing individual bacteria from both lineages were found to be connected to ER cisternae and thus to constitute integral parts of the ER network (Fig. 5D).

DISCUSSION

Several intracellular pathogens are known to thrive inside vacuoles that display at least some characteristics of host cellular organelles [6]. Once it has been successfully established a vacuolar replicative compartment requires constant remodeling by membrane fusion and fission events in order to facilitate the evasion of host cell defenses, the acquisition of nutrients, and volume and shape changes to adjust to pathogen growth. EM has provided invaluable information about the ultrastructural details of such pathogen-containing vacuoles inside host cells [13, 20, 32, 33]. Most studies, however, are based on flat ultrathin sections, which fail to resolve the 3D membrane assemblies of cellular organelles and their complex interactions. The facultative intracellular pathogen *Brucella* is an interesting example in this respect. Ultrastructural analysis in combination with cell biology studies has suggested a relationship between the rBCV and the ER [13, 22]. However, the lack of 3D ultrastructural information has hampered a thorough characterization of the role of the ER in establishing and maintaining rBCVs. By combining FIB/SEM tomography with SIM super-resolution fluorescent imaging, we were able to visualize the complex structure of the ER and its interactions with rBCVs formed by two species of brucellae, *B. abortus* and *B. melitensis*, in human and mouse cells, respectively.

Our FIB/SEM data indicate that seemingly isolated rBCVs are often connected to other rBCVs as well as to extended membranous cisternae. We

demonstrated that these membranes can be traced back to the outer nuclear membrane in the reconstructed 3D volumes. Moreover, by correlating fluorescent SIM data with EM, we could demonstrate that the marker GFP-Sec61β colocalizes with both the rBCVs of *B. abortus* and the membranes that are continuous with them. This confirms that at a given time some of the rBCVs share a continuous lumen with the ER. These observations in infected HeLa cells, were confirmed by FIB/SEM imaging of trophoblasts in the placenta of pregnant mice infected with *B. melitensis*. Similar to *B. abortus* in HeLa cells, the rBCVs were often found connected directly to ER cisternae and the outer nuclear membrane.

Not all rBCVs in a given cell volume were found to be integrated into the ER network. In part, this may result from technical limitations of the FIB/SEM tomography approach, as this method does not allow all membranous structures to be resolved and thus systematically underestimates connectivity. However, incomplete continuity between rBCVs and ER may also reflect dynamic remodeling that constantly takes place within the ER [25]. In agreement, the numerous seemingly discontinuous contact sites between rBCVs and the ER observed in addition to direct membrane continuity most likely reflect tethering events between these compartments. We speculate that they may be snapshots of dynamic fusion/fission events responsible for the assembly and disassembly of connections between rBCVs and the remaining ER volume. Apparent continuity between rBCVs containing bacteria of two distinct strains in co-infected cells, indicates that they dynamically undergo fusion with other rBCVs and possibly also with distant ER structures.

A striking characteristic of rBCVs is the tight wrapping of individual bacteria by its host-derived membranes. During intracellular infection, bacteria numbers double roughly every three hours [34] until large parts of the host cytoplasm are occupied by rBCVs. Segregation of dividing bacteria by host membranes is fast and efficient. Already at late stages of bacterial division - before the separation of daughter cells is completed - the rBCV membranes invaginate at the site of septation. Homotypic fusion of rBCV to produce large vacuoles containing multiple bacteria was hardly ever observed. Thus, the overall membrane surface area of the rBCVs seems to be higher than for most other intracellular bacteria, which do typically grow in more spacious vacuoles that accommodate multiple bacteria [21]. This suggests that substantial amounts of membrane must be recruited to keep bacteria in relatively

confined spaces. If the replicative niche indeed represents stretched ER cisternae, as indicated by our findings, it seems that the volume of the organelle is kept to a minimum at the cost of generating more membrane surface. We speculate that rBCVs undergo fusion/fission events that are orchestrated by host factors normally responsible for the remodeling of the ER [25, 35]. It has been shown that one of the ways of alleviating ER stress is the expansion of cisternae volume through lipid biosynthesis [36]. In future experiments, it would thus be interesting to test whether the presence of *Brucella* inside the ER network triggers this or other mechanisms to increase the membrane surface.

It will also be important to clarify if these processes of membrane expansion in the replicative niche require active signaling by bacteria or are merely a consequence of physical forces caused by growing bacteria. It is well established that the T4SS and possibly its effectors are required for the formation of the rBCV [12]. Recent evidence suggests that the effector BspB is needed for efficient division of *Brucella* in the rBCV [37]. Additionally, the effector VceC was shown to cause ER stress via triggering of the unfolded protein response (UPR) [38, 39]. However, both these effectors play only modulatory roles as they are not essential for rBCV expansion. Moreover, there is evidence that T4SS inactivation in bacteria residing already within an rBCV has limited influence on the rate of *Brucella* replication [40]. Although we cannot rule out the activity of yet unidentified T4SS-independent factors, these data may suggest that following initial entry into the ER lumen bacteria may not need to actively induce membrane acquisition in order to expand the rBCV.

Together, the data support the hypothesis that following entry and initial trafficking along the endocytic network *Brucella* escapes into the ER lumen, rather than isolated ER-derived vacuoles, to establish its replicative niche. This allows the pathogen not only to nurture on nutrients contained within the extended ER network, but also to rely on homeostatic mechanisms of membrane expansion and structure to sustain bacterial growth. Further studies of the replicative niche will provide details about the unique interactions of *Brucella* with ER, and might also shed new light on the fundamental cellular processes responsible for controlling the structure and metabolism of the ER.

MATERIALS AND METHODS

Bacteria strains and plasmids

The plasmid pJC44 encoding the DsRed gene was a kind gift from Jean Celli [41]. The plasmid pJS17 encoding Tet-DsRed and mTagBFP2 was generated from pAC042.08 [42] by replacing the GFP cassette with DsRed for inducible expression and the DsRed cassette with mTagBFP for constitutive expression. Both plasmids were conjugated into *B. abortus* strain 2308. *B. melitensis* strain 16M (Biotype1, ATCC 23456) carrying the plasmid pKSoriT-bla-kan-PsojA-mCherry as described previously [43].

Mammalian cell lines and plasmids

Human cervical carcinoma epithelial cell line (Hela) (ATCC, CCL-2) was maintained in Dulbecco Modified Eagle Medium (DMEM) supplemented with 10% fetal calf serum (FCS). The plasmid carrying the Sec61β-Emerald construct containing an Emerald-GFP gene followed by Sec61β was a kind gift from J. Lippincott-Schwartz [25]. The plasmid carrying the Calnexin-GFP gene was a kind gift from F. van der Goot [29]. Plasmids MDK124-Emerald-Sec61β and MDK124-GFP-Calnexin were generated by cloning the respective constructs it into the pMDK124 vector using the EcoRI and BamHI restriction sites. The plasmids were then used for lentivirus generation and transduction of HeLa cells.

Mammalian cell culture infection

HeLa cells were seeded onto 32 mm gridded glass coverslips (MatTek, Ashland, MA) in a 6-well plate at 150,000 cells per well and incubated overnight. *B. abortus* 2308 strains carrying either pJC44 or pJS17 were grown overnight in TSB medium containing 50 µg/ml kanamycin at 37°C to an OD of 0.8- 1.0. Bacteria were then diluted in DMEM/10% FCS and added to HeLa cells at a final MOI of 2'000. Plates were centrifuged at 400 x *g* for 20 min at 4°C to synchronize bacterial entry. After 2 h of incubation at 37°C and 5% CO_2, extracellular bacteria were killed by exchanging the infection medium by DMEM/10% FCS supplemented with 100 µg/ml gentamicin. After the total infection time indicated in the figure legends, cells were fixed using PHEM fixation buffer (4% formaldehyde, 0.2% glutaraldehyde, 60 mM PIPES, 25 mM HEPES, 10mM EGTA, 4 mM $MgCl_2$) for 90 min. at room temperature. Following fixation, the coverslips were washed in PHEM buffer (60 mM PIPES, 25

mM HEPES, 10 mM EGTA, 4 mM $MgCl_2$) and mounted to 38mm glass slides (BioSystems, Muttenz, Switzerland) using Vectashield H1000 mounting medium (Vector Laboratories, Burlingame, CA) and sealed with nail polish.

Fluorescence microscopy

3D-SIM was performed using a DeltaVision OMX-Blaze system (version 4; GE Healthcare), equipped with 488 and 568 nm solid-state lasers. Images were acquired using a Plan Apo N 60x, 1.42 NA oil immersion objective lens (Olympus) and 4 liquid-cooled sCMOs cameras (pco Edge, full frame 2560 x 2160; Photometrics). Optical z-sections were separated by 0.125 µm. The laser lines 488 and 568 nm were used for 3D-SIM acquisition. Exposure times were typically between 3 and 10 ms, and the power of each laser was adjusted to achieve optimal intensities of between 2,000 and 5,000 counts in a raw image of 15-bit dynamic range at the lowest laser power possible to minimize photobleaching. Multichannel imaging was achieved through sequential acquisition of wavelengths by separate cameras. First, the channels were aligned in the image plane and around the optical axis using predetermined shifts measured using a target lens and the SoftWoRx alignment tool. Afterwards, they were carefully aligned using alignment parameters from control measurements made with 0.5 µm diameter multi-spectral fluorescent beads (Invitrogen, Thermo Fisher Scientific). Raw 3D-SIM images 256 x 256 pixels in size, were recorded. These were processed and reconstructed using the DeltaVision OMX SoftWoRx software package (GE Healthcare) [44]. The resulting size of the reconstructed images was of 512 x 512 pixels from an initial set of 256 x 256 pixel raw images, with a final voxel size of 40 nm x 40 nm x 125 nm.

Confocal images were acquired with an LSM 800 confocal microscope (Zeiss) using a 63x oil objective. Grid coordinates of imaged cells were saved for correlation with electron microscopy. Following image acquisition, coverslips were detached from slides and fixed in cacodylate fixation buffer (2.5% glutaraldehyde, 150 mM sodium cacodylate, 2 mM $MgCl_2$) at 4°C overnight.

Mouse infection and organ collection

Bacterial growth of *B. melitensis* cultures was measured through the culture optical density at 600 nm. Bacterial cultures were spun down, washed with RPMI medium (Gibco) and resuspended for injection in the same medium at a density of 2 x 10^5

CFU/ml. Oestrus of 8–14 weeks old BALB/c females was synchronised 3 days before mating pairs were set up with 3- to 4-month-old males. The following morning, the presence of a vaginal plug was checked and the potentially fertilised females were isolated. That day corresponded to day 0 post-fecundation (PF). At day 10 PF, pregnant females were infected intraperitoneally with 500 µl of bacterial suspension (10^5 bacteria). At day 15 PF, mice were anaesthetised with isoflurane and sacrificed by cervical dislocation, as previously described [45]. All infections were performed at an Animal Biosafety Level 3 facility. Conceptuses were removed from maternal uterine horns and fixed overnight at 4°C in PBS supplemented with 2.5% glutaraldehyde. Tissue fragments were washed several times in cacodylate buffer (150 mM sodium cacodylate, 2 mM $MgCl_2$) at 4°C. The samples were then fixed overnight in 2.5% glutaraldehyde in cacodylate buffer (150 mM sodium cacodylate, 2 mM $MgCl_2$) at 4°C.

Electron microscopy sample preparation

Both cell monolayers and placenta fragments were processed for electron microscopy using the same protocol. Following overnight fixation, samples were washed 3 times with cacodylate buffer (150 mM sodium cacodylate, 2 mM $MgCl_2$) at 4°C. They were then immersed in freshly prepared reduced osmium buffer (2% osmium tetroxide, 150 mM sodium cacodylate, 2 mM $MgCl_2$, 40 mM potassium ferrocyanide) for 1 hour at 4°C. After this initial staining/fixation step, the samples were washed with deionized water at room temperature and immersed in 100 mM thiocarbohydrazide solution for 20 min at room temperature. They were then washed with deionized water and incubated in 2% osmium tetroxide for 30 min at room temperature. This was followed by overnight incubation in 1% uranyl acetate at 4°C. The following morning, the samples were washed in deionized water and incubated in freshly prepared 20mM lead aspartate solution for 30 min at 60°C. They were then dehydrated with ethanol and immersed in 50% solution of durcupan in ethanol for 1 hour. Afterwards, the samples were incubated 2 times in fresh durcupan and placed at 60°C for 48 hours for polymerization.

Focused ion beam scanning electron microscopy

For cell monolayers, the cells of interest were located in the polymerized resin block, trimmed and attached to pre-tilt 45° SEM stubs (Agar Scientific, Stansted, UK) using colloidal silver paint (Ted Pella, Redding, CA), sputter-coated with platinum and

subjected to FIB/SEM tomography. For placenta samples, the resin blocks were cut into small pieces and mounted to flat SEM stubs (Ted Pella, Redding, CA). The blocks were then processed using the EM UC7 microtome (Leica, Wetzlar, Germany). The blocks were initially polished with a glass knife and then a series of 70 nm ultrathin sections was cut using a diamond knife (Diatome, Nidau, Switzerland). Cells carrying bacteria where located in the ultrathin sections using a T12 TEM (FEI, Hillsboro, OR). The corresponding locations were found in the resin blocks and imaged by FIB/SEM. The images were acquired with a Helios NanoLab 650 Dual Beam FIB/SEM using the Slice and View software (FEI, Hillsboro, OR). They had 3072 x 2048 or 2048 x 1780 pixel and were collected using an Elstar in-lens BSE detector at 1.5 kV with a horizontal field width of 15 μm at a working distance of 4.01 mm. The milling was performed with a FIB operating at 30 kV and 0.78 nA beam current. The thickness of the slices was between 10 and 20 nm. Image stacks were aligned using the TrackEM2 plugin of ImageJ [46]. Image analysis and quantification was performed using the IMOD software package [47]. The manual segmentations and 3D representations of the electron microscopy datasets were done using the FEI Amira software (FEI, Hillsboro, OR).

Acknowledgements

We are grateful to the Jean Celli (Washington State University, Pullman, WA) for providing the JC44 plasmid. We thank Dr. Jennifer Lippincott-Schwartz for providing the Emerald-Sec61β construct. We thank Dr. Gisou van der Goot for providing the Calnexin-GFP construct. The authors acknowledge the technical assistance of Marcel Düggelin (ZMB, University of Basel, Switzerland) and Daniel Mathys (SNI, University of Basel, Switzerland) for the assistance with FIB/SEM imaging. We thank the Imaging Core Facility (IMCF, University of Basel, Switzerland) and in particular Alexia Ferrand for the technical assistance provided on the OMX microscope. We would like to thank Maxime Québatte for critical reading of the manuscript.

Competing interests

We have no competing interest to declare.

Funding

This work was supported by grant 31003A_173119 to C.D. from the Swiss National Science Foundation (SNSF, www.snf.ch), advanced grant 340330 to C.D. (FicModFun) from the European Research Council (ERC), grant 51RTP0_151029 to C.D. for the Research and Technology Development (RTD) project TargetInfectX in the frame of SystemsX.ch (www.systemX.ch), the Swiss Initiative for System Biology, and to H.S. The research at UNamur was supported by the Interuniversity Attraction Poles Program initiated by the Belgian Science Policy Office (PAI n° P7/28).

REFERENCES

1. Creasey EA, Isberg RR. Maintenance of vacuole integrity by bacterial pathogens. Curr Opin Microbiol. 2014;17:46-52. doi: 10.1016/j.mib.2013.11.005. PubMed PMID: 24581692; PubMed Central PMCID: PMC4009691.
2. Vergne I, Chua J, Singh SB, Deretic V. Cell biology of mycobacterium tuberculosis phagosome. Annu Rev Cell Dev Biol. 2004;20:367-94. doi: 10.1146/annurev.cellbio.20.010403.114015. PubMed PMID: 15473845.
3. Fratti RA, Chua J, Vergne I, Deretic V. *Mycobacterium tuberculosis* glycosylated phosphatidylinositol causes phagosome maturation arrest. Proc Natl Acad Sci U S A. 2003;100(9):5437-42. doi: 10.1073/pnas.0737613100. PubMed PMID: 12702770; PubMed Central PMCID: PMC154363.

4. Gutierrez MG, Vazquez CL, Munafo DB, Zoppino FC, Beron W, Rabinovitch M, et al. Autophagy induction favours the generation and maturation of the *Coxiella*-replicative vacuoles. Cell Microbiol. 2005;7(7):981-93. doi: 10.1111/j.1462-5822.2005.00527.x. PubMed PMID: 15953030.
5. Delevoye C, Nilges M, Dehoux P, Paumet F, Perrinet S, Dautry-Varsat A, et al. SNARE protein mimicry by an intracellular bacterium. PLoS Pathog. 2008;4(3):e1000022. doi: 10.1371/journal.ppat.1000022. PubMed PMID: 18369472; PubMed Central PMCID: PMC2265411.
6. Celli J, Tsolis RM. Bacteria, the endoplasmic reticulum and the unfolded protein response: friends or foes? Nat Rev Microbiol. 2015;13(2):71-82. doi: 10.1038/nrmicro3393. PubMed PMID: 25534809; PubMed Central PMCID: PMC4447104.
7. Pappas G, Akritidis N, Bosilkovski M, Tsianos E. Brucellosis. N Engl J Med. 2005;352(22):2325-36. doi: 10.1056/NEJMra050570. PubMed PMID: 15930423.
8. Archambaud C, Salcedo SP, Lelouard H, Devilard E, de Bovis B, Van Rooijen N, et al. Contrasting roles of macrophages and dendritic cells in controlling initial pulmonary *Brucella* infection. Eur J Immunol. 2010;40(12):3458-71. doi: 10.1002/eji.201040497. PubMed PMID: 21108467.
9. Atluri VL, Xavier MN, de Jong MF, den Hartigh AB, Tsolis RM. Interactions of the human pathogenic *Brucella* species with their hosts. Annu Rev Microbiol. 2011;65:523-41. doi: 10.1146/annurev-micro-090110-102905. PubMed PMID: 21939378.
10. Pizarro-Cerda J, Meresse S, Parton RG, van der Goot G, Sola-Landa A, Lopez-Goni I, et al. *Brucella abortus* transits through the autophagic pathway and replicates in the endoplasmic reticulum of nonprofessional phagocytes. Infect Immun. 1998;66(12):5711-24. PubMed PMID: 9826346; PubMed Central PMCID: PMC108722.
11. Pizarro-Cerda J, Moreno E, Sanguedolce V, Mege JL, Gorvel JP. Virulent *Brucella abortus* prevents lysosome fusion and is distributed within autophagosome-like compartments. Infect Immun. 1998;66(5):2387-92. PubMed PMID: 9573138; PubMed Central PMCID: PMC108212.
12. Comerci DJ, Martinez-Lorenzo MJ, Sieira R, Gorvel JP, Ugalde RA. Essential role of the VirB machinery in the maturation of the *Brucella abortus*-containing vacuole. Cell Microbiol. 2001;3(3):159-68. PubMed PMID: 11260139.
13. Celli J, de Chastellier C, Franchini DM, Pizarro-Cerda J, Moreno E, Gorvel JP. *Brucella* evades macrophage killing via VirB-dependent sustained interactions with the endoplasmic reticulum. J Exp Med. 2003;198(4):545-56. doi: 10.1084/jem.20030088. PubMed PMID: 12925673; PubMed Central PMCID: PMC2194179.
14. Bellaire BH, Roop RM, 2nd, Cardelli JA. Opsonized virulent *Brucella abortus* replicates within nonacidic, endoplasmic reticulum-negative, LAMP-1-positive phagosomes in human monocytes. Infect Immun. 2005;73(6):3702-13. doi: 10.1128/IAI.73.6.3702-3713.2005. PubMed PMID: 15908400; PubMed Central PMCID: PMC1111828.
15. Porte F, Liautard JP, Kohler S. Early acidification of phagosomes containing *Brucella suis* is essential for intracellular survival in murine macrophages. Infect Immun. 1999;67(8):4041-7. PubMed PMID: 10417172; PubMed Central PMCID: PMC96697.
16. Boschiroli ML, Ouahrani-Bettache S, Foulongne V, Michaux-Charachon S, Bourg G, Allardet-Servent A, et al. The *Brucella suis* virB operon is induced intracellularly in macrophages. Proc Natl Acad Sci U S A. 2002;99(3):1544-9. doi: 10.1073/pnas.032514299. PubMed PMID: 11830669; PubMed Central PMCID: PMC122227.
17. Myeni S, Child R, Ng TW, Kupko JJ, 3rd, Wehrly TD, Porcella SF, et al. *Brucella* modulates secretory trafficking via multiple type IV secretion effector proteins. PLoS Pathog. 2013;9(8):e1003556. doi: 10.1371/journal.ppat.1003556. PubMed PMID: 23950720; PubMed Central PMCID: PMC3738490.

18. Lestrate P, Delrue RM, Danese I, Didembourg C, Taminiau B, Mertens P, et al. Identification and characterization of in vivo attenuated mutants of *Brucella melitensis*. Mol Microbiol. 2000;38(3):543-51. PubMed PMID: 11069678.
19. Taguchi Y, Imaoka K, Kataoka M, Uda A, Nakatsu D, Horii-Okazaki S, et al. Yip1A, a novel host factor for the activation of the IRE1 pathway of the unfolded protein response during *Brucella* infection. PLoS Pathog. 2015;11(3):e1004747. doi: 10.1371/journal.ppat.1004747. PubMed PMID: 25742138; PubMed Central PMCID: PMC4350842.
20. Starr T, Child R, Wehrly TD, Hansen B, Hwang S, Lopez-Otin C, et al. Selective subversion of autophagy complexes facilitates completion of the *Brucella* intracellular cycle. Cell Host Microbe. 2012;11(1):33-45. doi: 10.1016/j.chom.2011.12.002. PubMed PMID: 22264511; PubMed Central PMCID: PMC3266535.
21. Case ED, Smith JA, Ficht TA, Samuel JE, de Figueiredo P. Space: A Final Frontier for Vacuolar Pathogens. Traffic. 2016;17(5):461-74. doi: 10.1111/tra.12382. PubMed PMID: 26842840.
22. Detilleux PG, Deyoe BL, Cheville NF. Entry and intracellular localization of *Brucella* spp. in Vero cells: fluorescence and electron microscopy. Vet Pathol. 1990;27(5):317-28. doi: 10.1177/030098589002700503. PubMed PMID: 2122572.
23. Anderson TD, Cheville NF, Meador VP. Pathogenesis of placentitis in the goat inoculated with *Brucella abortus*. II. Ultrastructural studies. Vet Pathol. 1986;23(3):227-39. doi: 10.1177/030098588602300302. PubMed PMID: 3088810.
24. Detilleux PG, Deyoe BL, Cheville NF. Penetration and intracellular growth of *Brucella abortus* in nonphagocytic cells in vitro. Infect Immun. 1990;58(7):2320-8. PubMed PMID: 2114362; PubMed Central PMCID: PMC258815.
25. Nixon-Abell J, Obara CJ, Weigel AV, Li D, Legant WR, Xu CS, et al. Increased spatiotemporal resolution reveals highly dynamic dense tubular matrices in the peripheral ER. Science. 2016;354(6311). doi: 10.1126/science.aaf3928. PubMed PMID: 27789813.
26. Knott G, Rosset S, Cantoni M. Focussed ion beam milling and scanning electron microscopy of brain tissue. J Vis Exp. 2011;(53):e2588. doi: 10.3791/2588. PubMed PMID: 21775953; PubMed Central PMCID: PMC3196160.
27. Mellouk N, Weiner A, Aulner N, Schmitt C, Elbaum M, Shorte SL, et al. Shigella subverts the host recycling compartment to rupture its vacuole. Cell Host Microbe. 2014;16(4):517-30. doi: 10.1016/j.chom.2014.09.005. PubMed PMID: 25299335.
28. Alcantara CL, Vidal JC, de Souza W, Cunha ESNL. The cytostome-cytopharynx complex of *Trypanosoma cruzi* epimastigotes disassembles during cell division. J Cell Sci. 2017;130(1):164-76. doi: 10.1242/jcs.187419. PubMed PMID: 27363990.
29. Lakkaraju AK, Abrami L, Lemmin T, Blaskovic S, Kunz B, Kihara A, et al. Palmitoylated calnexin is a key component of the ribosome-translocon complex. EMBO J. 2012;31(7):1823-35. doi: 10.1038/emboj.2012.15. PubMed PMID: 22314232; PubMed Central PMCID: PMC3321195.
30. Okiyoneda T, Harada K, Takeya M, Yamahira K, Wada I, Shuto T, et al. Delta F508 CFTR pool in the endoplasmic reticulum is increased by calnexin overexpression. Mol Biol Cell. 2004;15(2):563-74. doi: 10.1091/mbc.E03-06-0379. PubMed PMID: 14595111; PubMed Central PMCID: PMC329241.
31. Zeuschner D, Geerts WJ, van Donselaar E, Humbel BM, Slot JW, Koster AJ, et al. Immuno-electron tomography of ER exit sites reveals the existence of free COPII-coated transport carriers. Nat Cell Biol. 2006;8(4):377-83. doi: 10.1038/ncb1371. PubMed PMID: 16531996.
32. Tilney LG, Harb OS, Connelly PS, Robinson CG, Roy CR. How the parasitic bacterium *Legionella pneumophila* modifies its phagosome and transforms it into rough ER: implications for conversion of plasma membrane to the ER membrane. J Cell Sci. 2001;114(Pt 24):4637-50. PubMed PMID: 11792828.

33. Robinson CG, Roy CR. Attachment and fusion of endoplasmic reticulum with vacuoles containing *Legionella pneumophila*. Cell Microbiol. 2006;8(5):793-805. doi: 10.1111/j.1462-5822.2005.00666.x. PubMed PMID: 16611228.
34. Gamazo C, Vitas AI, Lopez-Goni I, Diaz R, Moriyon I. Factors affecting detection of *Brucella melitensis* by BACTEC NR730, a nonradiometric system for hemocultures. J Clin Microbiol. 1993;31(12):3200-3. PubMed PMID: 8308111; PubMed Central PMCID: PMC266375.
35. English AR, Voeltz GK. Rab10 GTPase regulates ER dynamics and morphology. Nat Cell Biol. 2013;15(2):169-78. doi: 10.1038/ncb2647. PubMed PMID: 23263280; PubMed Central PMCID: PMC3582403.
36. Schuck S, Prinz WA, Thorn KS, Voss C, Walter P. Membrane expansion alleviates endoplasmic reticulum stress independently of the unfolded protein response. J Cell Biol. 2009;187(4):525-36. doi: 10.1083/jcb.200907074. PubMed PMID: 19948500; PubMed Central PMCID: PMC2779237.
37. Miller CN, Smith EP, Cundiff JA, Knodler LA, Bailey Blackburn J, Lupashin V, et al. A *Brucella* Type IV Effector Targets the COG Tethering Complex to Remodel Host Secretory Traffic and Promote Intracellular Replication. Cell Host Microbe. 2017. doi: 10.1016/j.chom.2017.07.017. PubMed PMID: 28844886.
38. Wang X, Lin P, Li Y, Xiang C, Yin Y, Chen Z, et al. *Brucella suis* Vaccine Strain 2 Induces Endoplasmic Reticulum Stress that Affects Intracellular Replication in Goat Trophoblast Cells In vitro. Front Cell Infect Microbiol. 2016;6:19. doi: 10.3389/fcimb.2016.00019. PubMed PMID: 26904517; PubMed Central PMCID: PMC4746994.
39. Keestra-Gounder AM, Byndloss MX, Seyffert N, Young BM, Chavez-Arroyo A, Tsai AY, et al. NOD1 and NOD2 signalling links ER stress with inflammation. Nature. 2016;532(7599):394-7. doi: 10.1038/nature17631. PubMed PMID: 27007849; PubMed Central PMCID: PMC4869892.
40. Smith EP, Miller CN, Child R, Cundiff JA, Celli J. Postreplication Roles of the *Brucella* VirB Type IV Secretion System Uncovered via Conditional Expression of the VirB11 ATPase. MBio. 2016;7(6). doi: 10.1128/mBio.01730-16. PubMed PMID: 27899503; PubMed Central PMCID: PMC5137499.
41. Starr T, Ng TW, Wehrly TD, Knodler LA, Celli J. *Brucella* intracellular replication requires trafficking through the late endosomal/lysosomal compartment. Traffic. 2008;9(5):678-94. doi: 10.1111/j.1600-0854.2008.00718.x. PubMed PMID: 18266913.
42. Casanova A, Low SH, Emmenlauer M, Conde-Alvarez R, Salcedo SP, Gorvel JP, et al. Microscopy-based Assays for High-throughput Screening of Host Factors Involved in *Brucella* Infection of Hela Cells. J Vis Exp. 2016;(114). doi: 10.3791/54263. PubMed PMID: 27584799.
43. Copin R, Vitry MA, Hanot Mambres D, Machelart A, De Trez C, Vanderwinden JM, et al. In situ microscopy analysis reveals local innate immune response developed around *Brucella* infected cells in resistant and susceptible mice. PLoS Pathog. 2012;8(3):e1002575. doi: 10.1371/journal.ppat.1002575. PubMed PMID: 22479178; PubMed Central PMCID: PMC3315488.
44. Gustafsson MG. Surpassing the lateral resolution limit by a factor of two using structured illumination microscopy. J Microsc. 2000;198(Pt 2):82-7. PubMed PMID: 10810003.
45. Barbier T, Machelart A, Zuniga-Ripa A, Plovier H, Hougardy C, Lobet E, et al. Erythritol Availability in Bovine, Murine and Human Models Highlights a Potential Role for the Host Aldose Reductase during Brucella Infection. Front Microbiol. 2017;8:1088. doi: 10.3389/fmicb.2017.01088. PubMed PMID: 28659902; PubMed Central PMCID: PMC5468441.
46. Cardona A, Saalfeld S, Preibisch S, Schmid B, Cheng A, Pulokas J, et al. An integrated micro- and macroarchitectural analysis of the *Drosophila* brain by computer-assisted serial section electron microscopy. PLoS Biol. 2010;8(10). doi:

10.1371/journal.pbio.1000502. PubMed PMID: 20957184; PubMed Central PMCID: PMC2950124.
47. Kremer JR, Mastronarde DN, McIntosh JR. Computer visualization of three-dimensional image data using IMOD. J Struct Biol. 1996;116(1):71-6. doi: 10.1006/jsbi.1996.0013. PubMed PMID: 8742726.

FIGURE LEGENDS

Fig. 1. 3-dimensional structure of the rBCV revealed with correlative FIB/SEM tomography. (**A**) SIM microscopy of a HeLa cell expressing the ER marker Emerald-Sec61β (green), infected with *B. abortus*-dsRed (magenta). Emerald-Sec61β staining circumscribes bacteria and localizes to adjacent ER cisternae. Some of the bacteria are undergoing division (arrow heads). The yellow box indicates an area that was later imaged using FIB/SEM. (**B**) Single image from a FIB/SEM tomogram depicting the area marked in (A). rBCVs are seen as confined, single-membrane vacuoles. The BCVs containing dividing bacteria tighten next to the division septum formed as the daughter cells separate (arrow heads). Some rBCVs are occupied by more than one bacterium (arrow). The orange box indicates the rBCV shown as a 3D reconstruction in (C). (**C**) 3D reconstruction of the site marked in (B), showing the rBCV membrane and adjacent ER cisternae (yellow). The dividing bacteria (magenta) are efficiently enclosed by the rBCV membrane, which tightens around the septum formed as cell division progresses (arrow heads). (**D**) Single section from a FIB/SEM tomogram of a mouse trophoblast, 5 d.p.i with *B. melitensis*. Large areas of the cell are filled with dividing bacteria. The orange box indicates the rBCV that is shown in 3D in (E). (**E**) 3D reconstruction of the site marked in (D). The rBCV and neighboring ER structures are shown in yellow, mitochondria are shown in cyan. Similar to *B. abortus* in (C), cell division is followed by fission of the rBCV (arrow heads) eventually giving rise to daughter cells residing in separate rBCV subcompartments. M: mitochondria; G: Golgi stacks; N: nucleus. Scale bars: 3 μm (A); 1 μm (B, D); 500 nm (C, E)

Fig. 2. Interactions between BCVs and organelles revealed by 3D FIB/SEM

(**A**) FIB/SEM of a HeLa cell infected with *B. abortus* 24 h.p.i. Consecutive z-planes from a tomogram show a single rBCV (asterisk). Small protrusions can be observed originating from the surface of the vacuoles (left panel, arrow head). The protrusion

indicated was found to be continuous with the surrounding ER cisternae (right panel, arrow) upon examination of the entire 3D stack. (**B**) 3D reconstruction of the site in (A) reveals that the rBCV forms a connection (arrow) with the neighboring organelle membranes, which are a part of an extended ER mesh. (**C**) Images from a FIB/SEM tomogram of a mouse trophoblast at 5 d.p.i. with *B. melitensis*. The rBCV has extensions (arrow heads) that were traced across the tomogram and found to be continuous with other host membranes. (**D**) 3D reconstruction of the site from (C). The protrusions of the rBCVs (yellow) are continuous with a mesh of host ER membranes (yellow). The membranes form an interface with a Golgi stack (orange). A number of vesicles (green) are clustered at the interface and around the Golgi stack. (**E**) FIB/SEM of a HeLa cell infected with *B. abortus* 24 h.p.i. Two different z-planes (heights) of the same site in a FIB/SEM stack are shown. A protrusion from a BCV (left panel, arrow head) is continuous with an ER cisterna that originates from the outer nuclear membrane (right panel, arrow head). (**F**) 3D reconstruction of the site from (E) showing four bacteria (red) located in a large rBCV that is continuous with ER cisternae (arrow head) originating from the outer nuclear membrane (orange, arrow). (**G**) Images from a FIB/SEM tomogram of a mouse trophoblast at 5 d.p.i. with *B. melitensis*. The rBCVs visible in the images (asterisks) are continuous with the outer nuclear membrane of the host cell. Nuclear pore complexes (NPCs) are marked with arrow heads. (**H**) 3D reconstruction of the site from (G) indicates that the bacteria (red) are located in an extension of the nuclear envelope (yellow). NPCs are marked with arrow heads. (**I**) FIB/SEM of a HeLa cell infected with *B. abortus* 24 h.p.i. Consecutive z-planes from a tomogram show a group of rBCVs (asterisks). The membrane of the BCVs is continuous (arrow heads), resulting in several bacteria being located in the same lumen. (**J**) 3D reconstruction of the site depicted in (I). All the indicated bacteria (red) are located in a large, continuous rBCV (yellow), connected by narrow extensions of the membrane (arrow heads). (**K**) FIB/SEM of a HeLa cell infected with *B. abortus* 24 h.p.i. One of the rBCVs (asterisk) has several contact sites with surrounding ER cisternae (arrow heads). In some cases, we observed protrusions of the BCV membrane, indicating potential tethering between the lipid bilayers. (**L**) 3D reconstruction of the site depicted in (K). The tethered membranes (yellow) are ER cisternae that share contact sites (arrow heads) with the BCV (yellow). N: nucleus; NPC: nuclear pore complex. Scale bars: 600 nm

Fig. 3. CLEM reveals that BCV extensions colocalize with Emerald-Sec61β.
(**A**) SIM image of HeLa expressing Emerald-Sec61β infected with *B. abortus*-dsRed for 24 h. The bacteria (magenta) are dividing inside Sec61β-positive rBCVs (green). The resolution allows the ER mesh located in the proximity of the rBCVs to be distinguished. The marked area was imaged by FIB/SEM tomography. (**B**) Single frame from a FIB/SEM tomogram of the site marked in (A) showing stretches of flat cisternae distributed between the rBCVs (arrow heads). (**C**) 3D reconstruction of a site marked in (B). Volumes generated by SIM (top) and FIB/SEM (bottom). Reconstruction of the SIM data, showing bacteria (magenta) and Sec61β-positive structures (green). The FIB/SEM reconstruction reveals the location of rBCVs (orange) and the ER, including the nuclear envelope (yellow). The two volumes were superimposed (middle) to indicate the colocalization of the Sec61β-GFP marker with the ER structures as well as the rBCV membranes. (**D**) Two rBCVs from (C) displayed with the same color code. Extensions of the BCV membrane are continuous with ER cisternae (arrow heads). The ER characteristic of the membranes reconstructed from the FIB/SEM tomogram (yellow), is confirmed by the superimposed Sec61β-GFP signal from SIM microscopy (middle). Scale bars: 1.5 μm (A-C); 500 nm (D)

Fig. 4. The replicative niche of *Brucella* constitutes an extended, complex compartment that spans large volumes of the host cell. (**A**) Single frame from a FIB/SEM tomogram of a HeLa cell infected with *B. abortus* 24 h.p.i. Most of the bacteria appear to be located in individual, single membrane rBCVs. (**B**) 3D reconstruction of the FIB/SEM tomogram from (A). ER membranes (yellow) form an extended mesh that surrounds the rBCVs (orange and cyan). A large proportion of the rBCVs (orange) are continuous with the ER cisternae, sharing a common lumen with the entire ER network. rBCVs for which the connection was not visible in the EM data are colored in cyan. (**C, D**) Similar to (A, B), but the FIB/SEM data depicts a mouse trophoblast infected with *B. melitensis* at 5 d.p.i. The ER mesh forms connections with many of the rBCVs (orange), indicating that the vacuoles are to a large extent continuous with the ER network. N: nucleus. Scale bars: 1.5 μm (A, B); 1 μm (C, D)

Fig. 5. rBCVs undergo limited fusion. (**A**) Confocal microscope image of HeLa cell expressing Emerald-Sec61β (green), coinfected with *B. abortus*-BFP (blue) and *B. abortus*-dsRed (magenta), 24 h.p.i. Bacteria are located inside Sec61β-positive compartments. The marked area was imaged using FIB/SEM. (**B**) Single image form a FIB/SEM tomogram of the site marked in (A). Bacteria were colored magenta or blue based on the confocal data, depending on which of the two strains they represent. (**C**) 3D reconstruction of the site marked in (B), including bacteria from both strains. There is membrane continuity between rBCVs belonging to the same (arrow heads) or different strains (arrow), although the latter kind of connection is limited to small surfaces. (**D**) 3D reconstruction depicting several BCVs (blue or magenta bacteria visible inside) and parts of the ER mesh (yellow) across the FIB/SEM tomogram. All BCVs present in the reconstruction were found to be continuous with the same network of ER cisternae (arrow heads), constituting a single, extended organelle. Scale bars: 6 μm (A); 2 μm (B); 700 nm (C, D)

Fig. S1. Calnexin-GFP overexpression triggers multi-layered rBCVs consistent with ER localization. (**A**) SIM microscopy of a HeLa cell expressing Calnexin-GFP (green), infected with *B. abortus*-dsRed (magenta), 48 h.p.i. The ER marker is localized around the bacteria (arrow heads). (**B**) Slice from a FIB/SEM tomogram of the site marked in (A). There are multi-layered structures formed by ER membranes, often located around the BCVs (arrow heads). Scale bars: 3.5 μm (A); 1.3 μm (B)

Fig. S2. Resolution limitations of FIB/SEM tomograms. (**A**) Two slices of a FIB/SEM tomogram of a HeLa cell infected with B. abortus, 24 h.p.i. There are thin ER cisternae that touch the surface of the BCV (arrow heads). At this resolution some of the ER structures in HeLa cells are too narrow to determine whether the two organelles are continuous. (**B**) FIB/SEM tomogram of a mouse trophoblast, 5 d.p.i. The ER structures of trophoblasts were found to be typically more spacious and the connections with BCVs (arrow head) are thus resolved more faithfully. Scale bars: 500 nm

Movie 1. FIB/SEM reveals 3D organisation of ER and rBCVs. FIB/SEM tomogram of a HeLa cell 24 h.p.i. depicting an single rBCV. The ER cisternae in proximity of the rBCV (arrows) are connected to the vacuole through a thin membrane extension (arrow head).

3.1.3. Figures

Figure 1

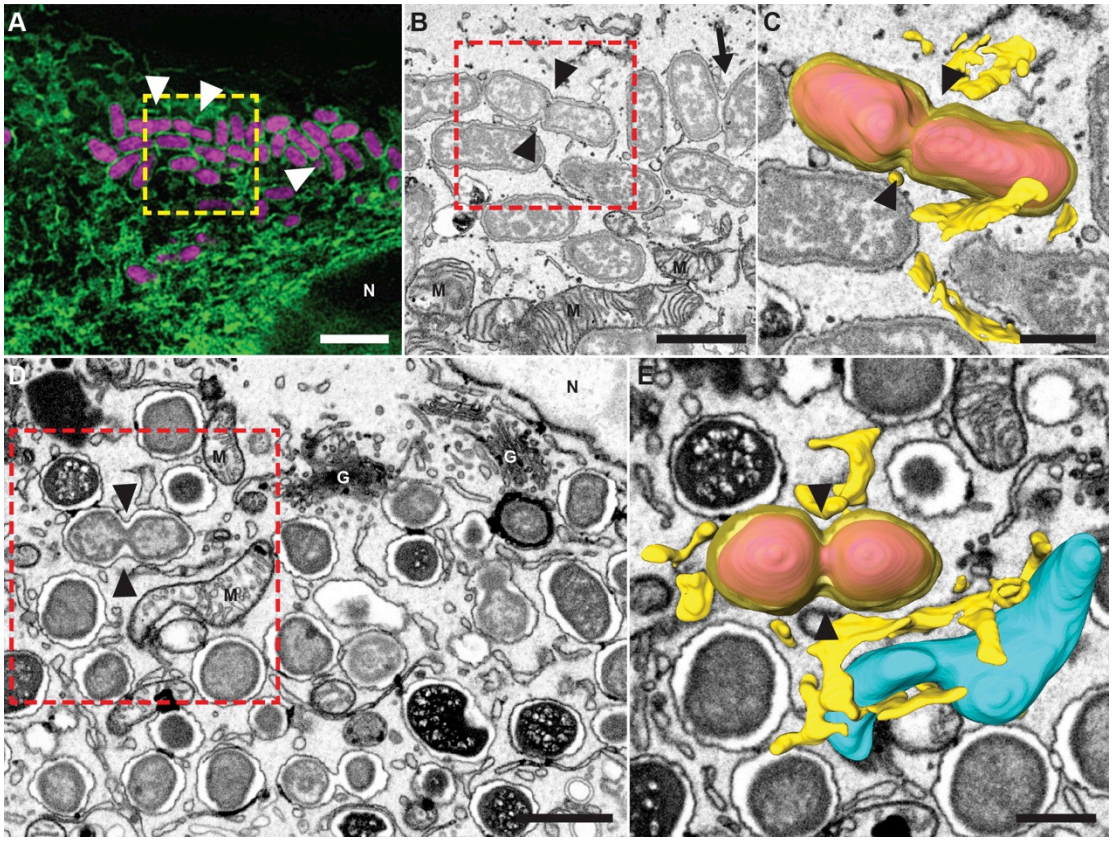

Figure 2

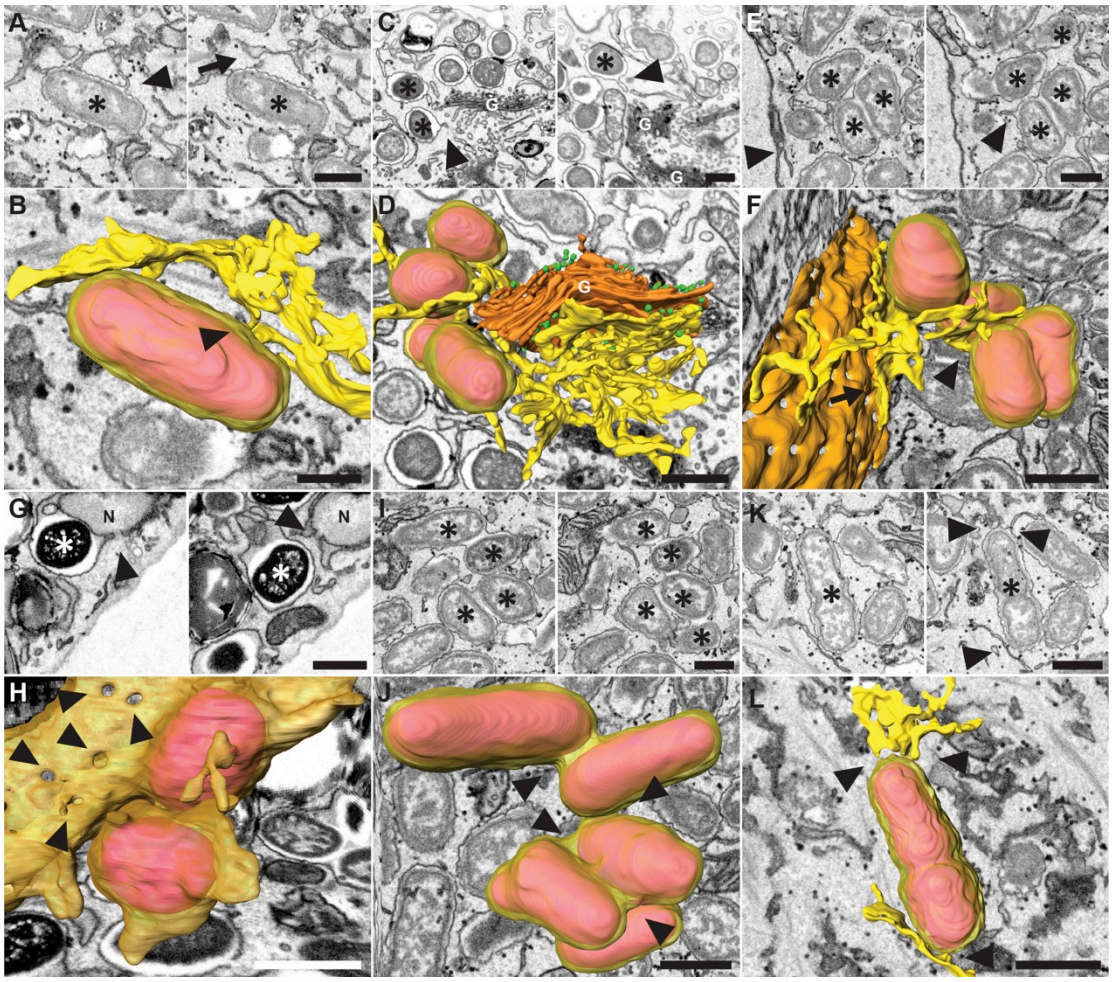

Figure 3

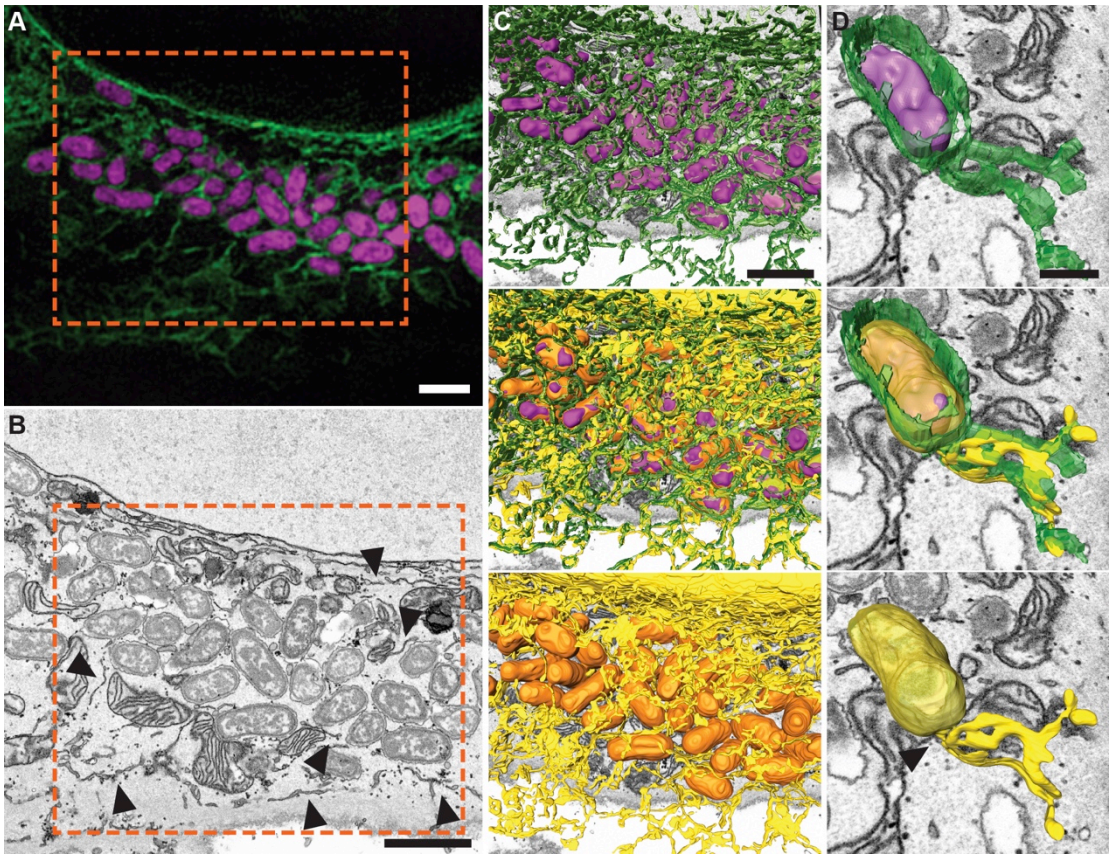

Figure 4

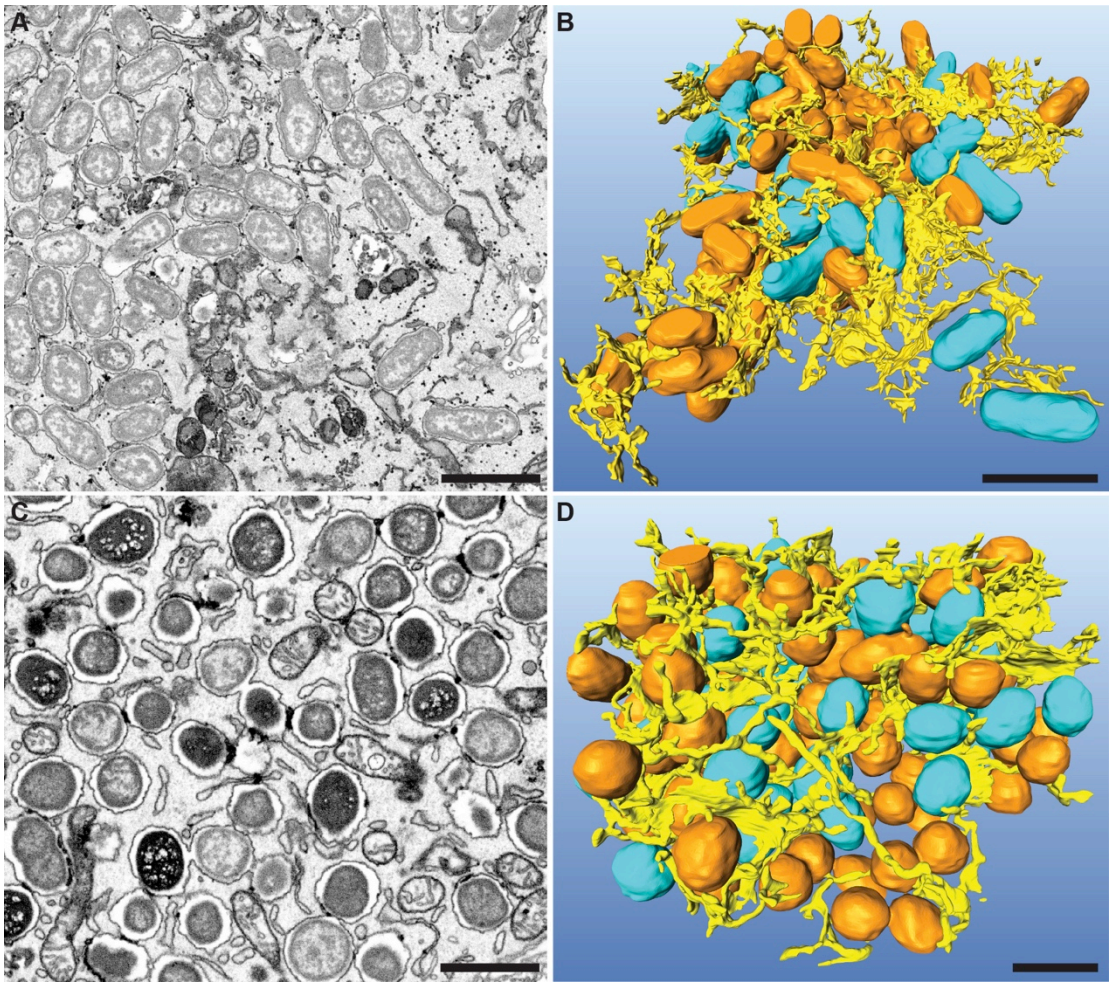

Figure 5

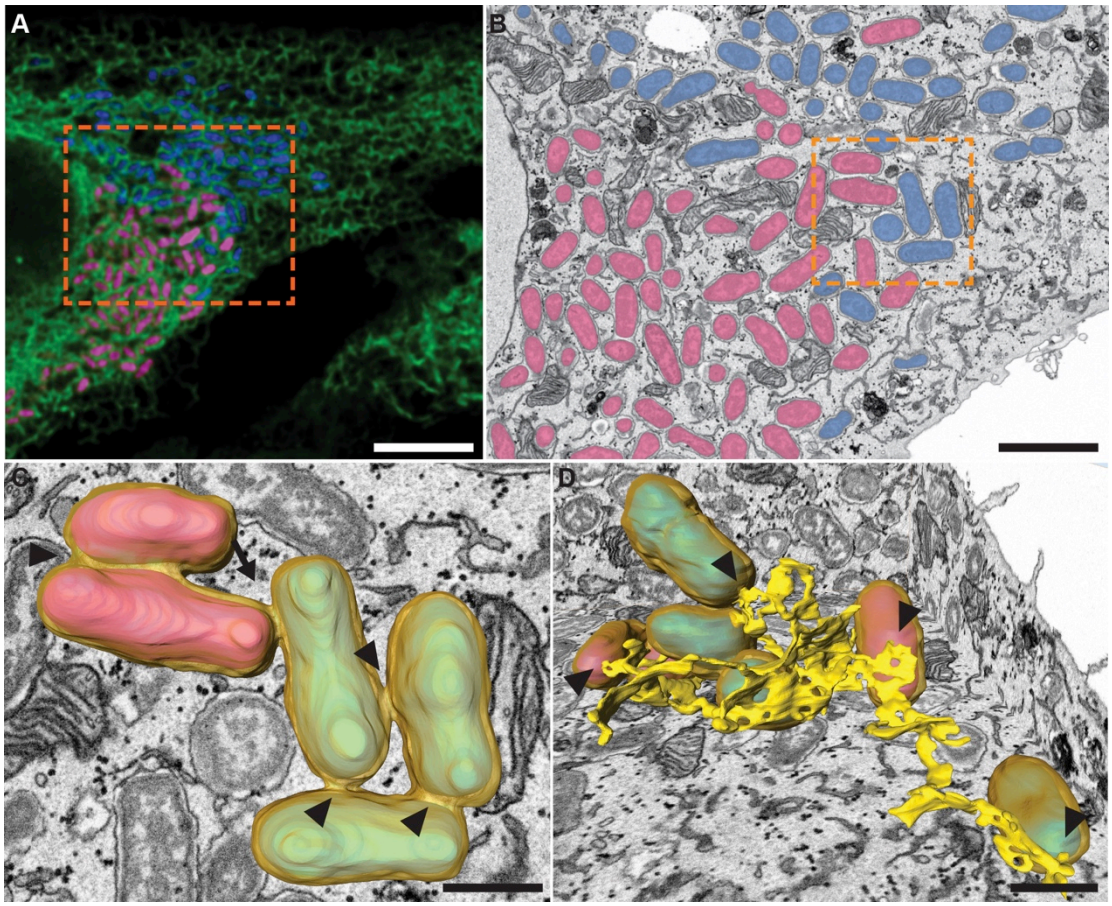

Figure S1

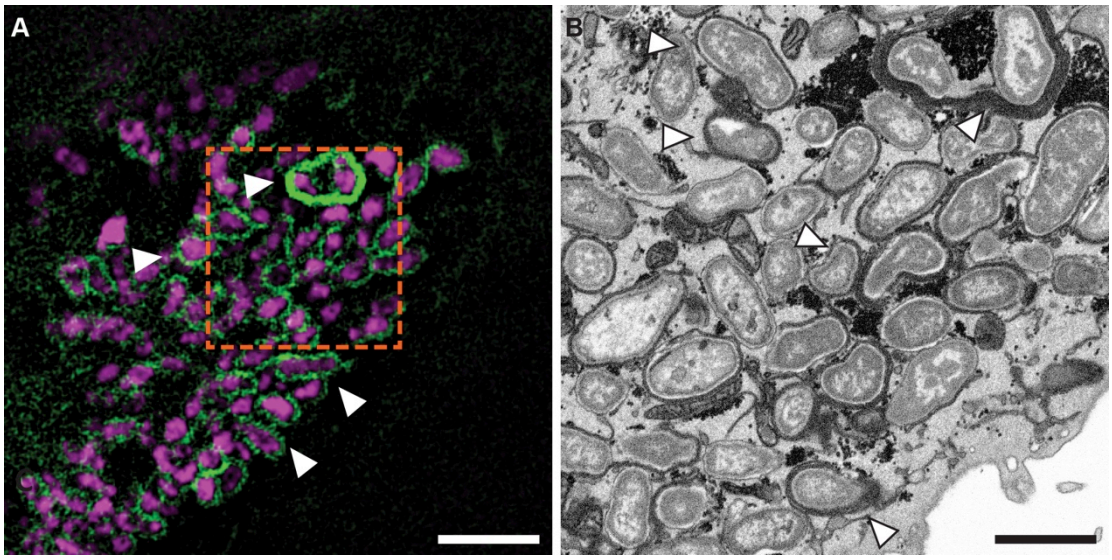

Figure S2

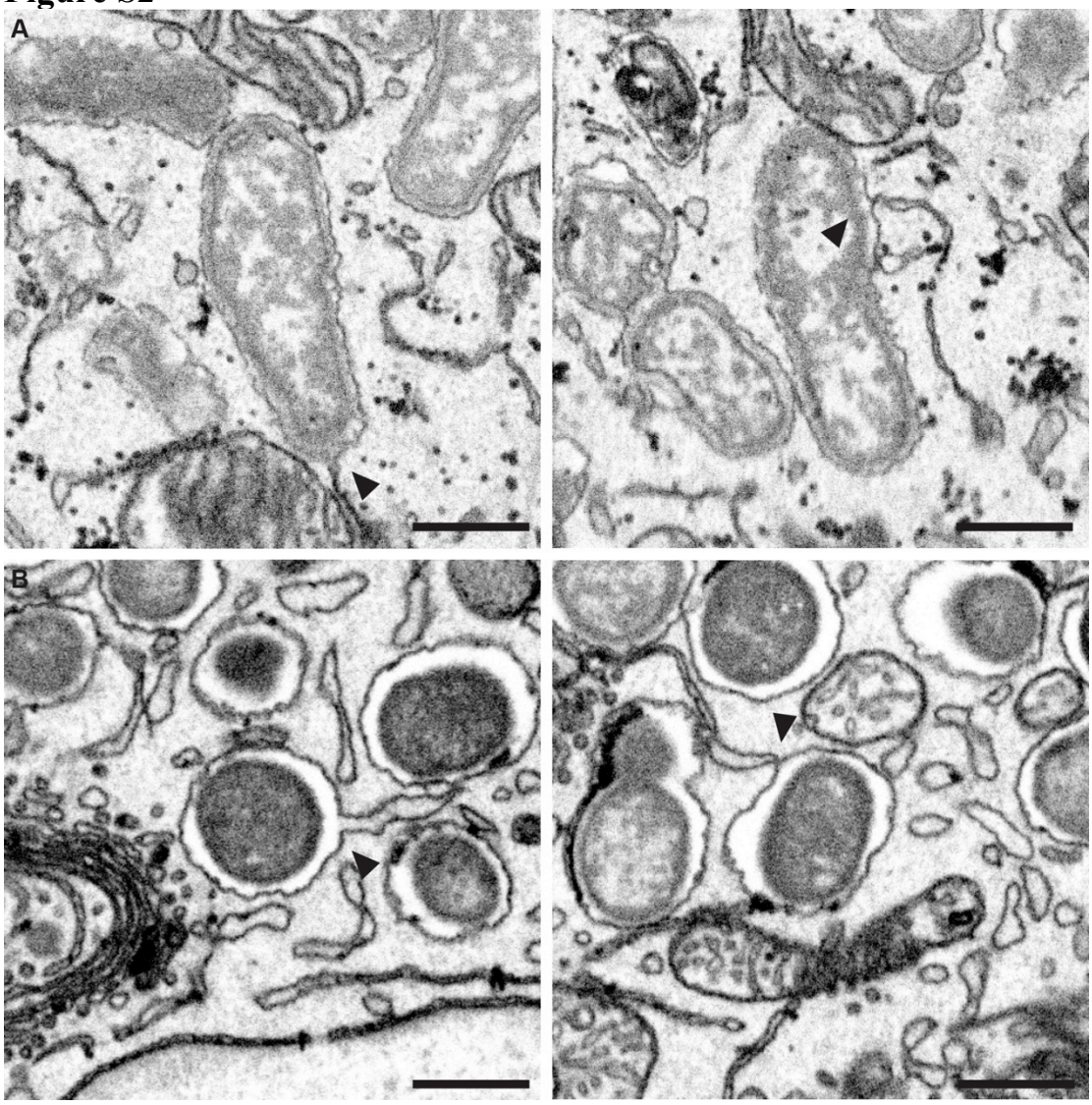

3.2. Research article II (in preparation)

A new role for endosome-to-Golgi transport in *Brucella* infection revealed by genome-wide siRNA screen

Alain Casanova, Shyan Huey Low, Therese Tschon, Jaroslaw Sedzicki, Mario Emmenlauer, Kevin Smith, Nicolas Bennett, Peter Bühlmann, Houchaima Ben-Tekaya, Maxime Québatte, and Christoph Dehio

Manuscript in preparation

3.2.1. Statement of own contribution

I was responsible for establishing a confocal microscopy-based approach for assessing the influence of siRNAs on the dynamics of *Brucella* intermediate trafficking. This was used to confirm the role of vps35 siRNA in the establishment of the replicative niche by Brucella abortus inside HeLa cells.

3.2.2. Manuscript

A new role for endosome-to-Golgi transport in *Brucella* infection revealed by genome-wide siRNA screen

Alain Casanova[1¶,#a], Shyan Huey Low[1¶,#b], Therese Tschon[1], Jaroslaw Sedzicki[1,2], Mario Emmenlauer[1, #c], Kevin Smith[1,#d], Nicolas Bennett[3], Peter Bühlmann[3], Houchaima Ben-Tekaya[1], Maxime Québatte[1], and Christoph Dehio[1*]

[1] Focal Area Infection Biology, Biozentrum, University of Basel, Switzerland

[2] C-CINA, Biozentrum, University of Basel, Switzerland

[3] Seminar for Statistics, ETH Zürich, Switzerland

[#a] Current address: Novartis AG, Basel, Switzerland

[#b] Current address: Lee Kong Chian School of Medicine, Nanyang Technological University

[#c] Current address: BioDataAnalysis GmbH, Munich, Germany

[#d] Current address: Science for Life Laboratory, KTH Royal Institute of Technology, School of Computer Science and Communication, Solna, Sweden

* Corresponding author

Email: **christoph.dehio@unibas.ch**

[¶]These authors contributed equally to this work

Author Summary

With about 500,000 new cases of human brucellosis annually worldwide *Brucella* is regarded as the most important zoonotic bacterial pathogen. The causing agent of brucellosis resides inside host cells within vacuoles termed *Brucella* containing vacuoles (BCVs). Although several host components important for escape of the degradative lysosomal pathway and the establishment of an ER-derived replicative BCV have been identified, a global understanding of this highly coordinated process is still missing. In this study we took a systems level approach to gain a deeper insight into these fundamental questions by performing a genome-wide RNA interference (RNAi) screen aiming at identifying host factors involved in *Brucella* cellular entry, intracellular trafficking, and replication. We identified more than 500 host proteins that contribute to *Brucella* intracellular replication, which could be assigned to major cellular pathways. Among these, we identified a critical role for the retromer – a trafficking pathway that mediates endosome-to-Golgi transport. Taken together, this study sheds light on previously unidentified host pathways required during *Brucella* infection cycle and identifies the role played by the retromer in the establishment of *Brucella* replicative niche.

Abstract

Brucella, the causing agent of brucellosis, is a major zoonotic pathogen that resides and replicates inside infected host cells in membrane-bound vacuoles called BCVs (*Brucella*-containing vacuoles). Following uptake, *Brucella* interacts with host components to avoid the fusion of the BCVs with lysosomes and to eventually allow the establishment of an endoplasmic reticulum-derived replicative niche. Despite the importance of host-components for the *Brucella* life cycle, a holistic view on the factors controlling *Brucella* cell entry, trafficking and replication is still missing. Here we used a systematic cell-based siRNA knockdown screen in HeLa cells infected with *Brucella abortus* and identified 507 components of the human infectome for *Brucella* infection, including multiple components of pathways involved in mitotic cell cycle, actin remodeling, TOR, TGF-β or FGF signaling and endosome-to-Golgi transport. Using a pathogen entry assay we revealed the importance of endosome-to-Golgi trafficking components for post-entry infection processes. Further, using complementation assays, chemical inhibition, and single-cell resolution co-localization assay, we demonstrate the requirement of the retromer − and more specifically its cargo recognition complex component Vps35 − for *Brucella* to escape the lysosomal degradative pathway and to establish its intracellular replicative niche. We thus reveal a novel trafficking route critical for *Brucella* intracellular infection and describe a new role of the retromer complex during *Brucella* infection.

INTRODUCTION

Cellular invasion is a common strategy to escape host defenses and to establish a protected replicative niche that is shared by intracellular bacterial pathogens of human and animals, such as *Salmonella*, *Shigella*, *Listeria*, *Legionella*, *Bartonella* and *Brucella* [1]. Knowledge of the host cellular pathways that are subverted by these pathogenic bacteria to reach their intracellular replicative niches might be instructive for the development of new treatment strategies to control the resulting infectious diseases.

Brucella is a facultative intracellular zoonotic pathogen causing animal and human brucellosis. With about 500,000 new cases of human brucellosis annually worldwide *Brucella* is regarded as the most important zoonotic bacterial pathogen [2, 3]. There is currently no effective vaccination for humans and even a prolonged combinatory antibiotic treatment is not able to completely protect against relapses [4]. Therefore, *Brucella* remains a significant threat to the economy as well as public health in endemic areas.

At the cellular level, *Brucella* infects phagocytic as well as non-phagocytic cells where bacteria replicate and persist inside membrane-bound vesicles – the *Brucella* containing vacuoles (BCVs). BCVs sequentially interact with components of the host endocytic pathway to reach the replicative niche, a network of endoplasmic reticulum (ER) - derived vesicles labeled with ER-specific markers, such as Sec61 and calnexin [5, 6]. Several critical steps for the intracellular journey of *Brucella* have been identified together with their associated host factors through various studies. Adherence to the host cell surface is mediated via interaction with sialic acid residues or binding to fibronectin and vitronectin [7, 8]. Internalization requires actin remodeling via the activity of the small GTPases Rac, Rho and direct activation of Cdc42 [9]. Upon internalization, *Brucella* is contained within a BCV that successively associates with a subset of endosomal markers, starting from Rab5, the early endosomal antigen (EEA1), the transferrin receptor (TfR), as well as the lipid rafts component flotillin-1 [5, 10-12]. Next, the BCV associates with the late endosomal markers Rab7, RILP (Rab7's effector Rab interacting lysosomal protein), LAMP-1, and transiently with autophagosomal markers [5, 6].

Acidification of the BCV upon reaching a late endosomal compartment serves as a trigger for the expression of the VirB type IV secretion system (T4SS)[13, 14],

which enables a fraction of *Brucella* to avoid fusion of their BCVs with lysosomes and their subsequent degradation [12, 14]. These bacteria diverting from the endocytic pathway were shown to interact with ER exit sites (ERES) with the small GTPase Sar1 and the COPII complex [12, 15]. Which of the effector protein(s) are responsible for the escape of the BCVs from the degradative pathway have not yet resolved, but a growing repertoire of candidates have been identified [16]. Moreover, the *Brucella* effector RicA was shown to interact with Rab2, which is involved in the control of the vesicular-trafficking from Golgi to ER in the ER-Golgi intermediate compartment (ERGIC) and is required for fusion of BCVs with ER-derived vesicles and subsequent intracellular replication of *Brucella* [17, 18]. This indicates that anterograde as well as retrograde trafficking components are required during infection.

Despite identification of numerous individual host components recruited to or important for *Brucella* to reach its replicative niche, a global understanding of this highly coordinated process is still missing. Essentially, the actual mechanism resulting in the diversion of BCVs from the lysosomal pathway towards an ER-derived compartment remains elusive. Moreover, host factors that are needed for the maintenance of the BCVs in the replicative niche are still largely unexplored. In this study we took a systems level approach to gain a deeper insight into these fundamental questions and therefore performed a genome-wide RNA interference (RNAi) screen aiming at identifying host factors involved in *Brucella* cellular entry, trafficking, and replication. We identified 507 host proteins for which we show that their knock-down either increases (251) or decreases (255) *Brucella* intracellular replication, which clustered in seven and eight major cellular pathways, respectively. Among these, we identified a role for the retromer-mediated endosome-to-TGN (trans-Golgi network) trafficking pathway. Validation experiments combined with pharmacological inhibition of endosome-to-TGN trafficking confirmed the requirement of the retromer and its component Vps35 for *Brucella* trafficking towards its replicative niche. Taken together, this study reveals a novel trafficking route critical for intracellular infection by *Brucella* and describes a new role of the retromer complex during bacterial infection.

RESULTS

A genome-wide siRNA screen uncovers the human infectome for *Brucella* infection

To identify the cellular factors involved in the infection of epithelial cells by *Brucella*, we performed a genome-wide siRNA screen on HeLa cells combined with bacterial infection at biosafety-level 3 and a high-throughput microscopy-based read-out [19]. HeLa cells were reverse siRNA-transfected for 3 days, followed by infection with a GFP-expressing *Brucella abortus* strain for a total of 44 h. During the first 4 h of infection, bacteria were allowed to enter cells after which extracellular bacteria were killed by addition of gentamicin. Intracellular bacteria were then allowed to replicate intracellularly before fixation and staining. Data were acquired by automated microscopy and explored by a tailored high-content analysis workflow that determined infection rates based on cell number and GFP fluorescence (See Material and Methods, Fig. 1). A model of *Brucella* replication was fitted to the pathogen intensity distribution to gain an infection classification independent of absolute fluorescence intensity. Image intensity normalization and a novel association of pathogen to cells were used to enable quantitative measurement of the pathogen intensity distribution. The overall workflow used for analyzing the screening data is presented in Figure 1 (see also Material and Methods). In order to identify host factors involved in *Brucella* infection in an unbiased way, two genome-wide siRNA libraries were screened. These consisted of a Dharmacon library containing a pool of 4 siRNA per gene, as well as a Qiagen library with 4 individual siRNAs for each target. These data were then supplemented with up to 6 additional siRNAs (Ambion) for about 1000 genes and 1900 esiRNAs (Sigma) which were selected in a larger consortium studying a number of bacterial and viral pathogens. In order to make full use of the available data, we also included the previously published kinome screens [20].

To account for the well-known confounding off-target effects in siRNA technology [21, 22], we performed statistical analysis of all available screening data with the Redundant siRNA Analysis (RSA) algorithm [23], reducing the number of false positives caused by off-target effects of single siRNAs and favors genes with a reproducible phenotype from different siRNAs. As input for the RSA algorithm, data that did not pass quality control or contained too few cells were removed. Then

technical replicates were averaged and the algorithm was run separately to identify genes that promote or reduce *Brucella* infection. This resulted in a list comprising 251 up- and 255 down-hits (RSA p-value < 0.01, Table S1 and S2). Hits were further classified using the STRING database [24] and high confidence protein-protein interaction network of top ranking genes from the RSA analysis are presented in Figure 2 for targets that reduced (Fig. 2A) or increased (Fig. 2B) *Brucella* infection upon knockdown. Our approach confirmed the role of known components critical for *Brucella* infection, including Rab7A, Rac1, and Cdc42 [6, 9, 25], thereby validating our experimental approach. Multiple components of pathways involved in mitotic cell cycle, actin remodeling, TOR, TGF-β or FGF signaling, endosome-to-Golgi transport and further vesicular trafficking were found in our top ranking gene lists suggesting an important role of these signaling pathways during *Brucella* infection. Representative images for a selected subset of identified target are presented in Fig. 2C. Results of a gene ontology enrichment analysis are presented in Fig. 2D (down-hits) and Fig. 2E (up-hits).

Brucella entry assay identifies Vps35, a component of the retromer complex, as host factor involved in post-entry trafficking

To dissect the role of the identified genes in the progression of *Brucella* infection, we performed an entry assay previously developed in our laboratory [19], which allows studying the early infection steps in a high-throughput format. After 4 h of bacterial entry, extracellular *Brucella* were killed by gentamicin and the GFP-reporter was induced simultaneously in intracellular bacteria by Anhydrotetracycline for 4 h, giving a total of 8 h before fixation. This approach allowed us to robustly identify individual intracellular bacteria and quantify the bacterial load before intracellular replication is initiated (Fig. 3A and Material and Methods). For this assay, a number of genes from different pathways identified in the genome-wide screen as well as additional genes supplementing these pathways were selected for follow up (for full list see Table S3). Results of the entry assay were then plotted against the end point assay (microcolony formation 48 hpi). For ease of visualization, only the averages over all RNAi products targeting a certain gene are displayed. Strikingly, most of the tested genes displayed a direct correlation between the results of the entry assay and the endpoint assay. This was the case for most components from the TGF-β and FGF signaling, Golgi to ER transport, or the actin-remodeling

pathway, indicating a contribution of these pathways in the entry process of *Brucella* into HeLa cells (Fig. 3B). Noteworthy, these results do not exclude an additional role for these pathways at any further stage of the infection. In fact, we could observe a tendency that siRNA knockdown effects that reduce infection were more pronounced in endpoint assay compared to the entry assay.

In order to find genes which are predominantly involved in a post-entry process we focused on those that mainly affected colony formation and had little effect on bacterial entry. 14 genes were identified that showed less than 50% reduction on *Brucella* entry although their knockdown resulted in at least 50% reduction in the endpoint assay (upper left quarter separated by dotted lines, Fig 2B). Among these, we found several components of the retromer or endosome-to-Golgi trafficking (highlighted in yellow). Knockdown of Vps35, an essential component of the retromer complex [26, 27] had the strongest negative effect on colony formation in the endpoint assay with only a mild reduction in bacterial entry. This indicates that Vps35, and potentially other components of the retromer complex, are involved in a post-entry step during *Brucella* infection but do not affect bacterial entry into cells.

Endosome-to-Golgi transport and the retromer are required for *Brucella* infection

In mammalian cells, the retromer complex is composed of two functional sub-complexes: Vps26-Vps29-Vps35 that is involved in cargo selection and generally known as the cargo recognition complex (CRC) or cargo selective trimer (CST), and proteins from the sorting nexin (SNX) family [28] that interact with the CRC. Vps35 is the core component of the CRC with a direct role in cargo binding [29, 30] while Vps26 and Vps29 independently associates at either end of the complex (Fig. 4A). Further, recruitment of the CRC to the endosome is dependent on the GTPase Rab5 and Rab7 [28]. To decipher the contribution of the different retromer-associated factors we specifically browsed our genome-wide siRNA data for retromer components or associated proteins (Fig. 4B). Besides Vps35, Vps26a knockdown also strongly reduced *Brucella* infection, to a comparable level than the positive controls ArpC3 and Rab7a (Fig. 4B). In contrast, siRNA depletion of Vps26b, the paralogue of Vps26a, and Vps29, the third unit of the CRC, only resulted in mild reduction in *Brucella* infection, below our significance threshold. Depletion of SNX1 and SNX5, two of the four sorting nexins associated with the SNX-BAR-retromer,

showed an enhanced *Brucella* infection (below significance threshold) while the other two components, SNX2 and SNX6 showed no effect. SNX3, a component of the SNX3-retromer, showed a mild reduction in infection (not significant) while USP6NL, a Rab GTPase activating protein (GAP) for Rab43 shown to be involved in Shiga toxin endosome-to-TGN trafficking [31] increased *Brucella* infection upon knockdown. Taken together, these results suggest that the CRC function of the retromer complex is the critical element for *Brucella* to reach its replicative niche.

To confirm the effect of Vps35 knockdown on *Brucella* infection and to rule out any off-target effect, a complementation experiment with a Vps35 cDNA insensitive to a co-expressed shRNA was performed. While shRNA knockdown of Vps35 inhibited *Brucella* infection, co-expression of the shRNA-insensitive cDNA of Vps35 could rescue the phenotype (Fig. 4C and D), confirming that depletion of Vps35 indeed negatively affects *Brucella* infection.

Retro-2 inhibits *Brucella abortus* infection

To further investigate the importance of retrograde transport from endosomes to Golgi for *Brucella*, we performed infection in the presence of the small molecule inhibitor Retro-2, isolated in a screen for compounds that prevents cellular toxicity of ricin and Shiga-like toxins [32]. Retro-2 specifically acts on the retrograde trafficking from endosomes to the TGN although it neither affected the morphology of membrane compartments nor the transport of endogenous cargo (with the exception of the syntaxins 5, 6, and 16)[32]. Retro-2 titration at the onset of *Brucella* infection resulted in a dose-dependent reduction of infected cells (Fig. 5A). Unless stated differently, a final concentration of 50 μM Retro-2 was used for all follow-up experiments as this concentration showed the maximal inhibition without marked effect on cell number. We then addressed the timing of Retro-2 dependent inhibition of *Brucella* replication by adding the drug from 0 to 24 hpi, keeping the inhibitor throughout the experiment and analyzing the infection rate after a total of 48 h (Fig. 5B). Retro-2 still markedly reduced *Brucella* infection when added at 4 hpi together with gentamicin, which terminates further infection. This indicates that a post-entry process of *Brucella* infection is blocked by Retro-2. Strikingly, the inhibitory effect of Retro-2 gradually decreases the later the drug was added - and virtually disappears when added at 16 hpi or 24 hpi. Taken together, these results confirmed our finding

that retrograde trafficking from endosome to TGN is critical for the *Brucella* to reach is replicative niche. Moreover, we concluded that this trafficking step represent an early event in the intracellular cycle of *Brucella* - taking place between 0 h and 9 h post entry.

Having shown that Vps35 and Retro-2 both have an inhibitory effect on *B. abortus* infection, we addressed the combinatorial effect of both treatments. To this end, we performed siRNA knockdown of endogenous Vps35 for 72 h followed by infection and concomitant treatment with a single dose of Retro-2 or mock treatment for 44 h (Fig. 5C, D). The results clearly indicated an additive effect of this dual treatment with a decrease of the infection rate on top of inhibition obtained by the knockdown of Vps35. Strikingly, the relative contribution of Vps35 knockdown to the *Brucella* infection was independent of the Retro-2 treatment, with a relative inhibition of ca. 60% regardless whether the cells were treated or not with the drug. This finding strongly suggests that a Vps35-independent function of the endosome-to-Golgi retrograde trafficking is involved in *Brucella* trafficking towards its intracellular replicative niche.

Vps35 knockdown prevents *Brucella* escape from the lysosomal pathway

To investigate how Vps35 knockdown influences *Brucella* trafficking and how it prevents BCVs to converge towards the replicative niche we quantified *Brucella* co-localization with the lysosomal marker LAMP-1 in siRNA-treated and control cells. Early and transient association with LAMP-1 is a well-established signature of BCV trafficking during the first hours of infection [6]. This association eventually gets lost for bacteria that manage to escape the degradative pathway prior to intracellular replication [6], a process that is dependent on a functional VirB T4SS [12]. We analyzed *Brucella*-infected HeLa cells at 6 and 18 hpi and determined the percentage of LAMP-1 colocalization for each detected bacteria using immunostaining and confocal microscopy (Fig. 6A and Material and Methods). At 6 hpi, most *Brucella* were found within LAMP-1 positive vesicles in both control and siRNA-treated cells (Fig. 6B, C, D, F), confirming that Vps35 function is not required for the early trafficking of the BCVs. At 18 hpi, loss of LAMP-1 association (Fig 6B, C) and early intracellular replication (Fig. 6E) was mainly detected in control cells. In contrast, most *Brucella* remained in a LAMP-1 positive compartment in Vps35-knockdown

cells (Fig 6B, C) and failed to replicate intracellularly (Fig. 6G). Our single cell co-localization analysis thus supports the requirement of Vps35 and the retromer complex for BCV diversion from the lysosomal pathway and for the establishment of a successful replicative niche.

DISCUSSION

The different membrane-bound organelles that compose the secretory pathway and the endo-lysosomal system of eukaryotic cells constitute targets of choice for many intracellular pathogens, which evolved an impressive and highly diverse panel of strategies to hijack and/or subvert these trafficking pathways to their benefit. To date, studies aiming at understanding *Brucella* interaction with host cells have been mainly hypothesis driven with only few unbiased approaches, including small-scale RNAi screen in Drosophila S2 cell and proteomics studies to identify host components of the BCV [6, 12, 15, 18, 33, 34]. Here we have taken a systems level approach using a genome-wide RNAi screen in HeLa cells and identified a set of 507 host factors important for *Brucella* infection, most of which had not been reported previously. These hits span several important signaling pathways, providing new insights into *Brucella* infection cycle. By combining these results with a high-throughput entry assay, we further classified a subset of the newly identified host factors according to their impact on *Brucella* entry into the host cells. With this means we identified Vps35, a component of the retromer complex as a pivotal component of the post-entry trafficking of *B. abortus*. Consistently, we could show that knockdown of Vps35 prevents *Brucella* escape from degradative pathway – BCVs remaining associated with LAMP-1, confirming the importance of retrograde trafficking for *Brucella* to reach and/or establish its replicative niche. The requirement for endosome-to-Golgi trafficking was further confirmed using Retro-2, a specific chemical inhibitor of that pathway [32].

The retromer has recently been identified as an important component for the intracellular infection cycle of viruses (e.g. papilloma virus [35] or poxvirus [1]), bacterial pathogens (e.g. *Coxiella burnetti* [36], *Salmonella typhimurium* [37], or *Simkania* [38]) as well as for the parasite *Leishmania* [39] as demonstrated by siRNA knockdown and/or chemical inhibition using Retro-2. In human cells, the retromer complex is composed of three vacuolar protein sorting associated proteins (Vps) Vps35, Vps26 and Vps29 forming the cargo recognition complex (CRC) and a

complex of membrane deforming proteins consisting of sorting nexins (SNX). Of note, the molecular target of Retro-2 has not yet been described, and its effects do not fully recapitulate the effect of siRNA knockdown of the CRC.

Our data show that not only Vps35 but also Vps26a and to a lesser extent Vps29 and Vps26b reduce *Brucella* infection upon knockdown, which corroborates the need for an intact CRC for its components to be functional in this process. It has been reported that Vps26a and Vps26b have preferences towards different cargoes [40] and our data points towards a preference for Vps26a requirement for *Brucella* infection. At least two different types of retromer complexes have been described, defined by the sorting nexin (SNX) components associated to the CRC. The SNX-BAR-retromer, which is comprises an heterodimer formed by SNX1 or SNX2 and SNX5 or SNX6 in association with the CRC, is able to induce and stabilize the formation of membrane tubules [41-43]. That property is mediated by the membrane curvature sensing BAR (Bin/amphiphysin/Rv) domain and phosphatidylinositol 3-phosphate [PtdIns(3)P] or phosphatidylinositol 3,5-bisphosphate [PtdIns(3,5)P2] binding PX (phox homology) domain [44, 45] of the SNX. The SNX3-retromer however only consists of the complex of SNX3 and CRC [43, 46]. Our data do not conclusively resolve which CRC-SNX interaction(s) are mediating the observed phenotype. Whereas no significant effect was observed for the SNX1/5 knockdown, depletion of SNX2 or SNX6 appeared to promote *Brucella* intracellular replication. In contrast, SNX3 knockdown resulted in a decrease in *Brucella* infection, although none of these data point passed our stringent statistical cut-off. Combinatorial knockdown of SNXs and co-localization approaches should be addressed in future studies, to understand the possible redundancy between SNX and resolve the individual contribution of these factors to *Brucella* trafficking.

Besides the retromer complex, our study highlighted the involvement of several other pathways in *Brucella* infection. The most prominent clusters that negatively affected infection upon knockdown comprised signaling pathways involved in actin-remodeling, TGF-β or FGF signaling, endosome-to-Golgi transport and further vesicular/endocytic pathways. Among these components we can highlight Rab7A, which is needed for trafficking to the replicative niche [6], Rac1 and Cdc42, which are involved in *Brucella* internalization into non-phagocytic cells [9], or the COPB subunit of the COPI complex that is implicated in *Brucella* replication [18]. Although the role of these individual components had already been described in the

context of *Brucella* infection, they can be considered as benchmark to our results, and globally validate our systems-level perspective of the human infectome for *Brucella* infection. We believe that many of these identified genes will provide a rich resource for future discoveries. These include numerous components of the actin-remodeling pathway that have not yet been described in that context. Interestingly, members of the TGF-β and FGF signaling pathways were also found to promote *Brucella* infection as their depletion resulted in a decrease in *Brucella* infection. It has previously been reported that patients with brucellosis show higher levels of TGF-β1 in their sera that is correlated with depressed function of T cell responses [47]. Further, B cells were also shown to produce TGF-β at early stages of infection with *Brucella* in mice [48]. A possible immunosuppressive role for this pathway during *Brucella* infection should be further investigated.

Summarizing, our study specifically revealed the importance of Vps35 and of retrograde trafficking in particular for the establishment of *Brucella* replicative niche. Considering the central role of Vps35 in the retromer complex, and as key regulator of the endosome-to-Golgi transport [28], it is tempting to hypothesize that this route constitute the missing link in *Brucella* trafficking, possibly explaining the transition between its early non-replicative vacuole (characterized by its association with the endosomal markers LAMP-1 and RAB7A) and its ER-derived replicative niche - a hypothesis that is supported by our co-localization data. An alternative - yet non-exclusive hypothesis is that the retromer complex is involved in the establishment and/or maintenance of *Brucella* intracellular replicative niche, potentially by providing host factors that follow retrograde trafficking. Future studies will be needed to decipher the detailed contribution of the other host factors identified by our screening approach, as well as how secreted T4SS effector may contribute to their subversion.

MATERIALS AND METHODS

Cell lines and plasmid constructs

All experiments were performed in the human cervical carcinoma epithelial cell line (Hela) ATCC, CCL-2. Infections were performed using *Brucella abortus* 2308 carrying the constitutive GFP expression plasmid pJC43 (*aphT::GFP* [15]), pAC042.08 for entry assay (*apht::dsRed,tetO::tetR-GFP* [19]) or pAC037 (*apht::cerulean*, this study) for rescue experiments. Cells and bacteria were grown as described in [19, 20]. pAC037 was constructed by replacing dsRed from pJC44 [6] with Cerulean from pCERC-1 [49]. Cerulean was amplified using prAC082 (TTTTTGGATCCGAAAGGAGGTTTATTAAATGGTGAGCAAGGGCGAGGAG C) and prAC083 (TTTTTTCTAGAGC-TAGCTTACTTGTACAGCTCGTC) and cloned into pJC44 by restriction/ligation using BamHI and XbaI. The ribosomal binding site was which was lost on pJC44 using the above restriction was re-introduced on prAC082.

siRNA reverse transfection

Reverse siRNA transfection was performed as described in [19, 20] with minor adjustments. In brief, Genome-wide screens were performed with Dharmacon ON-TARGETplus SMART pool and Qiagen Human Whole Genome siRNA Set HP GenomeWide (QU) siRNA libraries. For the validation screens Ambion Silencer, Ambion Silencer Select and Sigma MISSION esiRNA libraries were used. In addition kinome libraries were included: Ambion (Silencer Select) with 3 siRNAs per gene, Qiagen (Human Kinase siRNA Set V4.1) with 4 siRNAs per gene and Dharmacon (Human ON-TARGETpIus) with 4 siRNAs per gene. All screening experiments were conducted in a 384-well plate format. Each plate contained general siRNA controls for transfection efficiency and toxicity (e.g. Kif11) as well as positive controls (e.g. Cdc42, Rac1) that are known to have an effect on *Brucella* infection [9]. In addition, negative controls such as mock (transfection reagent only) and scrambled (non-targeting siRNA) were added to each plate. The following specifications apply to all siRNA screens except the QU siRNA library where specifications are given in brackets. RNAiMAX in DMEM without foetal calf serum (FCS) was added to each well containing 1.6 pmol siRNA (QU: 1 pmol) or 15 ng esiRNA. Screening plates were then incubated at room temperature (RT) for 1 h.

Following incubation, 500 HeLa cells were added per well in DMEM (FCS 10% final). Plates were incubated at 37°C and 5% CO_2 for 72 h prior to infection. Secondary screens for all selected targets were performed with up to three siRNAs each from the Ambion Silencer and Ambion Silencer Select un-pooled libraries as well as one esiRNA from the pooled Sigma MISSION library For assays in 96-well plates and 24-well formats reverse transfections were performed in 6-well plates and subsequently reseeded in the respective plate format. On-target or control siRNAs were added to reach a final siRNA concentration of 20 nM together with RNAiMAx transfection reagent in DMEM without FCS. After 30 min of complex formation at room temperature, 110'000 HeLa cells in DMEM/10% FCS were added to each well. After 48 h transfection, cells were harvested by trypsinization and reseeded in DMEM/10%FCS (96-well plates: 2'800 cells per well; 24-well plates: 50'000 cells per well). The next day cells were infected as described before.

The following siRNAs used for the colocalization experiments were purchased from Qiagen (Hilden/Germany): hVPS35-2 (ID: SI00760690); all star negative (ID: 0001027281); all star death kif11 (ID: 0001027299). Retro-2 siRNA was purchased from Calbiochem/Merck (Darmstadt/Germany) (ID: 554715).

Infection

For the genome-wide and confirmation screens, infections were performed in 384-well plates as described in [19, 20]. In short, *B. abortus* 2308 pJC43 (*aphT::GFP* [15]) was grown in TSB medium containing 50 µg/ml kanamycin at 37°C to an OD of 0.8- 1.1. Bacteria were then diluted in DMEM/10% FCS and added at a final MOI of 10'000. Plates were centrifuged at 400 x *g* for 20 min at 4°C to synchronize bacterial entry. After 4 h incubation at 37°C and 5% CO_2, extracellular bacteria were killed by exchanging the infection medium by DMEM/10% FCS supplemented with 100 µg/ml gentamicin. After a total infection time of 44 h, cells were fixed with 3.7% PFA for 20 min at RT. For the entry assay, infections were performed as described in [19]. In brief, transfected cells were infected with *B. abortus* 2308 pAC042.08 for 4 h after what GFP expression was induced for 4 h by the addition of Anhydrotetracycline (100 ng/ml) during the gentamicin killing of extracellular bacteria. Follow up experiments and colocalization assays were done accordingly to the protocol described but performed in 96-well and 24-well plates, respectively. For the colocalization assay cells were infected at a MOI 2'000. 2 hpi cells were washed

three times with DMEM/10% FCS containing gentamicin (100 µg/ml). After the indicated incubation time cells were washed three times with PBS and finally fixed in 3.7% PFA in PBS.

Inhibitor experiment

HeLa cells were seeded in 96-well plates (2,800 cells/well) one day before infection. Retro-2 (2,3-Dihydro-2-(5-methyl-2-thienyl)-3-phenyl-4(1H)-quinazolinone, Sigma-Aldrich) was added to cells together with *B. abortus* 2308 pJC43 or during gentamicin wash at 4 hpi, Cells were maintained at 37°C with 5% CO_2 and Retro-2 was kept throughout the experiment.

Rescue experiment

The shRNA suppression/rescue constructs for Vps35 were kind gifts from Daniel Billadeau [50]. HeLa cells were seeded in a 6-well plate and transfected 4 h later with 0.9 µg of plasmid DNA using Fugene HD according to the manufacturer's protocol. 72 h post-transfection cells were reseeded into a 96-well plate (2'800 cells / well) and infected on the following day. Cells were infected with *Brucella abortus* carrying pAC037 for 48 h. After PFA fixation and staining, cells were analyzed by image analysis. Infection scoring was performed on YFP positive cells - indicative of successful transfection.

Immunofluorescence

Following fixation with 3.7% PFA in PBS for 20 min, HeLa cells were incubated in PBS containing 250 mM glycine for 20 min to quench remaining aldehyde residues. Cells were then permeabilized with saponin buffer (PBS containing 0.2% saponin and 3% bovine serum albumin) for 1 h. Immunostaining was performed by incubating coverslips with saponin buffer containing antibodies against LAMP-1 (Abcam ab25630) and *Brucella abortus* LPS polyclonal rabbit serum (kind gift from Xavier De Bolle [51]) overnight in a humidified chamber at 4°C. The coverslips were then washed three times with PBS and incubated with saponin buffer containing respective fluorophore-conjugated secondary antibodies: goat anti-mouse Alexa Fluor 488 (Thermo Fisher A11029) and anti-rabbit Alexa Fluor 647 (Cell Signaling #4414) for 3 h in a humidified chamber at room temperature. The coverslips were then washed

three times with PBS and mounted onto glass slides using Vectashield H-100 Antifade Mounting Medium (Vector Laboratories) and sealed with nail polish.

Confocal microscopy

The images were captured with the LSM-800 Confocal Microscope (Carl Zeiss) using a 63x oil objective. For each condition, 40 images were obtained at random locations across the coverslip, representing more than 50 individual cells per conditions. The images were deconvolved using Huygens software (Scientific Volume Imaging). The presence of Lamp-1 signal around the bacteria was quantified from the images by assessing the overlap between the anti-LPS and the anti-LAMP-1 staining for each individual bacterium (more than 400 per condition).

Imaging with high-throughput microscopy

Microscopy was performed with Molecular Devices ImageXpress microscopes. MetaXpress plate acquisition wizard with no gain, 12 bit dynamic range, 9 sites per well in a 3x3 grid was used with no spacing and no overlap and laser-based focusing. DAPI channel was used for imaging nucleus, GFP for bacteria, and RFP for F-actin or dsRed of bacteria in the entry assay. Robotic plate handling was used to load and unload plates (Thermo Scientific). The objective was a 10X S Fluor with 0.45NA. The Site Autofocus was set to “All Sites” and the initial well for finding the sample was set to “First well acquired”. Z-Offset for Focus was selected manually and manual correction of the exposure time was applied to ensure a wide dynamic range with low overexposure.

Image analysis

Images were analyzed with the screeningBee analysis framework from BioDataAnalysis GmbH. To correct for uneven illumination inherent in widefield microscopic imaging, an illumination correction model was computed for every plate using Cidre [52]. To ensure that the Cidre-corrected image intensities fall within the range [0.0, 1.0] a linear transformation for pixel intensities was computed that maps the 0.001-quantile to 0.01 and the 0.999-quantile to 0.99 post-illumination correction. Illumination correction and intensity scaling were performed as pre-processing steps for every image prior to analysis.

To reduce the signal of *Brucella* DNA in the DAPI channel, a linear transform of the GFP channel was subtracted from the DAPI channel, with the linear transformation parameters f, o estimated in the following way: a mapping of GFP pixels to DAPI pixels was constructed so that for all intensities in the GFP images, the list of corresponding intensities in the DAPI images were recorded. For every list of DAPI intensities, only the mean intensities were retained. This creates a mapping of GFP intensities to their corresponding mean DAPI intensities. A linear regression was performed to obtain the linear parameters f, o that map the GFP channel image to the DAPI channel image. Cleaned DAPI images with a reduced Brucella signal were obtained by subtracting the linear transform of the GFP channel from the DAPI channel $I'_{DAPI} = I_{DAPI} - (f\, I_{GFP} + o)$ as pre-processing steps for every image prior to analysis. On a random subset of 128 images, CellProfiler [53] was executed to identify Nucleus objects using "OTSU Global" segmentation in the DAPI channel, and the median, lower quartile and upper quartile segmentation thresholds of the images were retained as $T_{DAPI\text{-}m}$, $T_{DAPI\text{-}lq}$ and $T_{DAPI\text{-}uq}$. On the same images, the GFP background intensity B_{GFP} was obtained as the position of the peak in the GFP intensity histogram, the dynamic range of the histogram D_{GFP} was obtained as the difference between the 99% quantile and the 1% quantile of intensity values, and the Bacteria segmentation threshold was computed as $T_{GFP} = B_{GFP} + \frac{2}{100} D_{GFP}$. On all images, screeningBee CellProfiler was executed to perform object segmentation and measurements with the following steps: (a) Nuclei were detected as primary objects using manual threshold setting. For each plate it was manually chosen to use $T_{DAPI\text{-}m}$, $T_{DAPI\text{-}lq}$ or $T_{DAPI\text{-}uq}$, depending on visual inspection of the segmentation results. Using the same threshold on all images improved site-to-site comparability. (b) Cells were detected as secondary objects around the Nuclei, with "OTSU Global" segmentation in the RFP channel. (c) Bacteria were detected as primary objects using manual threshold setting with threshold T_{GFP}. Using the fixed background intensity as a reference for T_{GFP} allowed for segmenting even rather dim objects while avoiding site-to-site variability. In order to accurately measure infection scoring, a reliable method to associate pathogen colonies to individual cells is necessary. A straightforward approach is to assume that pathogen colonies must be contained within the body of the host cell. However, high cell confluence can make actin channel-based cell body segmentation inaccurate. Single microcolonies are often split

into pieces that are incorrectly assigned to neighboring cells using this approach (Fig. 1B). To address this issue, we developed a novel algorithm to intelligently assign pathogen colonies to robust nucleus objects (Fig. 1C). First, inexpensive 'bridge' and 'majority' morphological operations were applied to the pathogen objects to connect broken clumps. Next, a weighted distance metric was used to measure an attraction score $a_{N,P}$ between a pathogen P and individual nuclei N within a close proximity d_{prox}. The attraction score is computed as the surface integral of the nucleus area in a continuous field emanating from the pathogen defined by an exponential function that is strongest within the microcolony itself, and decays exponentially as distance from the microcolony increases: $a_{N,P} = \sum_{n \in N} e^{-\lambda d_{n,p}}$, where $n$is an element (pixel) belonging to nucleus object N, $d_{n,p}$is the distance transform from the edge of microcolony P to n, and λ is a parameter controlling the strength of the decay. Attraction scores for all nuclei proximate to microcolony P are normalized such that the strongest nucleus attraction score is 1, $\underline{a}_{N,P} = \frac{a_{N,P}}{max(a_{N,P})} \; \forall \; N \quad s.t. \, d_{n,p} < d_{prox}$. Nuclei objects with normalized attraction scores above a threshold $a_{min}$are associated with the pathogen microcolony. In the case that multiple nuclei are associated with the same microcolony, the microcolony is split so that each element is associated to the nearest nuclei. Large microcolonies are encouraged to split with greater ease than small microcolonies by weakening the minimum attraction score linearly according to area of the microcolony $a'_{min} = 0.5 \, a_{min}$ if $A_P < A_{large}$, or $a'_{min} = 1 - 0.5 \, \frac{A_P - A_{large}}{A_{large}} a_{min}$ if $A_{large} \leq A_P \leq 2A_{large}$, and $a'_{min} = 0.5 \, a_{min}$ otherwise (where A_P is the area of the pathogen microcolony). Parameters settings $d_{prox} = 45$, $\lambda = 0.2$, $a_{min} = 0.5$, and A_{large} =8,000 were optimized by grid search on a dataset of 7,566 hand-labeled segmentations resulting in a 95.58% correct association rate.

Nucleus to pathogen microcolonies associations were aggregated. The area and integrated intensity of the pathogen objects associated to each cell and the mean intensity of the Nuclei in the GFP channel was computed as readout.

Infection scoring for endpoint assay

Wells that contain only 32 Cells or less were excluded from infection scoring. In the remaining wells, Bacteria were filtered in a decision tree (DT) classification to

exclude objects of only one pixel area. Based on the relation of Bacteria to Nuclei, for the remaining Bacteria objects, the integrated GFP intensity was integrated over all Bacteria relating to a Cell. To reduce the impact of background intensity, an estimate for GFP background was computed using the 1% lower quantile of mean GFP intensity in the Nuclei. For every Cell, the estimated GFP background intensity was multiplied with the area of Bacteria relating to this cell, and the result was subtracted from the integrated Bacteria GFP intensity of the Cell, to arrive at a background-free estimate of "bacterial load" in each Cell. The value range for this intensity was zero for Cells with no segmented Bacteria objects, and higher than zero for all other Cells. This integrated GFP intensity was then log2-scaled, to reflect the exponential growth of replicating *Brucella*. Before log2-scaling, a small epsilon value of 2^{-20} was added to every Cell, so that the log2 value of Cells with no segmented Bacteria will not be negative infinity. The arbitrary value 2^{-20} is by a large margin smaller than the smallest actual intensity of our assays, but large enough to be used in histogram binning. For every plate, the histogram of the log2-scaled integrated cellular GFP intensity was computed (Fig. 1D) with a bin size of 0.025. The histograms were normalized to an arbitrary "virtual plate cell count" of 10^{10}. To extrapolate a continuous distribution from the possibly sparse histogram, kernel density estimation (KDE) was used with a manually optimized Gaussian kernel of standard deviation 16. The histogram shows a bimodal distribution. By correlating the plate histogram distributions to selected images from the plate, we could identify that the first mode of the distribution is composed of cells with a low number of infection events ranging from single *Brucella* to small clusters (denoted as), whereas the second mode is composed of large colonies (denoted as). The two peak positions of the bimodal distribution were identified. Normal distributions G_S and G_L were fitted to the peak positions for small and large colonies, respectively. For the fitting of G_S and G_L, the mean was given by the position of the peak, the height was given by the height of the peak, and the variance was optimized such that the distance between the KDE and the sum of G_S and G_L became minimal. To arrive at a binary infection scoring threshold, we identified a suitable value three standard deviations below the mean of G_L. This threshold includes 99.8% of the events in G_L. Cells with an integrated GFP intensity exceeding this threshold were considered true positive infections, and were labeled infected. The infection index was computed as the ratio of infected Cells to the total number of Cells in the well.

Infection Scoring Entry Assay

Wells that contain only 32 Cells or less were excluded from infection scoring. In the remaining wells, Bacteria were filtered in a decision tree (DT) classification to exclude objects of only one pixel area. The remaining Bacteria were filtered in a DT classification to exclude objects of less than a manually set threshold on the upper quartile of the object intensity. The remaining Bacteria were considered true positive infections. Based on the relation of Bacteria to Nuclei, Cells were labeled infected if and only if a true positive Bacteria is related to the Cells Nuclei. The infection index was computed as the ratio of infected Cells to the total number of Cells in the well. For quantification of bacterial load in infected cells, the median of integrated GFP intensity of all true positive Bacteria was computed. The final infection readout was the product of the infection rate and bacterial load, which gives a robust approximation of the amount of intracellular bacteria [19].

Redundant siRNA Analysis (RSA)

Redundant siRNA Analysis RSA, [23] ranks genes by iteratively assigning hypergeometric p-values to each of the multiple siRNAs targeting the same gene and picking the minimum value within a given group to represent this gene. The ranking score indicates whether the distribution of ranks corresponding to a gene is shifted towards the top, thereby aggregating the information provided by several siRNA sequences with the same target in a robust manner. To account for varying numbers of available siRNAs per gene, Bonferroni correction was applied within siRNA groups. Furthermore, as both up- and down hits are of interest to this analysis, RSA was run twice, once with Z-scored infection scores ranked from low to high values and once ranked oppositely. The parameters for lower and upper score thresholds which specify cutoffs for definite hits and non-hits, were chosen as the 2% and 88% quantiles respectively (this roughly corresponds to Z-scored infection scores of -1.5 and 1). Data was filtered prior to RSA by removing wells that do not pass quality control as well as wells where cell count is below 50% of the initially seeded cell number. Control wells were excluded from RSA and technical replicates (repeated experiments with identical siRNA) were averaged. Additionally, instead of relying solemnly on manufacturer information and in order to ensure comparability between libraries, siRNA targets were re-identified by searching against ENSEMBL cDNA

and the REFSEQ mRNA nucleotide data. Cases where matching failed were also excluded from this analysis.

Acknowledgments

We want to thank Julia Feldmann and Sonia Borrell from the SwissTPH, Basel, Switzerland for great assistance and support with BSL-3 environment. We also are thankful to the Imaging Core Facility of the Biozentrum, Basel for excellent assistance and advice with confocal microscopy.

REFERENCES

1. Hsiao JC, Chu LW, Lo YT, Lee SP, Chen TJ, Huang CY, et al. Intracellular transport of vaccinia virus in HeLa cells requires WASH-VPEF/FAM21-Retromer Complexes and Recycling Molecules Rab11 and Rab22. Journal of virology. 2015;89(16):8365-82. doi: 10.1128/JVI.00209-15. PubMed PMID: 26041286; PubMed Central PMCID: PMC4524218.
2. Moreno E. Retrospective and prospective perspectives on zoonotic brucellosis. Frontiers in microbiology. 2014;5:213. doi: 10.3389/fmicb.2014.00213. PubMed PMID: 24860561; PubMed Central PMCID: PMC4026726.
3. Pappas G, Papadimitriou P, Akritidis N, Christou L, Tsianos EV. The new global map of human brucellosis. The Lancet Infectious diseases. 2006;6(2):91-9. doi: 10.1016/S1473-3099(06)70382-6. PubMed PMID: 16439329.
4. Ariza J, Bosilkovski M, Cascio A, Colmenero JD, Corbel MJ, Falagas ME, et al. Perspectives for the treatment of brucellosis in the 21st century: the Ioannina recommendations. PLoS medicine. 2007;4(12):e317. doi: 10.1371/journal.pmed.0040317. PubMed PMID: 18162038; PubMed Central PMCID: PMC2222927.
5. Pizarro-Cerda J, Meresse S, Parton RG, van der Goot G, Sola-Landa A, Lopez-Goni I, et al. *Brucella abortus* transits through the autophagic pathway and replicates in the endoplasmic reticulum of nonprofessional phagocytes. Infection and immunity. 1998;66(12):5711-24. PubMed PMID: 9826346; PubMed Central PMCID: PMC108722.
6. Starr T, Ng TW, Wehrly TD, Knodler LA, Celli J. *Brucella* intracellular replication requires trafficking through the late endosomal/lysosomal compartment. Traffic. 2008;9(5):678-94. doi: 10.1111/j.1600-0854.2008.00718.x. PubMed PMID: 18266913.
7. Castaneda-Roldan EI, Avelino-Flores F, Dall'Agnol M, Freer E, Cedillo L, Dornand J, et al. Adherence of *Brucella* to human epithelial cells and macrophages is mediated by sialic acid residues. Cellular microbiology. 2004;6(5):435-45. doi: 10.1111/j.1462-5822.2004.00372.x. PubMed PMID: 15056214.
8. Castaneda-Roldan EI, Ouahrani-Bettache S, Saldana Z, Avelino F, Rendon MA, Dornand J, et al. Characterization of SP41, a surface protein of *Brucella* associated with adherence and invasion of host epithelial cells. Cellular microbiology. 2006;8(12):1877-87. doi: 10.1111/j.1462-5822.2006.00754.x. PubMed PMID: 16817909.
9. Guzman-Verri C, Chaves-Olarte E, von Eichel-Streiber C, Lopez-Goni I, Thelestam M, Arvidson S, et al. GTPases of the Rho subfamily are required for *Brucella abortus* internalization in nonprofessional phagocytes: direct activation of Cdc42. The Journal

of biological chemistry. 2001;276(48):44435-43. doi: 10.1074/jbc.M105606200. PubMed PMID: 11579087.
10. Arellano-Reynoso B, Lapaque N, Salcedo S, Briones G, Ciocchini AE, Ugalde R, et al. Cyclic beta-1,2-glucan is a *Brucella* virulence factor required for intracellular survival. Nature immunology. 2005;6(6):618-25. doi: 10.1038/ni1202. PubMed PMID: 15880113.
11. Bellaire BH, Roop RM, 2nd, Cardelli JA. Opsonized virulent *Brucella abortus* replicates within nonacidic, endoplasmic reticulum-negative, LAMP-1-positive phagosomes in human monocytes. Infection and immunity. 2005;73(6):3702-13. doi: 10.1128/IAI.73.6.3702-3713.2005. PubMed PMID: 15908400; PubMed Central PMCID: PMC1111828.
12. Celli J, de Chastellier C, Franchini DM, Pizarro-Cerda J, Moreno E, Gorvel JP. *Brucella* evades macrophage killing via VirB-dependent sustained interactions with the endoplasmic reticulum. The Journal of experimental medicine. 2003;198(4):545-56. doi: 10.1084/jem.20030088. PubMed PMID: 12925673; PubMed Central PMCID: PMC2194179.
13. Boschiroli ML, Ouahrani-Bettache S, Foulongne V, Michaux-Charachon S, Bourg G, Allardet-Servent A, et al. The *Brucella suis virB* operon is induced intracellularly in macrophages. Proceedings of the National Academy of Sciences of the United States of America. 2002;99(3):1544-9. doi: 10.1073/pnas.032514299. PubMed PMID: 11830669; PubMed Central PMCID: PMC122227.
14. Comerci DJ, Martinez-Lorenzo MJ, Sieira R, Gorvel JP, Ugalde RA. Essential role of the VirB machinery in the maturation of the *Brucella abortus*-containing vacuole. Cellular microbiology. 2001;3(3):159-68. PubMed PMID: 11260139.
15. Celli J, Salcedo SP, Gorvel JP. *Brucella* coopts the small GTPase Sar1 for intracellular replication. Proceedings of the National Academy of Sciences of the United States of America. 2005;102(5):1673-8. doi: 10.1073/pnas.0406873102. PubMed PMID: 15632218; PubMed Central PMCID: PMC547823.
16. Ke Y, Wang Y, Li W, Chen Z. Type IV secretion system of *Brucella* spp. and its effectors. Frontiers in cellular and infection microbiology. 2015;5:72. doi: 10.3389/fcimb.2015.00072. PubMed PMID: 26528442; PubMed Central PMCID: PMC4602199.
17. de Barsy M, Jamet A, Filopon D, Nicolas C, Laloux G, Rual JF, et al. Identification of a *Brucella* spp. secreted effector specifically interacting with human small GTPase Rab2. Cellular microbiology. 2011;13(7):1044-58. doi: 10.1111/j.1462-5822.2011.01601.x. PubMed PMID: 21501366.
18. Fugier E, Salcedo SP, de Chastellier C, Pophillat M, Muller A, Arce-Gorvel V, et al. The glyceraldehyde-3-phosphate dehydrogenase and the small GTPase Rab 2 are crucial for *Brucella* replication. PLoS pathogens. 2009;5(6):e1000487. doi: 10.1371/journal.ppat.1000487. PubMed PMID: 19557163; PubMed Central PMCID: PMC2695806.
19. Casanova A, Low SH, Emmenlauer M, Conde-Alvarez R, Salcedo SP, Gorvel JP, et al. Microscopy-based assays for high-throughput screening of host factors involved in *Brucella* infection of Hela Cells. Journal of visualized experiments : JoVE. 2016;(114). doi: 10.3791/54263. PubMed PMID: 27584799.
20. Ramo P, Drewek A, Arrieumerlou C, Beerenwinkel N, Ben-Tekaya H, Cardel B, et al. Simultaneous analysis of large-scale RNAi screens for pathogen entry. BMC genomics. 2014;15:1162. doi: 10.1186/1471-2164-15-1162. PubMed PMID: 25534632; PubMed Central PMCID: PMC4326433.
21. Schultz N, Marenstein DR, De Angelis DA, Wang WQ, Nelander S, Jacobsen A, et al. Off-target effects dominate a large-scale RNAi screen for modulators of the TGF-beta pathway and reveal microRNA regulation of TGFBR2. Silence. 2011;2:3. doi: 10.1186/1758-907X-2-3. PubMed PMID: 21401928; PubMed Central PMCID: PMC3068080.

22. Sigoillot FD, King RW. Vigilance and validation: Keys to success in RNAi screening. ACS chemical biology. 2011;6(1):47-60. doi: 10.1021/cb100358f. PubMed PMID: 21142076; PubMed Central PMCID: PMC3306249.
23. Konig R, Chiang CY, Tu BP, Yan SF, DeJesus PD, Romero A, et al. A probability-based approach for the analysis of large-scale RNAi screens. Nature methods. 2007;4(10):847-9. doi: 10.1038/nmeth1089. PubMed PMID: 17828270.
24. Szklarczyk D, Franceschini A, Wyder S, Forslund K, Heller D, Huerta-Cepas J, et al. STRING v10: protein-protein interaction networks, integrated over the tree of life. Nucleic acids research. 2015;43:D447-52. doi: 10.1093/nar/gku1003. PubMed PMID: 25352553; PubMed Central PMCID: PMC4383874.
25. Porte F, Liautard JP, Kohler S. Early acidification of phagosomes containing *Brucella suis* is essential for intracellular survival in murine macrophages. Infection and immunity. 1999;67(8):4041-7. PubMed PMID: 10417172; PubMed Central PMCID: PMC96697.
26. Liu JJ. Retromer-Mediated Protein Sorting and Vesicular Trafficking. Journal of genetics and genomics = Yi chuan xue bao. 2016;43(4):165-77. doi: 10.1016/j.jgg.2016.02.006. PubMed PMID: 27157806.
27. Trousdale C, Kim K. Retromer: Structure, function, and roles in mammalian disease. European journal of cell biology. 2015;94(11):513-21. doi: 10.1016/j.ejcb.2015.07.002. PubMed PMID: 26220253.
28. Wassmer T, Attar N, Harterink M, van Weering JR, Traer CJ, Oakley J, et al. The retromer coat complex coordinates endosomal sorting and dynein-mediated transport, with carrier recognition by the trans-Golgi network. Developmental cell. 2009;17(1):110-22. doi: 10.1016/j.devcel.2009.04.016. PubMed PMID: 19619496; PubMed Central PMCID: PMC2714578.
29. Arighi CN, Hartnell LM, Aguilar RC, Haft CR, Bonifacino JS. Role of the mammalian retromer in sorting of the cation-independent mannose 6-phosphate receptor. Journal of Cell Biology. 2004;165(1):123-33. doi: DOI 10.1083/jcb.200312055. PubMed PMID: WOS:000220880300012.
30. Nothwehr SF, Ha SA, Bruinsma P. Sorting of yeast membrane proteins into an endosome-to-Golgi pathway involves direct interaction of their cytosolic domains with Vps35p. Journal of Cell Biology. 2000;151(2):297-309. doi: DOI 10.1083/jcb.151.2.297. PubMed PMID: WOS:000089948700012.
31. Fuchs E, Haas AK, Spooner RA, Yoshimura S, Lord JM, Barr FA. Specific Rab GTPase-activating proteins define the Shiga toxin and epidermal growth factor uptake pathways. The Journal of cell biology. 2007;177(6):1133-43. doi: 10.1083/jcb.200612068. PubMed PMID: 17562788; PubMed Central PMCID: PMC2064371.
32. Stechmann B, Bai SK, Gobbo E, Lopez R, Merer G, Pinchard S, et al. Inhibition of retrograde transport protects mice from lethal ricin challenge. Cell. 2010;141(2):231-42. doi: 10.1016/j.cell.2010.01.043. PubMed PMID: 20403321.
33. Qin QM, Pei J, Ancona V, Shaw BD, Ficht TA, de Figueiredo P. RNAi screen of endoplasmic reticulum-associated host factors reveals a role for IRE1alpha in supporting *Brucella* replication. PLoS pathogens. 2008;4(7):e1000110. doi: 10.1371/journal.ppat.1000110. PubMed PMID: 18654626; PubMed Central PMCID: PMC2453327.
34. Starr T, Child R, Wehrly TD, Hansen B, Hwang S, Lopez-Otin C, et al. Selective subversion of autophagy complexes facilitates completion of the *Brucella* intracellular cycle. Cell Host Microbe. 2012;11(1):33-45. doi: 10.1016/j.chom.2011.12.002. PubMed PMID: 22264511; PubMed Central PMCID: PMC3266535.
35. Lipovsky A, Popa A, Pimienta G, Wyler M, Bhan A, Kuruvilla L, et al. Genome-wide siRNA screen identifies the retromer as a cellular entry factor for human papillomavirus. Proceedings of the National Academy of Sciences of the United States of America. 2013;110(18):7452-7. doi: 10.1073/pnas.1302164110. PubMed PMID: 23569269; PubMed Central PMCID: PMC3645514.

36. McDonough JA, Newton HJ, Klum S, Swiss R, Agaisse H, Roy CR. Host pathways important for *Coxiella burnetii* infection revealed by genome-wide RNA interference screening. Mbio. 2013;4(1). doi: ARTN e00606-1210.1128/mBio.00606-12. PubMed PMID: WOS:000315814300042.
37. McGourty K, Thurston TL, Matthews SA, Pinaud L, Mota LJ, Holden DW. *Salmonella* inhibits retrograde trafficking of mannose-6-phosphate receptors and lysosome function. Science. 2012;338(6109):963-7. doi: 10.1126/science.1227037. PubMed PMID: 23162002.
38. Herweg JA, Pons V, Becher D, Hecker M, Krohne G, Barbier J, et al. Proteomic analysis of the *Simkania*-containing vacuole: the central role of retrograde transport. Molecular microbiology. 2016;99(1):151-71. doi: 10.1111/mmi.13222. PubMed PMID: 26374382.
39. Canton J, Kima PE. Targeting host syntaxin-5 preferentially blocks *Leishmania parasitophorous* vacuole development in infected cells and limits experimental *Leishmania* infections. The American journal of pathology. 2012;181(4):1348-55. doi: 10.1016/j.ajpath.2012.06.041. PubMed PMID: 22885104.
40. Bugarcic A, Zhe Y, Kerr MC, Griffin J, Collins BM, Teasdale RD. Vps26A and Vps26B subunits define distinct retromer complexes. Traffic. 2011;12(12):1759-73. doi: 10.1111/j.1600-0854.2011.01284.x. PubMed PMID: WOS:000297573500009.
41. Carlton J, Bujny M, Peter BJ, Oorschot VMJ, Rutherford A, Mellor H, et al. Sorting nexin-1 mediates tubular endosome-to-TGN transport through coincidence sensing of high-curvature membranes and 3-phosphoinositides. Curr Biol. 2004;14(20):1791-800. doi: 10.1016/j.cub.2004.09.077. PubMed PMID: WOS:000224784200017.
42. Carlton JG, Bujny MV, Peter BJ, Oorschot VMJ, Rutherford A, Arkell RS, et al. Sorting nexin-2 is associated with tubular elements of the early endosome, but is not essential for retromer-mediated endosome-to-TGN transport. J Cell Sci. 2005;118(19):4527-39. doi: 10.1242/jcs.02568. PubMed PMID: WOS:000233258900020.
43. Cullen PJ, Korswagen HC. Sorting nexins provide diversity for retromer-dependent trafficking events. Nature cell biology. 2012;14(1):29-37. PubMed PMID: WOS:000298421100006.
44. Cozier GE, Carlton J, McGregor AH, Gleeson PA, Teasdale BD, Mellor H, et al. The Phox Homology (PX) domain-dependent, 3-phosphoinositide-mediated association of sorting nexin-1 with an early sorting endosomal compartment is required for its ability to regulate epidermal growth factor receptor degradation. Journal of Biological Chemistry. 2002;277(50):48730-6. doi: 10.1074/jbc.M206986200. PubMed PMID: WOS:000179789600099.
45. Peter BJ, Kent HM, Mills IG, Vallis Y, Butler PJG, Evans PR, et al. BAR domains as sensors of membrane curvature: The amphiphysin BAR structure. Science. 2004;303(5657):495-9. doi: 10.1126/science.1092586. PubMed PMID: WOS:000188316400030.
46. Harterink M, Port F, Lorenowicz MJ, McGough IJ, Silhankova M, Betist MC, et al. A SNX3-dependent retromer pathway mediates retrograde transport of the Wnt sorting receptor Wntless and is required for Wnt secretion. Nature cell biology. 2011;13(8):914-U358. doi: 10.1038/ncb2281. PubMed PMID: WOS:000293373700009.
47. Elfaki MG, Al-Hokail AA. Transforming growth factor beta production correlates with depressed lymphocytes function in humans with chronic brucellosis. Microbes and infection / Institut Pasteur. 2009;11(14-15):1089-96. doi: 10.1016/j.micinf.2009.08.001. PubMed PMID: 19665058.
48. Goenka R, Parent MA, Elzer PH, Baldwin CL. B cell-deficient mice display markedly enhanced resistance to the intracellular bacterium *Brucella abortus*. The Journal of infectious diseases. 2011;203(8):1136-46. doi: 10.1093/infdis/jiq171. PubMed PMID: 21451002.

49. Thanbichler M, Iniesta AA, Shapiro L. A comprehensive set of plasmids for vanillate- and xylose-inducible gene expression in *Caulobacter crescentus*. Nucleic acids research. 2007;35(20):e137. doi: 10.1093/nar/gkm818. PubMed PMID: 17959646; PubMed Central PMCID: PMC2175322.
50. Liu TT, Gomez TS, Sackey BK, Billadeau DD, Burd CG. Rab GTPase regulation of retromer-mediated cargo export during endosome maturation. Molecular biology of the cell. 2012;23(13):2505-15. doi: 10.1091/mbc.E11-11-0915. PubMed PMID: 22593205; PubMed Central PMCID: PMC3386214.
51. Deghelt M, Mullier C, Sternon JF, Francis N, Laloux G, Dotreppe D, et al. G1-arrested newborn cells are the predominant infectious form of the pathogen *Brucella abortus*. Nature communications. 2014;5:4366. doi: 10.1038/ncomms5366. PubMed PMID: 25006695; PubMed Central PMCID: PMC4104442.
52. Smith K, Li Y, Piccinini F, Csucs G, Balazs C, Bevilacqua A, et al. CIDRE: an illumination-correction method for optical microscopy. Nature methods. 2015;12(5):404-6. doi: 10.1038/nmeth.3323. PubMed PMID: 25775044.
53. Carpenter AE, Jones TR, Lamprecht MR, Clarke C, Kang IH, Friman O, et al. CellProfiler: image analysis software for identifying and quantifying cell phenotypes. Genome biology. 2006;7(10):R100. doi: 10.1186/gb-2006-7-10-r100. PubMed PMID: 17076895; PubMed Central PMCID: PMC1794559.

FIGURE LEGENDS

Fig 1. Overview of the high-content screening and analysis. (**A**) Summary of RNAi libraries screened and screening workflow. Reverse transfection of HeLa cells in 384-well format followed by infection with GFP expressing *B. abortus*, PFA fixation, and staining of HeLa cells with DAPI and DY-547-Phalloidin before automated imaging. (**B**) Image analysis with CellProfiler to segment nuclei and bacteria and to extract measurements. (**C**) Accurate association of segmented bacteria to nuclei enables quantitative single cell measurements. The naive association (middle image) of segmented pathogen can be affected by over-splitting in dense cell populations (left image). Our proposed solution (right image) based on a nucleus attraction score. (**D**) The plate histogram shows the bimodal distribution of integrated GFP intensity corresponding to *Brucella* replication. Intensity on the X-axes is log2-scaled to account for exponential growth. The normal distribution fitted (red curve) to the Kernel Density Estimation of the histogram allows to compute a robust binary infection threshold (dashed line). Associated are samples of single-cell images corresponding to the intervals of the intensity distribution (for more details see Material and Methods).

Fig 2. The *human* infectome for *Brucella* infection determined by genome-wide siRNA screening. (A, B**)** High confidence protein-protein interaction networks (x > 0.7) for the top 200 RSA down- (A) or up-hits (B) determined using STRING database. After removal of siRNAs that strongly reduced cell number, individual siRNAs from the Qiagen library and the averages of independent replicates of the Dharmacon, Ambion, and Sigma libraries were used as input (see Material and Methods). Clusters with common predicted cellular function are colored and their function is indicated. Disconnected nodes are not displayed. (**C**) Representative merged images from the genome wide screen showing nuclei (DAPI) and intracellular replication of GFP expressing *Brucella abortus* for either control conditions (scramble) or a set of identified hits (Rab7A, FGFR1, COPZ1, AP2S1, TGFBR2, Vps35). All images from the screen are available at http://www.targetinfectx.ch/data_access. (**D, E**) Results of gene ontology enrichment analysis (DAVID) for the identified down-hits (D) or up-hits (E). The log10 of P-value associated to the different categories are indicated (cut-off P-value: 0.05) as well as the number of individual components associated to the presented categories.

Fig 3. Entry assay identifies components of the endosome-to-Golgi trafficking required for post-entry processes during *Brucella* infection. (A) Representative images from the entry assay showing nuclei (DAPI) of HeLa cells and intracellular *Brucella abortus* (GFP) for control condition (mock) and cells treated with siRNAs against Cdc42 or Vps35. Scale bar =100 µm. HeLa cells were infected with *B. abortus* expressing GFP under a tetracycline inducible system for 8 h (see Materials and Methods). (B) Scatter plot showing infection rates of the entry assay versus the endpoint assay, normalized to the mock dataset (Table S3). For the entry assay, cells containing single bacteria were considered infected and the final readout considered the median amount of bacteria in infected cells. For the endpoint assay, only cell that contain replicating bacteria (as described in Fig.1) were considered. Each data point corresponds to the average of all siRNAs or esiRNAs targeted against the gene of interest. Dotted lines indicate a 50% reduction of the corresponding infection rate relative to mock wells. Coloring show involvement of selected genes in indicated cellular pathways. In addition, all genes that resulted in at least a 50% reduction in the endpoint assay, but did not reduce infection in the entry assay by 50% are labeled, in

addition to Cdc42 as a control. Diagonal shows identical effects of siRNA treatment on *Brucella* infection on both assays relative to the corresponding control conditions.

Fig 4. The cargo recognition complex of the retromer is a key component of *Brucella* intracellular trafficking. (A) Schematic representation of the components of the retromer complex. (**B**) Dotbox representation of the z-scored infection index for components of the retromer complex and selected target including the positive control ARPC3 and RAB7a. (**C**) Schematic representation of the shRNA constructs used in (D). The gray box on the shVPS35 / Rescue construct indicates the silent mutations that prevent recognition by to the co-expressed shRNA. (**D**) Infection index of transfected cells infected with *Brucella abortus* for 48 h. Displayed are the averaged infection index and associated standard deviation, normalized to the YFP only condition (N=3).

Fig 5. Retro-2 inhibits *Brucella* infection at an early trafficking stage. (A) Effect of titration of Retro-2 on *B. abortus* infection. Hela cells were treated with 1 to 100 μM Retro-2 and concomitantly infected with GFP-expressing *B. abortus* for 48 h. Displayed are the infection index normalized to DMSO treated cells and associated standard deviation (N ≥3). Relative cell counts for the corresponding samples are plotted on the secondary y-axis. (**B**) Retro-2 only acts on early *Brucella* trafficking. Retro-2 (50 μM final concentration) was added to *Brucella*-infected Hela cells at 0, 4, 9, 16 and 24 hpi. Represented are the infection rates determined 48 hpi and normalized to DMSO treated cells (not displayed). Relative cell counts for the corresponding samples are plotted on the secondary y-axis. (**C, D**) Additive effect of Retro-2 and Vps35 knockdown on *Brucella* infection. Hela cells transfected with siRNA directed against Vps35 were treated with 0, 25 or 50 μM Retro-2 at the onset of infection with *B. abortus*. Mock transfected cells were treated in parallel. (**C**) The relative infection rate was determined for each conditions 48 hpi. (**D**) The relative siRNA inhibition was determined for each concentration of Retro-2. (A-D) Represented are the averages and associated standard deviations (N=3). (**E**) Representative merged images from the experiment presented in (C, D) showing nuclei (DAPI) and intracellular replication of GFP expressing *Brucella abortus* for control conditions or for cells treated with 50 μM Retro-2. Scale bar: 100 μm.

Fig 6. Vps35 is required for *Brucella* to escape the lysosomal pathway. (**A**) Immunofluorescence approach used to quantify localization of *Brucella* within LAMP-1 positive vesicles. Individual channels and merged picture are presented. Arrows indicate examples of co-localization of bacteria with LAMP-1 positive compartments. Staining of *Brucella* LPS (αLPS) was used to confirm the presence of LAMP-1 in direct proximity of the bacterial surface. Asterisks indicate examples of LAMP-1 negative *Brucella*. (**B**) Representative images from *Brucella* infected cells either mock transfected (ctrl) or after Vps35 knockdown (siVPS35). Samples were fixed 6 and 18 hpi. For clarity only the LAMP-1 (cyan) and dsRed (magenta) channels are presented. Scale bar: 5 μm. (**C**) Global quantification of LAMP-1 negative *Brucella.* Displayed are the average and associated standard deviation for more than 500 bacteria and more than 50 Hela cells per time point and condition (N=3). (**D**) Single-cell data representation of the data presented in (C). Displayed is the distribution of LAMP-1 positive *Brucella* per cell as a function of the total number of bacteria counted in that given cell.

Supporting information legends

Supporting Table S1: List of the 255 down-hits resulting from the RSA analysis with associated p-value and infection score (cut-off: p-value <0.01, S1_Table.xlsx).

Supporting Table S2: List of the 251 up-hits resulting from the RSA analysis with associated p-value and infection score (cut-off: p-value <0.01, (S2_Table.xlsx).

Supporting Table S3: Hit-list of the entry assay analysis wit associated infection scores for both entry and endpoint assays (S3_Table.xlsx).

3.2.3. Figures

Figure 1

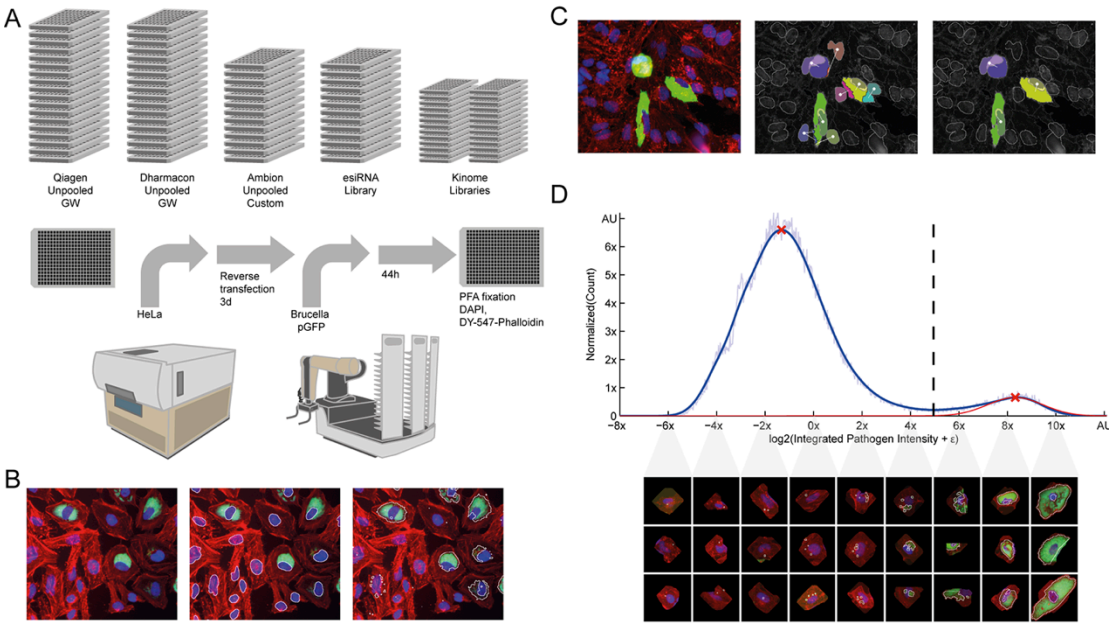

Figure 2

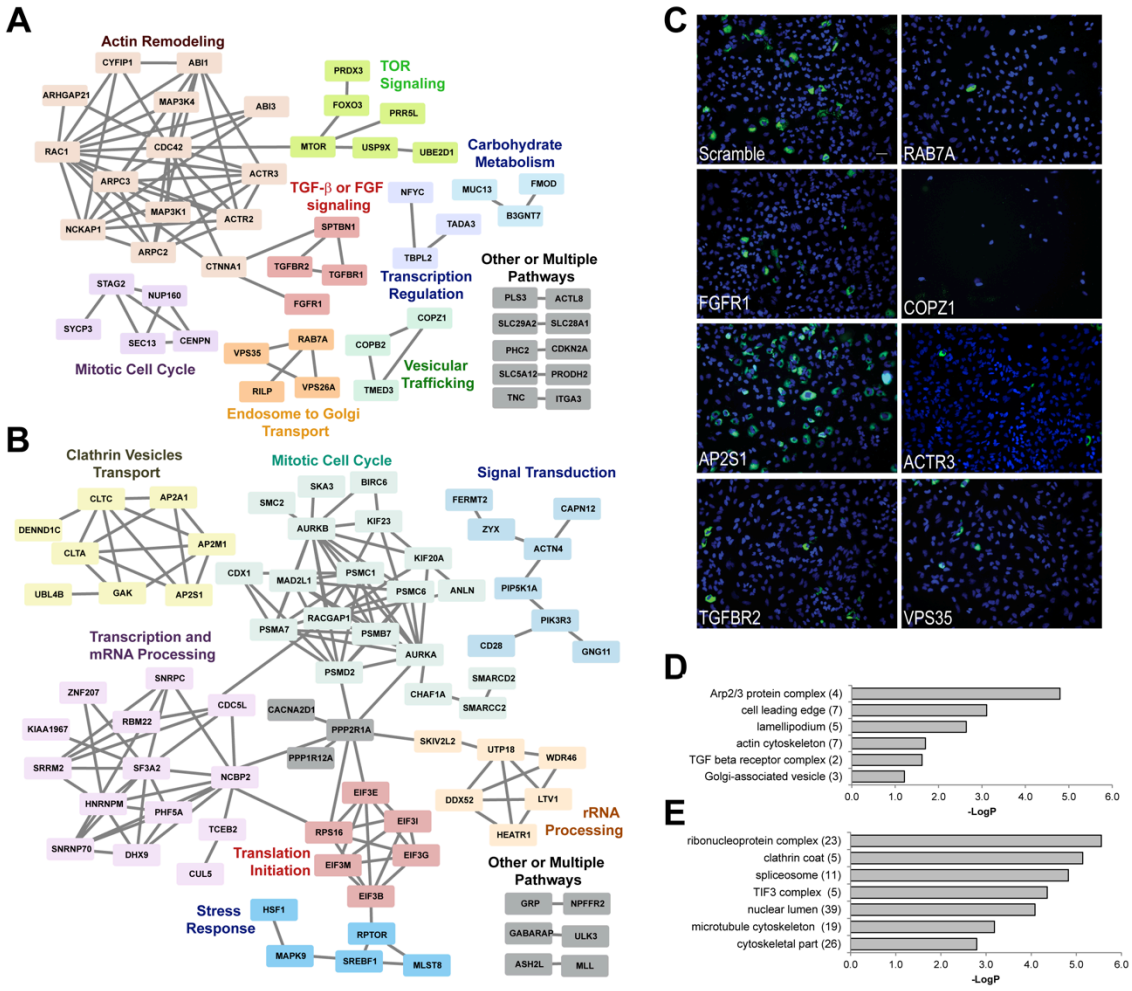
A
Actin Remodeling
CYFIP1
ABI1
ARHGAP21
MAP3K4
ABI3
RAC1
CDC42
ARPC3
ACTR3
MAP3K1
ACTR2
NCKAP1
ARPC2
CTNNA1
PRDX3
TOR Signaling
FOXO3
PRR5L
MTOR
USP9X
UBE2D1
Carbohydrate Metabolism
TGF-β or FGF signaling
NFYC
MUC13
FMOD
B3GNT2
SPTBN1
TADA3
TBPL2
TGFBR2
TGFBR1
FGFR1
Transcription Regulation
Other or Multiple Pathways
PLS3
ACTL8
SLC29A2
SLC28A1
PHC2
CDKN2A
SLC5A12
PRODH2
TNC
ITGA3
STAG2
NUP160
SYCP3
SEC13
CENPN
Mitotic Cell Cycle
COPZ1
COPB2
VPS35
RAB7A
RILP
VPS26A
TMED3
Vesicular Trafficking
Endosome to Golgi Transport
B
Clathrin Vesicles Transport
CLTC
AP2A1
DENND1C
AP2M1
CLTA
UBL4B
GAK
AP2S1
Mitotic Cell Cycle
SKA3
BIRC6
SMC2
AURKB
KIF23
CDX1
MAD2L1
PSMC1
KIF20A
PSMC6
ANLN
RACGAP1
PSMA7
PSMB7
AURKA
PSMD2
Signal Transduction
FERMT2
CAPN12
ZYX
ACTN4
PIP5K1A
PIK3R3
CD28
GNG11
Transcription and mRNA Processing
SNRPC
ZNF207
CDC5L
CACNA2D1
CHAF1A
SMARCD2
SMARCC2
RBM22
KIAA1967
PPP2R1A
SKIV2L2
UTP18
WDR46
SRRM2
SF3A2
PPP1R12A
NCBP2
EIF3E
DDX52
LTV1
HNRNPM
PHF5A
EIF3I
HEATR1
rRNA Processing
TCEB2
RPS16
SNRNP70
DHX9
Translation Initiation
EIF3G
EIF3M
CUL5
Other or Multiple Pathways
EIF3B
GRP
NPFFR2
Stress Response
HSF1
RPTOR
GABARAP
ULK3
MAPK9
SREBF1
MLST8
ASH2L
MLL
C
Scramble
RAB7A
FGFR1
COPZ1
AP2S1
ACTR3
TGFBR2
VPS35
D
Arp2/3 protein complex (4)
cell leading edge (7)
lamellipodium (5)
actin cytoskeleton (7)
TGF beta receptor complex (2)
Golgi-associated vesicle (3)
0.0
1.0
2.0
3.0
4.0
5.0
6.0
-LogP
E
ribonucleoprotein complex (23)
clathrin coat (5)
spliceosome (11)
TIF3 complex (5)
nuclear lumen (39)
microtubule cytoskeleton (19)
cytoskeletal part (26)
0.0
1.0
2.0
3.0
4.0
5.0
6.0
-LogP

Figure 3

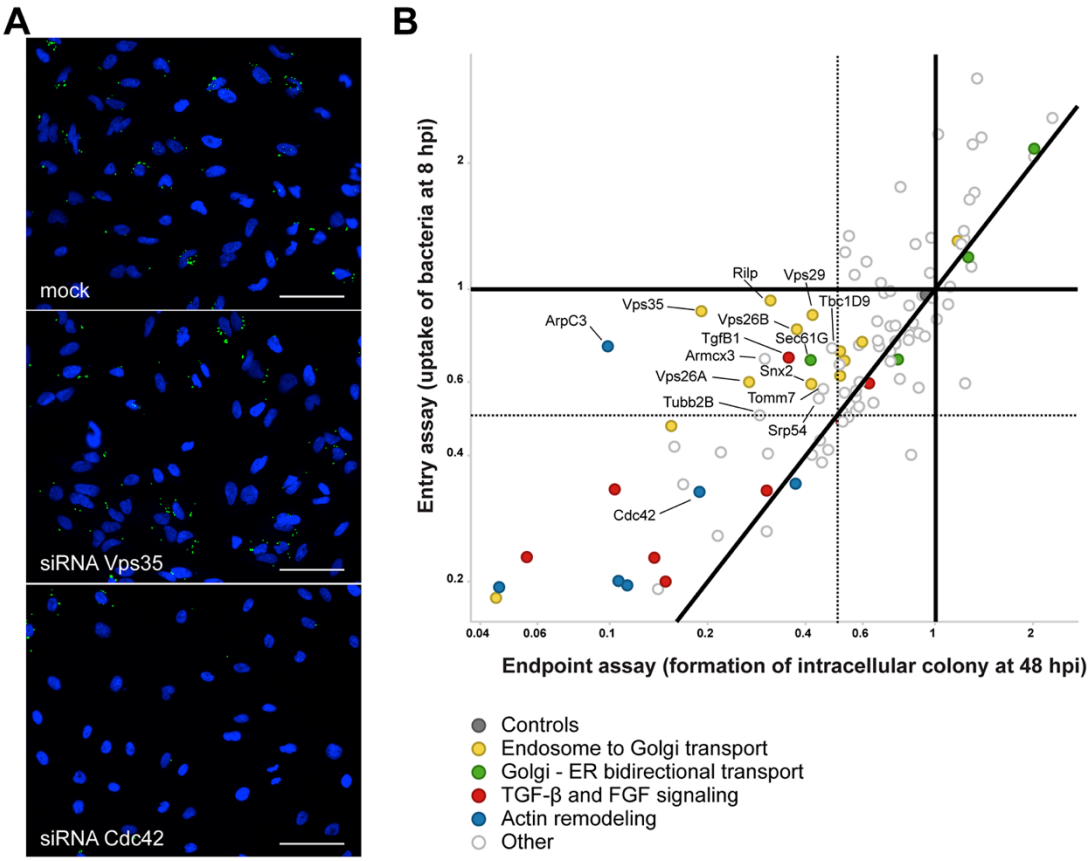
A
mock
siRNA Vps35
siRNA Cdc42
B
Entry assay (uptake of bacteria at 8 hpi)
Endpoint assay (formation of intracellular colony at 48 hpi)
Rilp
Vps29
Vps35
Tbc1D9
ArpC3
Vps26B
TgfB1
Sec61G
Armcx3
Snx2
Vps26A
Tubb2B
Tomm7
Srp54
Cdc42
Controls
Endosome to Golgi transport
Golgi - ER bidirectional transport
TGF-β and FGF signaling
Actin remodeling
Other

Figure 4

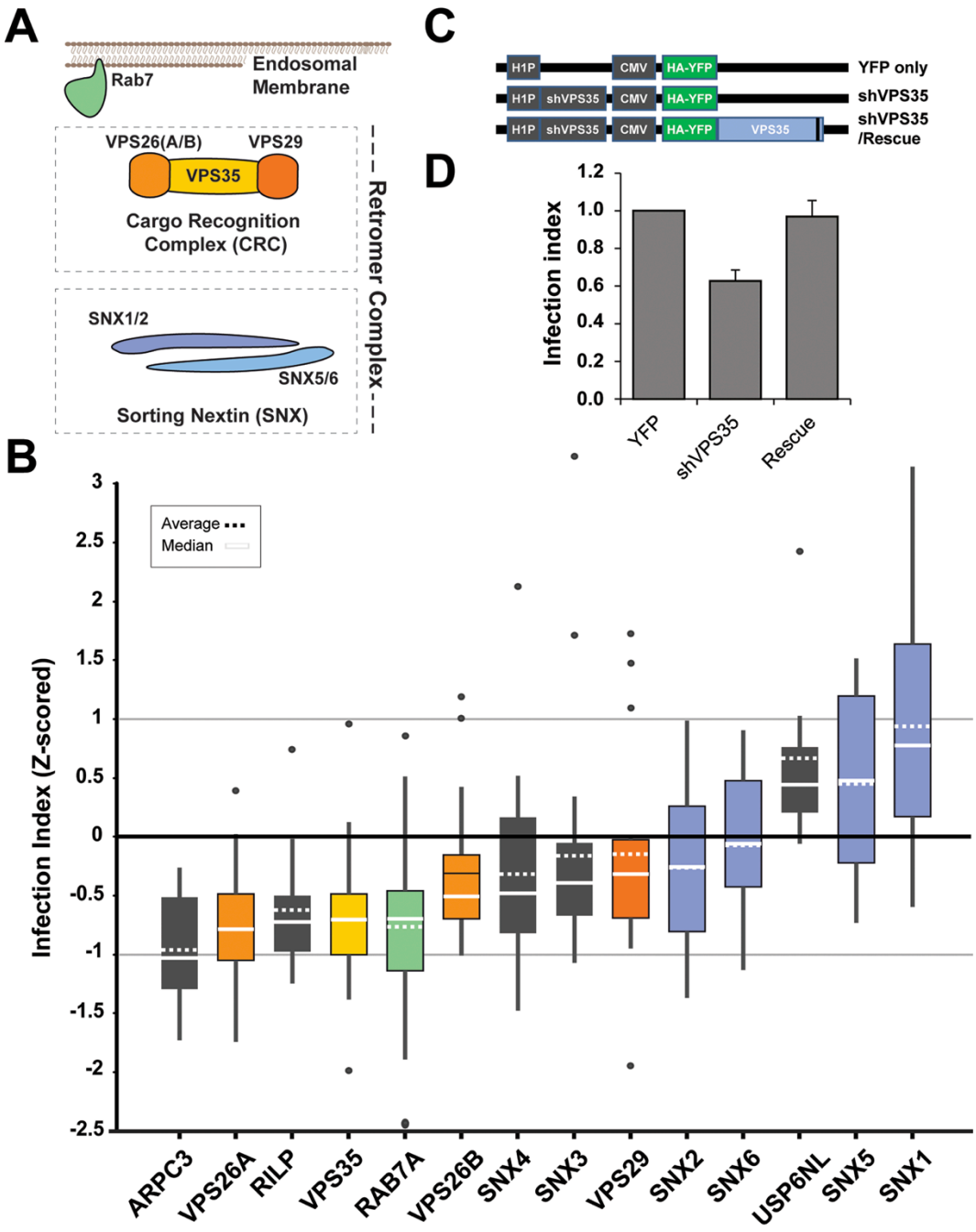
A
Rab7
Endosomal Membrane
VPS26(A/B)
VPS29
VPS35
Cargo Recognition Complex (CRC)
SNX1/2
SNX5/6
Sorting Nextin (SNX)
Retromer Complex
C
H1P
CMV
HA-YFP
YFP only
H1P
shVPS35
CMV
HA-YFP
shVPS35
H1P
shVPS35
CMV
HA-YFP
VPS35
shVPS35 /Rescue
D
Infection index
1.2
1.0
0.8
0.6
0.4
0.2
0.0
YFP
shVPS35
Rescue
B
Infection Index (Z-scored)
Average
Median
3
2.5
2
1.5
1
0.5
0
-0.5
-1
-1.5
-2
-2.5
ARPC3
VPS26A
RILP
VPS35
RAB7A
VPS26B
SNX4
SNX3
VPS29
SNX2
SNX6
USP6NL
SNX5
SNX1

Figure 5

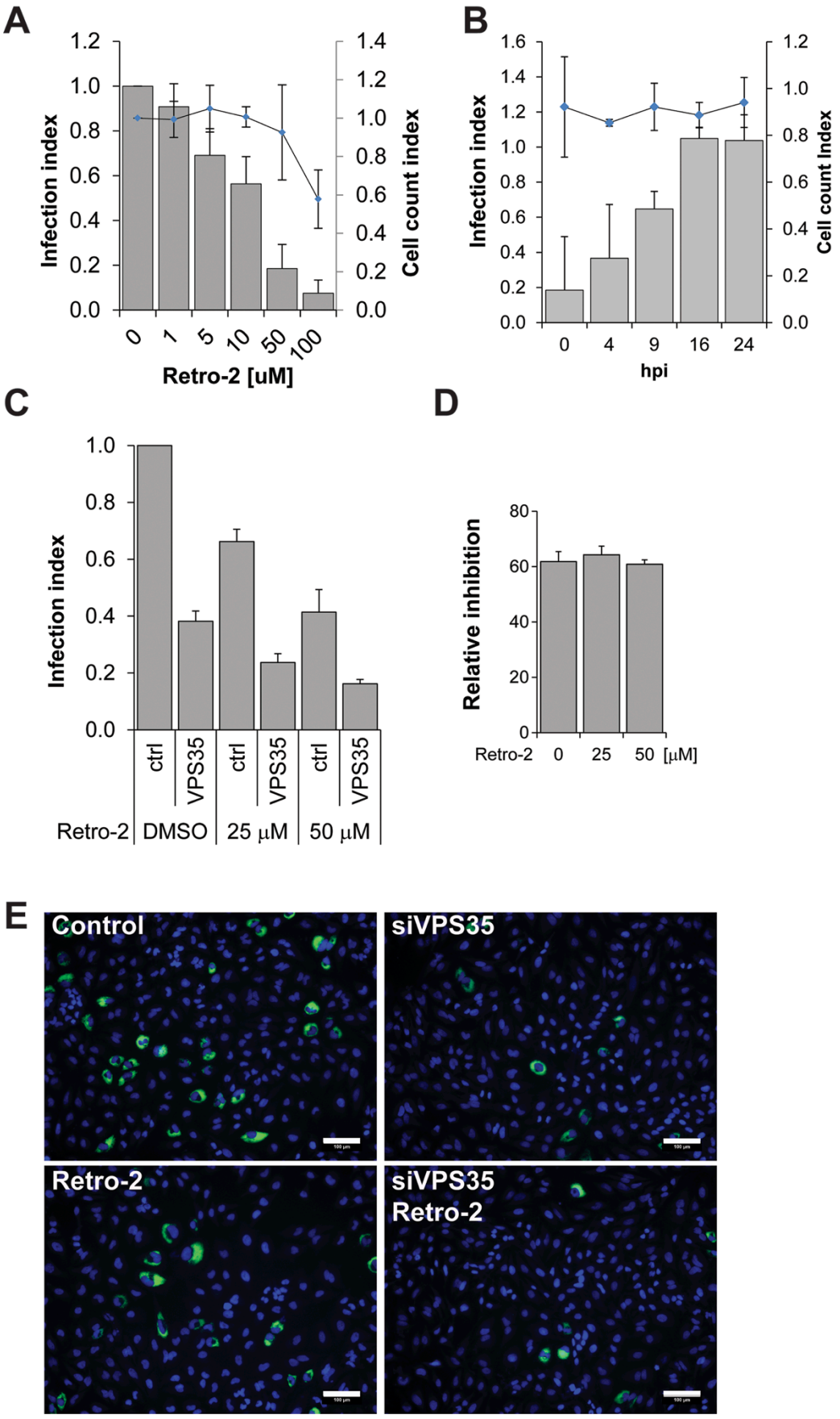
A
Infection index
Cell count index
Retro-2 [uM]
0
1
5
10
50
100
B
Infection index
Cell count Index
hpi
0
4
9
16
24
C
Infection index
ctrl
VPS35
Retro-2
DMSO
25 µM
50 µM
D
Relative inhibition
Retro-2
0
25
50 [µM]
E
Control
siVPS35
Retro-2
siVPS35
Retro-2

Figure 6

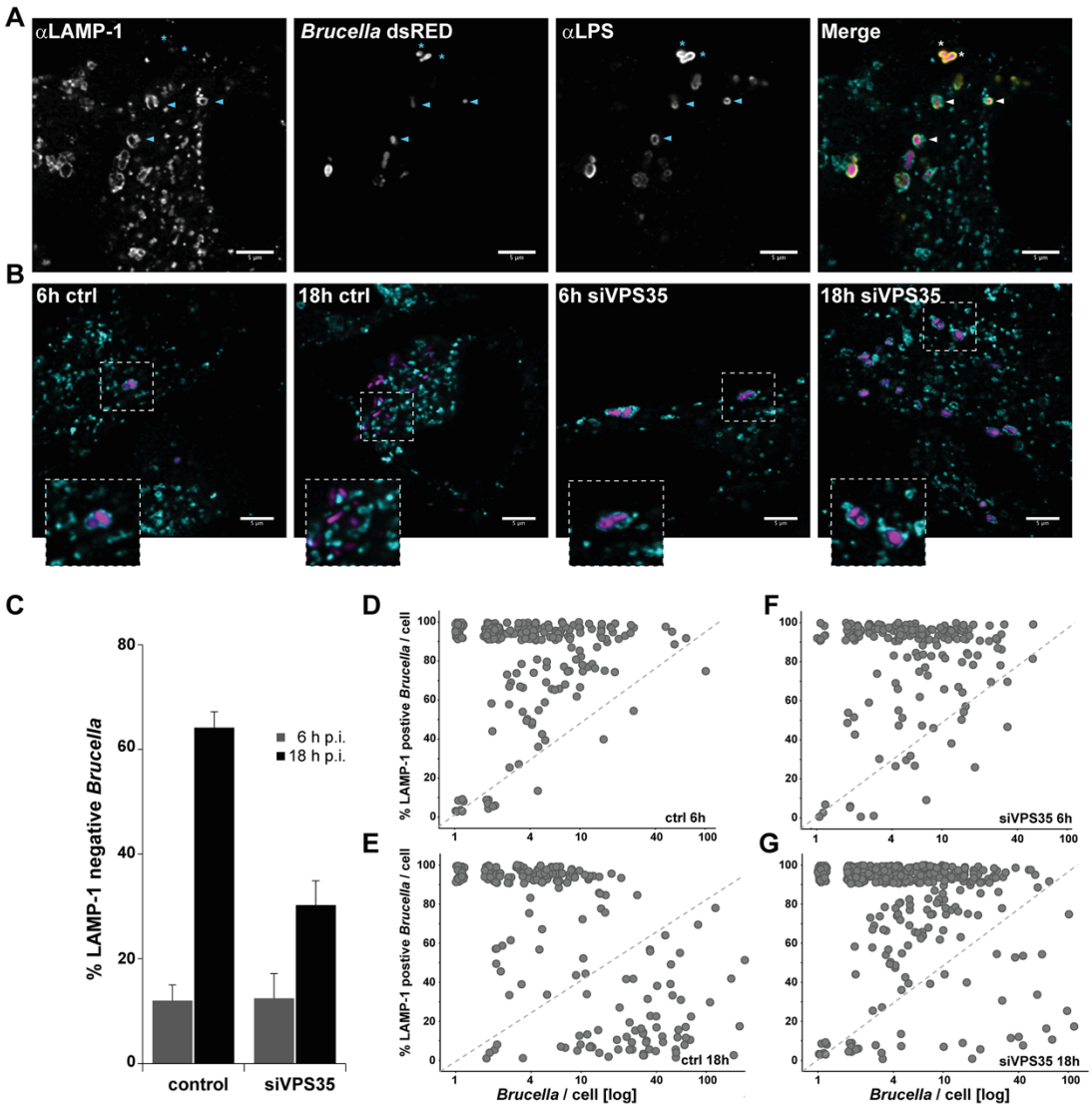
A
αLAMP-1
Brucella dsRED
αLPS
Merge
B
6h ctrl
18h ctrl
6h siVPS35
18h siVPS35
C
% LAMP-1 negative Brucella
6 h p.i.
18 h p.i.
control
siVPS35
D
% LAMP-1 postive Brucella / cell
ctrl 6h
E
ctrl 18h
F
siVPS35 6h
G
siVPS35 18h
Brucella / cell [log]

3.3. Unpublished results: Vacuolar escape of *Brucella abortus* during intermediate trafficking

3.3.1. Introduction

The intracellular trafficking of *Brucella* is a complex and carefully orchestrated process (see section 1.2.3). The initial non-replicative *Brucella*-containing vacuole (nrBCV) requires several hours until successful transition to the replicative niche (rBCV) can be achieved [1]. The vacuole traffics along the endocytic pathway, eventually interacting with late endosomes (LE) and, to a limited extent, with lysosomes. The essential factor in the establishment of the rBCV is the VirB T4SS, which introduces effector proteins into the host cell to alter trafficking processes [2-4]. There have been several reports providing insights into the nature and dynamics of the transition between the nrBCV and the rBCV. The acquisition of ER-derived membranes by the vacuole has been linked to interactions with the early secretory pathway, in particular with ER-exit sites (ERES) [4, 5]. There are also indications that the cell cycle of the bacteria is synchronized with the trafficking process, with the initial division occurring just before the transition [6]. However, the specific mechanism behind this process remains unclear and there is a need for a more integrated explanation.

Different microscopic approaches have been successfully used to study intracellular trafficking of numerous pathogens. The usage of various light microscopy (LM) and electron microscopy (EM) techniques led to many key discoveries about the localization of intracellular pathogens and their interactions with different host organelles. Through expression of different fluorescently tagged proteins, LM can provide useful information about the colocalization and interactions of pathogens with specific host cell structures. However, the approach is limited in resolution and only allows the recording of signals emitted by fluorophores, leaving information about non-tagged structures outside our scope. EM, on the other hand, allows the observation of actual cellular structures at much higher resolution, providing information that is normally unavailable to LM. By using correlative light and electron microscopy (CLEM), one can benefit from the advantages of both microscopic techniques and gain a richer insight into cellular processes.

The initial goal of the study was to visualize *Brucella* trafficking at intermediate stages of infection by using CLEM. This strategy solves many issues normally faced in the EM studies of *Brucella*. EM is a relatively low-throughput technique, which makes imaging of rare events challenging. Different aspects of *Brucella* infection in cell culture pose potential problems in this aspect. Due to low infection rates in mammalian cell culture (around 5-10%, personal communication) it is difficult to target infected cells. The percentage of bacteria that manage to establish the rBCV is also relatively low (10-40%, personal communication), resulting in most of the bacteria in a given sample representing off-pathway events that do not result in replication. In addition, the trafficking of *Brucella* lacks synchronization between different cells in the same sample.

The CLEM approach allowed us to localize infected cells with a fluorescent microscope and target them specifically using EM. Apart from localization of *Brucella*, we could use fluorescent markers to target cellular structures colocalizing with the bacteria. The study lead to the observation of a previously unreported cytosolic form of *Brucella*, suggesting that in some circumstances the pathogen is able to escape from the BCV into the host cell cytosol.

3.3.2. Results

CLEM reveals BCVs at different trafficking stages

The combination of fluorescence microscopy and EM allowed us to target BCVs at intermediate trafficking stages (Fig. 1). FIB/SEM of HeLa cells infected with *Brucella abortus* revealed that at 12-16 h.p.i., intracellular bacteria reside inside BCVs (Fig. 1A). The majority of BCVs contained one or two bacteria, with some exceptions suggesting the possibility of internalization of larger groups of Brucellae (Fig. 1A, B). The intracellular trafficking of *B. abortus* takes several hours, which results in lack of synchrony between different cells. The chosen time point allowed us to observe BCVs at different trafficking stages. Most of the BCVs hosted non-dividing bacteria and displayed features indicating their LE nature, with electron-dense deposits inside the vacuoles (Fig. 1A). In addition, we were able to find cases of initial *Brucella* division inside BCVs showing continuity with the ER, which suggest successful establishment of the rBCV (Fig. 1C,D).

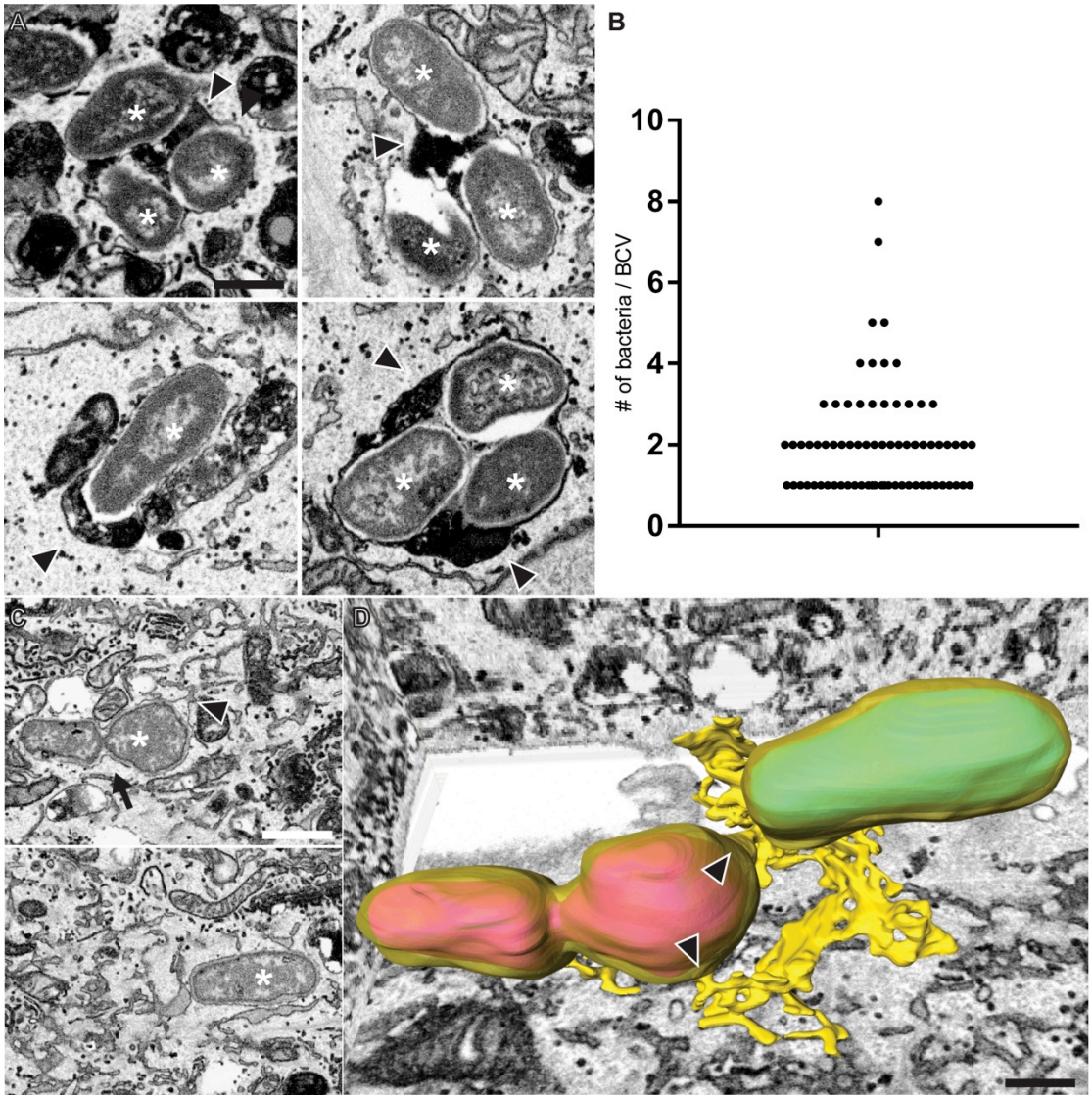

Figure 1. Intermediate stages of *Brucella* intracellular trafficking revealed by FIB/SEM. (A) Example frames from FIB/SEM stacks depicting BCVs inside HeLa cells 12-16 h.p.i. There are one to several bacteria located in each BCV (asterisks). The electron-dense deposits inside the vacuoles (arrow heads) indicate that they are still at the nrBCV stage. **(B)** Quantification of the amount of bacteria per BCV at 12-16 h.p.i. Only nrBCVs were taken into account (n=72). **(C)** FIB/SEM images of a HeLa cell infected with *B. abortus*, 12 h.p.i. The images represent two frames at the same location in a 3D stack. The bacteria (asterisks) are located inside BCVs. One bacterium is undergoing cell division (arrow). The BCV containing the dividing bacterium is continuous with host organelles (arrow head). **(D)** 3D reconstruction of (C). The BCV containing the dividing bacterium (magenta) is continuous with host ER cisternae (yellow) (arrow heads). The non-dividing bacterium is marked with cyan. G: Golgi apparatus; M: mitochondria. Scale bars: 500 nm (A, D); 1 μm (C).

***B. abortus* can be found directly in the cytosol at intermediate trafficking stages**

The next step was to employ CLEM in order to analyze interactions of the BCV with specific cellular structures. The cellular markers initially used in this study were GFP-fusions of two proteins, ERGIC53 [7] and syntaxin-6 (STX6) [8]. ERGIC53 is a mannose-binding type I membrane protein, which is a cargo receptor that facilitates export of glycoproteins from the ER. It is distributed mainly across ERGIC and in smaller quantities to ERES and cis-Golgi [7]. The marker was chosen based on previous reports suggesting interactions with the early secretory pathway as a key step during the trafficking towards the rBCV [5]. STX6 is a SNARE protein involved mainly in trafficking events between the plasma membrane and TGN [8].

For both EGFP-ERGIC53 and GFP-STX6, we were able to locate events where *Brucella* was colocalizing with the markers in LM images (Fig. 2A, B). Surprisingly, the FIB/SEM imaging indicated that some of the colocalizing bacteria were residing directly in the cytosol. The cytosolic bacteria were surrounded by host membranes (Fig. 2C, D, E, F). EGFP-STX6-positive structures were found to form an assembly of double membranes engulfing the bacteria (Fig. 2C, D), the whole structure resembling a growing autophagosome. The EGFP-ERGIC53-positive structures, on the other hand, were less tightly associated with the bacteria surface (Fig. 2E, F). They extended into a meshwork of membranes that resembled ERGIC structures.

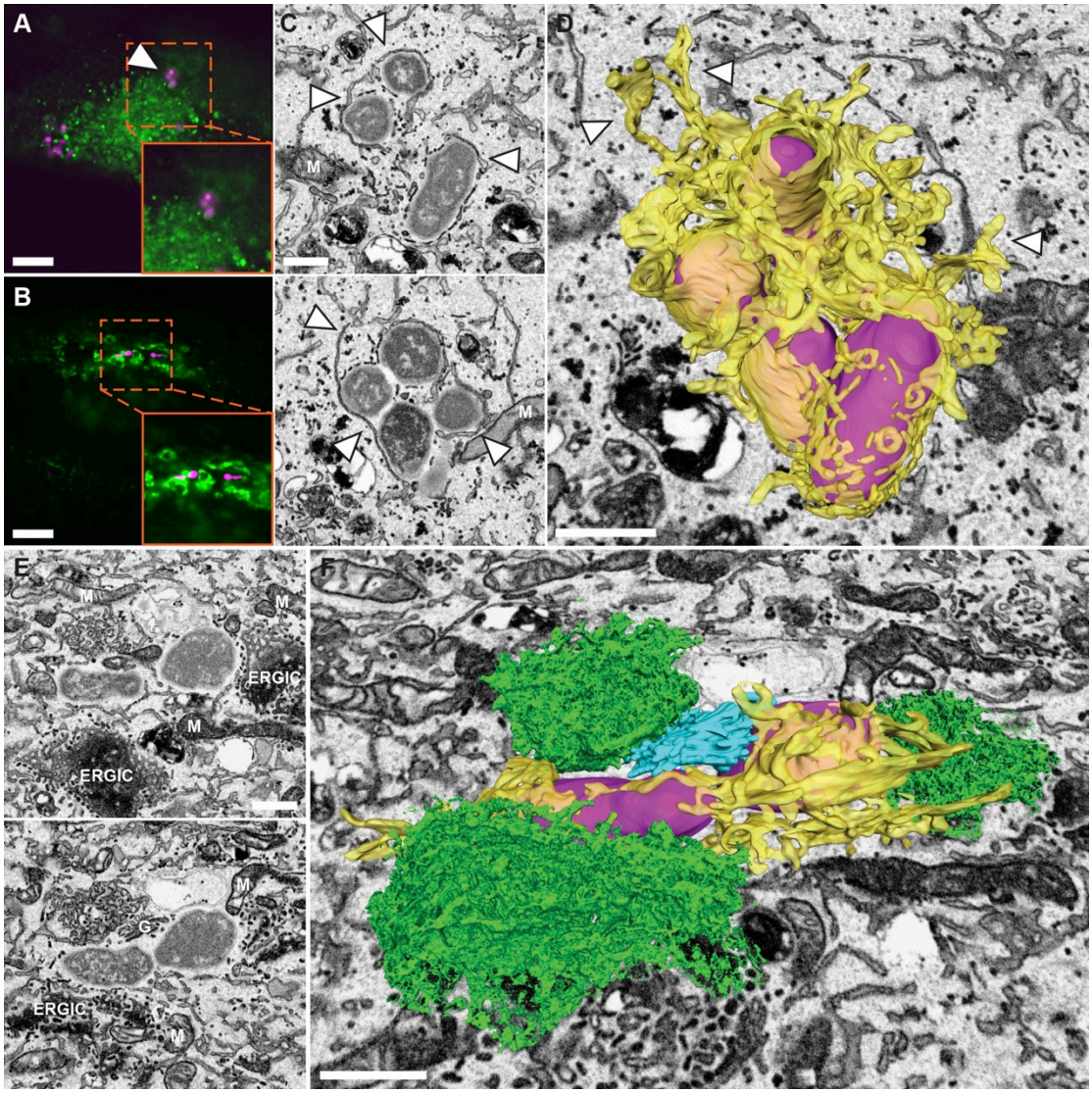

Figure 2. Correlative FIB/SEM reveals the presence of cytosolic *B. abortus* at intermediate stages of infection. (A) HeLa cell expressing GFP-STX6 (green) infected with *B. abortus*-dsRed (magenta) 16 h.p.i. Several bacteria have been taken up by the cell. In some cases, the marker can be seen localizing around a group of B. abortus (arrow head). The region marked with the orange box was imaged using FIB/SEM (C). **(B)** HeLa cell expressing GFP-ERGIC53 (green) infected with *B. abortus*-dsRed (magenta) 12 h.p.i. The region marked with the orange box was imaged using FIB/SEM (E). **(C)** Two frames from a FIB/SEM tomogram depicting a group of *B. abortus* from (A). The bacteria are located directly in the cytosol, surrounded by flattened cisternae (arrow heads). **(D)** 3D reconstruction of (C). The flattened cisternae (yellow) are a part of a membrane network that wraps around the bacteria (magenta), indicating autophagy. The membranes extend beyond the location and are continuous with the host ER (arrow heads). **(E)** Two frames from a FIB/SEM tomogram of the region marked in (B). The bacteria are located directly in the cytosol. Different organelles can be found in the proximity of the bacteria. **(F)** 3D reconstruction of (E). The bacteria are surrounded by a network of ER membranes (yellow), ERGIC structures (green) and Golgi apparatus (cyan). G: Golgi apparatus; M: mitochondria. Scale bars: 7 μm (A, B); 500 nm (C-F).

***B. abortus* colocalizes with Galectin-3 at intermediate trafficking stages in a VirB-dependent manner.**

In order to further explore the prevalence of the cytosolic form of *B. abortus*, we decided to use a phagosomal escape marker, GFP-Galectin-3 (GFP-Gal3). This fusion protein, when expressed in the cytosol of infected eukaryotic cells, has high affinity to sugar residues normally found on the outer side of the plasma membrane [9]. During phagocytosis, the membrane is incorporated into the growing phagosome, with the sugar residues present on the inner side. Vacuole rapture enables the access of the marker to the phagosome lumen, causing massive GFP-Gal3 recruitment to the membrane. GFP-Gal3 has been previously employed to visualize the escape of *Shigella* from the endosome [10].

Confocal microscopy of *Brucella*-infected HeLa cells expressing GFP-Gal3 revealed a small subpopulation of bacteria that is surrounded by the marker at 8 h.p.i. (Fig. 3A). GFP-Gal3-positive Brucellae were only found in a small portion of infected cells. Even in those cells, the proportion of bacteria colocalizing with the marker was often low, with mostly one positive bacterium located with several negative ones within the same host cell. Interestingly, we were unable to observe GFP-Gal3 binding in HeLa cells infected with the *B. abortus ΔvirB9*, which is unable to assemble a functional T4SS (Fig. 3A, right panel). This suggests that the process of phagosome rapture depends on a functional T4SS.

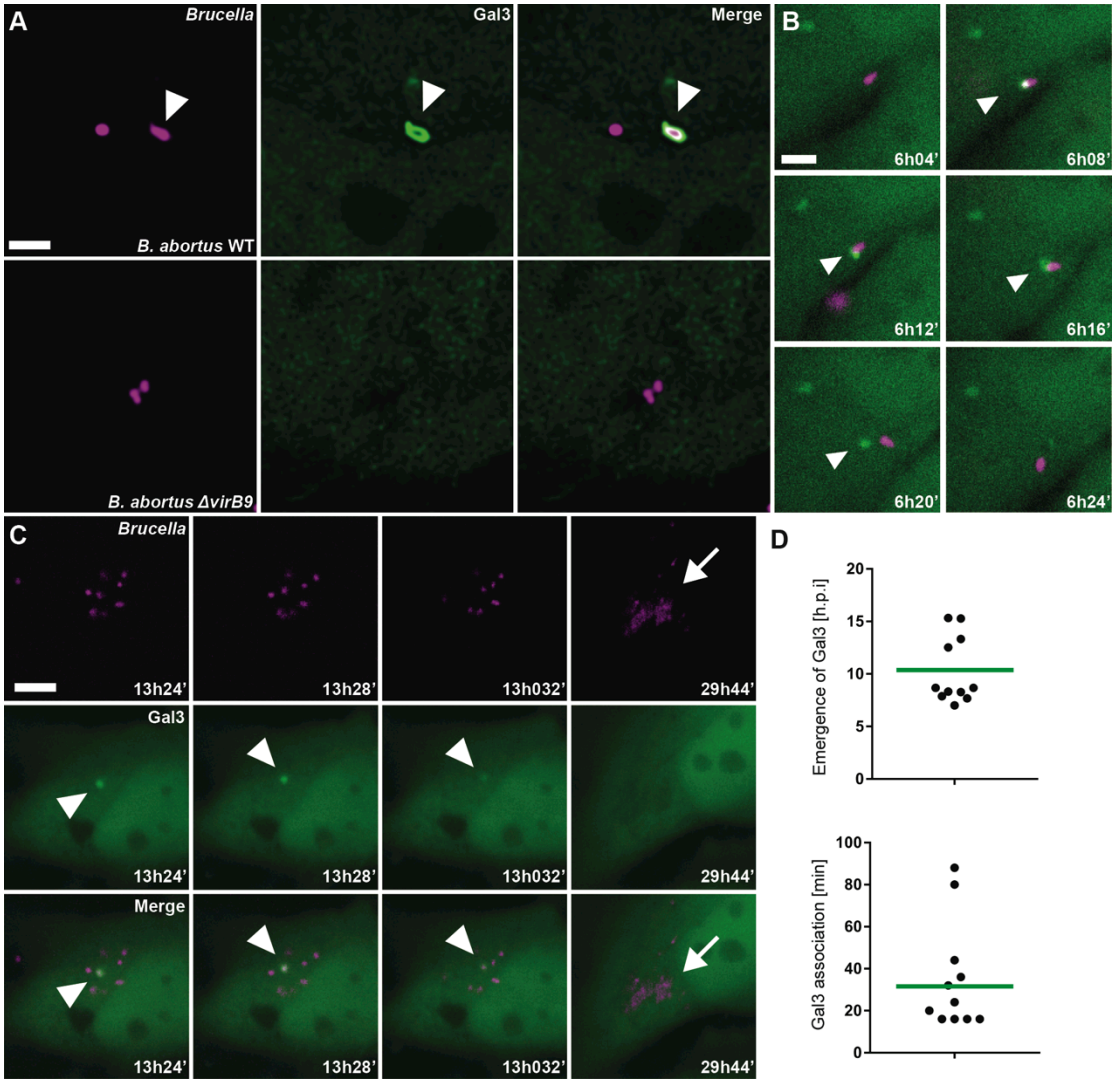

Figure 3. Colocalization of *B. abortus* with GFP-Gal3. (A) Representative confocal images of HeLa cells expressing GFP-Gal3 (green) infected with *B. abortus* (magenta) 8 h.p.i. The *B. abortus* strains used were either wild-type (top) or ***Δ****virB9* mutant (bottom). Some of the wild-type bacteria are surrounded by GFP-Gal3 (arrow head), suggesting phagosome rapture. Such events were not observed in the case of ***Δ****virB9* mutant. **(B)** Live-cell imaging HeLa cells expressing GFP-Gal3 (green) infected with *B. abortus* (magenta). Time post-infection is indicated for each frame. GFP-Gal3 transiently colocalizes with and then dissociates from the bacterium (arrow heads). **(C)** Live-cell imaging HeLa cells expressing GFP-Gal3 (green) infected with *B. abortus* (magenta). Association with GFP-Gal3 (arrow head) is followed by formation of the rBCV, indicated by the *Brucella* microcolony (arrow). **(D)** Quantification of GFP-Gal3 colocalization events in live-cell data form infected HeLa cells. Colocalization of *Brucella*-dsRed with GFP-Gal3 was evaluated in cells that were found to have a microcolony developing at later time points. Out of the whole population (n=15), GFP-Gal3 was transiently colocalizing with the bacteria in 11 cells. The top graph indicates the time point of infection (h.p.i.) of the colocalization events. The bottom graph indicates the total time (min.) of association between *Brucella* and GFP-Gal3. Scale bars: 4 μm (A, B); 8 μm (C).

Live cell imaging indicates that vacuole escape of *Brucella* coincides with the establishment of the replicative niche in HeLa cells

We speculated that vacuole rapture and escape of the bacteria is a relatively short process (up to several minutes) that can take place within a long timeframe (potentially up to few hours). This would make the probability of finding such an event in a fixed sample relatively low. For this reason, we turned towards live-cell imaging of HeLa cells stably expressing GFP-Gal3 (Fig. 3B-D). Due to technical limitations associated with *Brucella* being classified as a risk group 3 organism, the earliest time point possible in practice for starting the image acquisition is around 3 h.p.i. The movies revealed that there are a number of HeLa cells within the sample where *Brucella* transiently associates with a strong signal from GFP-Gal3 (Fig. 3B, Movie S1). The time of the interaction with the marker varied between cells, with an average time of 35 min (Fig. 3D, bottom) and ended with the bacteria dissociating from the GFP-Gal3 complex. This suggests that the BCV might recruit the marker due to rapture, which is followed by cytosolic escape. In some cases we could observe that this event is followed by the first bacteria division and eventual establishment of *Brucella* microcolonies, indicating successful transition to the rBCV (Fig. 3C, Movie 1). The timing of GFP-Gal3 colocalization varied between 7-15 h.p.i, indicating weak synchronization of the process between cells (Fig. 3D, top).

The presence of more than one bacterium inside most of the HeLa cells posed difficulty with the interpretation of the movies. Even in HeLa cells that developed microcolonies, we could find indications that non-dividing bacteria were present next to the dividing ones. This suggests that *Brucella*-infected HeLa cells may contain both dividing and non-dividing bacteria at the same time, which further complicates interpretation of the data. The depth and time resolution of the microscope used in the study did not allow us to track the GFP-Gal3-positive bacteria with full certainty. For this reason it remains to be determined if these bacteria are responsible for the formation of the rBCV, or rather represent an erroneous side pathway that leads to bacteria clearance.

***Brucella abortus* colocalizes with the autophagy nucleation factor OPTN in a VirB-dependent manner**

One of the possible outcomes of phagosome escape of bacteria into the cytosol is the recruitment of autophagy proteins and subsequent engulfment in an autophagosome [11]. Our initial EM data suggests that this is one of the possible outcomes for cytosolic *Brucella*. One of the autophagy proteins that have been shown to colocalize with cytosolic bacteria is optineurin (OPTN), an adaptor responsible for autophagosome assembly [12]. For this reason, we decided to examine the colocalization of *Brucella* with the marker EGFP-OPTN (Fig. 4).

Confocal microscopy images of HeLa cells infected with *B. abortus* indicated that at 8 h.p.i some bacteria are surrounded by GFP-OPTN-positive structures (Fig. 4A, top). However, the frequency of those events was low, resembling GFP-Gal3 colocalization observed earlier. In case of cells infected with the *ΔvirB9* strain, we were unable to find similar colocalization events at indicated time point (Fig. 4A, bottom).

We next decided to check if the bacteria colocalizing with GFP-OPTN are located within the eBCV, or have already exited the LE compartment. To determine this, we used antibody staining for the lysosome-associated membrane protein 1 (LAMP-1), a marker known to associate with eBCVs (Fig. 4C) [2]. Confocal microscopy confirmed that most (83%; n=41) of bacteria surrounded by GFP-OPTN structures were negative for LAMP-1. This suggests that these bacteria represent a subpopulation that has already exited the eBCV and is either located in the cytosol or inside the rBCV. In order to confirm this observation, we employed the CLEM approach. Correlative FIB/SEM tomography of GFP-OPTN-positive *Brucella* indicated that the bacteria are partially surrounded by a double membrane, which colocalizes with GFP-OPTN signal from the confocal microscopy data (Fig. 4C-E). Parts of the bacteria that were not encompassed by GFP-OPTN had a single membrane around them. This single membrane was, however, not present underneath the growing autophagosome (Fig. 4D, E).

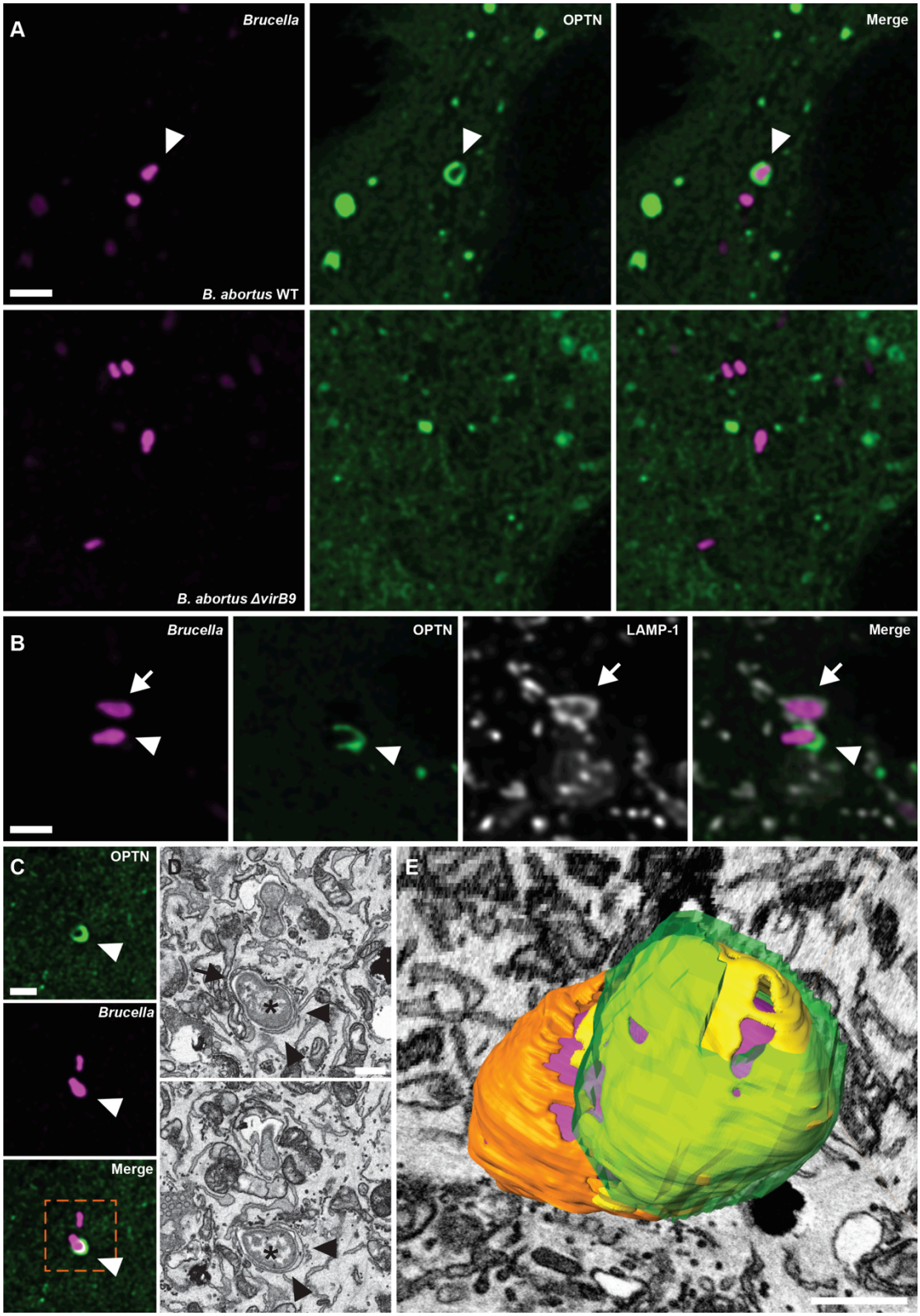

Figure 4. The role of OPTN in *Brucella* infection. (A) Representative confocal images of HeLa cells expressing GFP-OPTN (green) infected with *B. abortus* (magenta) 8 h.p.i. The *B. abortus* strains used were either wild-type (top) or *ΔvirB9* mutant (bottom). Some of the wild-type bacteria are surrounded by GFP-OPTN (arrow head). Such events were not observed in the case of *ΔvirB9* mutant. **(B)** Representative confocal images of HeLa cells expressing GFP-OPTN (green) infected with *B. abortus* (magenta) 8 h.p.i., stained for LAMP-1. One of the bacteria (top, arrow) is located within a LAMP-1-

positive compartment, while the other (bottom, arrow) is located outside the LAMP-1 compartment and partially engulfed by GFP-OPTN. **(C)** Confocal microscopy of a HeLa cell expressing GFP-OPTN (green) infected with *B. abortus* (magenta), 8 h.p.i. One of the bacteria is partially surrounded by the marker, indicating autophagy (arrow head). The box indicates an area imaged using FIB/SEM. **(D)** Two slices from a FIB/SEM tomogram of the site from (C). The bottom bacterium (asterisk) is partially surrounded by a double membrane (arrow heads) resembling an autophagosome. There is also a partial single membrane around the bacterium (arrow) **(E)** 3D reconstruction of the autophagy event in (D), with superimposed GFP signal from (C). The bacterium (magenta) is partially surrounded by a double membrane (yellow) that colocalizes with the GFP-OPTN signal (green). There is also a fragment of a single-membrane vacuole left around the bacterium (orange). Scale bars: 4 μm (A); 2 μm (B); 1.5 μm (C); 500nm (D); 300 nm (E).

Movie 1. Live-cell imaging of B. abortus vacuolar escape. Live-cell microscopy of HeLa cells expressing GFP-Gal3 (green) infected with *B. abortus*-dsRed (magenta). GFP-Gal3 (arrow) transiently colocalizes with *Brucella* (arrow head). Time post-infection is indicated for each frame.

3.3.3. Discussion and outlook

There are several intracellular pathogens that can reside directly in the cytosol of host cells at least at some stages of their intracellular lifestyle [13]. In case of *B. abortus*, there has been no evidence so far of phagosomal escape. By using a combination of CLEM and live-cell imaging, we were able to demonstrate that phagosome rapture and cytosolic escape take place during *B. abortus* infection of HeLa cells. The actual role of this process in the intracellular trafficking of *Brucella* and the establishment of the rBCV remains unclear. Our data indicates that vacuole rapture is T4SS-dependent, suggesting that the bacteria might actively induce the process through one or more effector proteins. There are known examples of pathogens that use secreted proteins to trigger vacuole escape [10, 14-16]. Unfortunately, our knowledge of the exact role of the T4SS in *Brucella* infection is limited to only few examples [4, 17]. To date, there are no reports indicating a *Brucella* protein that could potentially orchestrate cytosolic escape.

We could show that the escape of bacteria into the cytosol can be followed by the association of optineurin and engulfment by autophagy membrane, which is an outcome previously reported for *Salmonella* [12]. Our FIB/SEM data indicates that this process may occur relatively fast, since we could observe an autophagosome growing around a bacterium that was still partially surrounded by a single-membrane vacuole. This could explain why we observed LAMP1 colocalization of some of GFP-OPTN-positive bacteria.

The fate of the cytosolic *Brucella* remains unclear. There are several possible outcomes that follow phagosome rapture. The fundamental question in this case is whether the cytosolic bacteria are the ones responsible for the formation of the rBCV, or rather an erroneous off-pathway event that leads to their elimination by autophagy.

The most straightforward explanation is that phagosome escape leads to bacteria killing. The T4SS-dependence of the process may indicate that effector introduction or the secretion machinery itself induce membrane stress that in rare cases leads to vacuole rapture. The low frequency of galectin-3 colocalization suggests that these events are side effects that occur only to a small group of the bacteria. The association of optineurin with cytosolic bacteria has been shown to result in growth restriction during *Salmonella* infection [12]. It is probable that a similar process takes place during *Brucella* trafficking and eventually leads to

clearance of the pathogen. The risk of phagosome rapture and killing by autophagy may be one of the factors responsible for the low success rate during the trafficking between the nrBCV and the rBCV.

An alternative hypothesis is that the vacuole escape eventually leads to the formation of the rBCV. It is well established that the rBCV is a single-membrane compartment associated with the ER. Formation of the rBCV by the cytosolic bacteria would in this case require re-entry into a membranous organelle from the cytosol. A similar process takes place during *Francisella tularensis* trafficking inside host cells and is autophagy-dependent [18]. There is a possibility that the association of *Brucella* with optineurin and autophagy of cytosolic bacteria observed by EM are manifestations of a similar pathway. Autophagosome membranes are believed to be mostly of ER origin [19] and it is possible that *Brucella* could somehow use this process to enter the ER. This would, however, involve mechanisms that would strongly divert from known events following autophagosome formation and need to be approached with skepticism.

An alternative explanation could be that this process represents a “division of labor” between different bacteria inside the same host cell, where one sacrifices itself in order to introduce effector proteins that later orchestrate the formation of rBCV by the remaining bacteria [20].

At this point we do not possess enough data to determine the significance of cytosolic bacteria for the intracellular trafficking of *Brucella*. Regardless of its role, the phagosome escape represents an interesting observation that may potentially be of great importance for the survival of the pathogen inside host cells. Further research needs to shed light on the fate of cytosolic *Brucella* in trafficking and the role of different bacteria and host factors in this process.

3.3.4. Materials and methods

Reagents

In-fusion HD cloning kit (Clontech, 639649), HeLa (human cervical carcinoma epithelial cell line, ATCC, CCL-2); human embryonic kidney 293T (HEK-293T) (from Hwain Cornelis's lab); Dulbecco Modified Eagle Medium Glutamax (DMEM Glutamax) (Gibco, 61965-026); RPMI-1640 medium (Sigma, R0883); Fetal Calf Serum (FCS) (Gibco, 10270): heat inactivated at 56°C for 30 min.; tryptic soy broth (TSB) (Fluka, 22092); kanamycin sulfate (Sigma-Aldrich, 60615); ampicillin sodium salt (Applichem, A.8039.0025); gentamicin (Sigma, G1397); paraformaldehyde (Sigma, P6148); phosphate buffered saline (PBS) (Gibco, 20012); EcoRI (New England Biolabs, R3101); BamHI (New England Biolabs, R3130); polybrene (Sigma, H9268); Triton-x-100, sigma-ultra (Sigma-Aldrich, T9284); albumin from bovine serum (BSA) (Sigma, A9647); mouse monoclonal anti-Lamp1 [H4A3] antibody (Abcam, ab25630); Alexa Fluor 647 Goat Anti-mouse IgG (life technologies, A21236); Formaldehyde (Electron Microscopy Sciences, EMS, 15710); Glutaraldehyde (EMS, 16000); PIPES (Sigma, P8203); HEPES (AppliChem, A3724); EGTA (Fluka , 03779); $MgCl_2$ hexahydrate (M9272); sodium cacodylate (SERVA, 1554002); calcium chloride anhydrous (499609); potassium ferrocyanate (Sigma, P3289); osmium tetroxide (EMS, 19170); thiocarbohydrazide (Sigma, 88535); uranyl acetate (Fluka, 73943); L-Aspartic acid (Sigma, A9256); lead nitrate (EMS, 17900); coverslips for CLEM studies (MatTek, special order on demand).

Preparation of Walton's lead aspartate solution [21]:

L-Aspartic acid (Sigma) was dissolved in distilled water at a concentration of 30 mM for 30 min. at 60°C. The solution was then mixed with lead nitrate (EMS) at a proportion of 0.066 g of lead nintrate per 10 ml of aspartic acid solution. The mixture was then incubated for 30 min. at 60°C and filtered through a 0.22 µm filter

Durcupan resin preparation

Durcupan resin was purchased as 4 different components with commercial names. The resin was prepared by mixing Part A (Fluka, 44611), Part B (Fluka, 44612) and Part D (Fluka, 44614) at a ratio of 10:10:0.3 (by weight). After extensive mixing, the activator DMP-30 (EMS, 13600) was added at a ratio of 16 drops per 20 g of initial

solution and mixed extensively. The samples were polymerized for 48 h at 60°C.

Table 1: Primers used in this study

Name	Sequence
prSL021	5'-CGACTCTAGAGGATCCCCACCATGGACAGCAAAGG TTCG-3'
prSL022	5'-GATTGTCGACGAATTCTCAAAAGAATTTTTTGGCAGCTGC TTCT-3'
pJS145	5'-GACACCGACTCTAGAGGCCACCATGGTGAGCAAGGGCG-3'
prJS146	5'-GATTGTCGACGAATTATATCATGGTATATGAAGCACTGG-3'
prJS165	5'-ACACCGACTCTAGAGGCCACCATGGTGAGCAAGGGCG-3'
prJS166	5'-TGATTGTCGACGAATTCTTAAATGATGCAATCCATCACG-3'

Bacteria strains and plasmids

The plasmid pJC44 encoding the DsRed gene was a kind gift from Jean Celli [22]. The plasmid was conjugated into *B. abortus* strain 2308.

Mammalian cell lines and plasmids

Human cervical carcinoma epithelial cell line (Hela) (ATCC, CCL-2) and Human Embryonic Kidney cell line (HEK) (ATCC) were maintained in Dulbecco Modified Eagle Medium (DMEM) supplemented with 10% fetal calf serum (FCS). Plasmid pPRL-EGFP-ERGIC53 was a kind gift from professor Hans-Peter Hauri (Basel University, Basel, Switzerland). The PR-EGFP-ERGIC53 cassette was amplified using primers prSL021 and prSJ022. The Plasmid pEGFP-C1 containing galectin-3 was a kind gift from Dr. Jost Enninga (Institut Pasteur, Paris, France) [9]. The EGFP-galectin-3 cassette from was amplified by PCR using primers prJS145 and prJS146. Plasmid pEGFP-C1 containing optineurin was a kind gift from Dr. Ivan Dikic (Goethe University, Frankfurt, Germany) [23]. The EGFP-OPTN cassette from was amplified by PCR using primers prJS165 and prJS166. Plasmids MDK124-EGFP-ERGIC53, MDK124-EGFP-STX6, MDK124-EGFP-Gal3 and MDK124-EGFP-OPTN were generated by inserting the respective PCR products into plasmid pMDK124 (kind gift of Professor Oliver Pertz, unpublished) digested with EcoRI and BamHI (NEB, Ipswich, MA) using the InFusion cloning kit (Clontech, Mountain

View, CA). All four plasmids were then introduced into HEK cells using the Fugene HD transfection reagent (Promega, Madison, WI) along with helper plasmids pMDL, pVSV and pREV (kind gifts from Professor Oliver Pertz, unpublished) in order to generate lentivirus vectors. Cell supernatants were harvested 2 d.p.i., filtered through 0.45 μm filters and used to infect HeLa cells. 24 h.p.i. the cell medium was supplemented with 1μg/ml puromycin (producer) to select for transduced cells.

Mammalian cell culture and infection for confocal and electron microscopy

For experiments involving confocal microscopy of fixed samples, cells were seeded onto 13 mm glass coverslips (Marienfeld, Lauda-Koenigshofen, Germany) in 24-well plates at 70,000 cells per well. For experiments involving electron microscopy, HeLa cells were seeded onto 32 mm gridded glass coverslips (MatTek, Ashland, MA) in a 6-well plate at 150,000 cells per well. The seeding was done on the day preceding infection. *B. abortus* 2308 carrying the pJC44 was grown overnight in TSB medium containing 50 μg/ml kanamycin at 37°C to an OD of 0.8-1.0. Bacteria were then diluted in DMEM/10% FCS and added to HeLa cells at a final MOI of 2'000 (time 0 of infection). Plates were centrifuged at 400 x *g* for 20 min at 4°C to synchronize bacterial entry. After 2 h of incubation at 37°C and 5% CO_2, extracellular bacteria were killed by exchanging the infection medium by DMEM/10% FCS supplemented with 100 μg/ml gentamicin. After a total infection time as indicated in the figure legends, cells were fixed using appropriate fixation buffer (see below).

Light microscopy

Samples used in fixed time point confocal microscopy studies were fixed with PFA fixation buffer (3.7% paraformaldehyde in PBS) for 20 min. at room temperature. Samples were then washed with PBS and and mounted to 25mm glass slides (BioSystems, Muttenz, Switzerland) using Vectashield H1000 mounting medium (Vector Laboratories, Burlingame, CA) and sealed with nail polish. Correlative light and electron microscopy samples were fixed in PHEM fixation buffer (4% formaldehyde, 0.2% glutaraldehyde, 60 mM PIPES, 25 mM HEPES, 10 mM EGTA, 4 mM $MgCl_2$) for 90 min. at room temperature. Following fixation, the coverslips were washed in PHEM buffer (60 mM PIPES, 25 mM HEPES, 10 mM EGTA, 4 mM $MgCl_2$) and mounted to 38 mm glass slides (BioSystems, Muttenz, Switzerland) using Vectashield H1000 mounting medium (Vector Laboratories, Burlingame, CA)

and sealed with nail polish. Confocal images were recorded using the Leica SP8 confocal microscope (Leica, Wetzlar, Germany) equipped with a 63x oil immersion objective. The images were deconvolved using Huygens software. Wide-field images were acquired using the Deltavision Core system (GE Healthcare, Little Chalfont, UK) with an Olympus IX71 stand, equipped with a CoolSNAP HQ2 camera (Photometrics). The images were deconvolved using the built-in algorithm.

Processing of cell monolayers for electron microscopy

Following overnight fixation, samples were washed 3 times with cacodylate buffer (150 mM sodium cacodylate, 2 mM $MgCl_2$) at 4°C. The samples were then immersed in freshly prepared reduced osmium buffer (2% osmium tetroxide, 150 mM sodium cacodylate, 2 mM $MgCl_2$, 40 mM potassium ferrocyanide) for 1 hour at 4°C. The samples were subsequently washed with deionized water at room temperature and immersed in 100 mM thiocarbohydrazide solution for 20 min. at room temperature. The samples were then washed with deionized water and incubated in 2% osmium tetroxide for 30 min. at room temperature. This was followed by overnight incubation in 1% uranyl acetate at 4°C. Following morning, the samples were washed in deionized water and incubated in freshly prepared Walton's lead aspartate solution (see Materials section) for 30 min. at 60°C. The samples were then dehydrated with a series of ethanol solutions (20, 50, 70, 90 and 100%) and immersed in 50% solution of durcupan in ethanol for 1 hour. Afterwards the samples were incubated 2 times in freshly prepared durcupan (see Materials section) and placed at 60°C for 48 hours for polymerization.

Focused ion beam scanning electron microscopy

Cells of interest were located in the polymerized resin block, trimmed and attached to pre-tilt 45° SEM stubs (Agar Scientific, Stansted, UK) using colloidal silver paint (Ted Pella, Redding, CA), sputter-coated with platinum and subject to FIB/SEM tomography. FIB/SEM images were acquired with a Helios NanoLab 650 Dual Beam using the Slice and View software (FEI, Hillsboro, OR). 3072 by 2048 or 2048 by 1780 pixel images were collected using an Elstar in-lens BSE detector at 1.5 kV with a horizontal field width of 15 or 10 μm at a working distance of 4.01 mm. The milling was performed with a FIB operating at 30 kV and 0.78 nA beam current. The thickness of the slices was between 10 and 20 nm. Image stacks were aligned using

the TrackEM2 plugin of ImageJ [24]. The manual segmentations and 3D representations of electron microscopy datasets were done using the IMOD software package [25].

Live-cell imaging

HeLa cells carrying the indicated marker were seeded into 24-well glass-bottom plates (Greiner Bio-One, Kremsmuenster, Austria) at 40,000 cells per well. *B. abortus* 2308 carrying the pJC44 was grown overnight in TSB medium containing 50 μg/ml kanamycin at 37°C to an OD of 0.8-1.0. Bacteria were then diluted in DMEM/10% FCS and added to HeLa cells at a final MOI of 2'000 (time 0 of infection). Plates were centrifuged at 400 x *g* for 20 min at 4°C to synchronize bacterial entry. After 2 hours of incubation at 37°C and 5% CO_2, extracellular bacteria were killed by exchanging the infection medium by DMEM/10% FCS supplemented with 100 μg/ml gentamicin.

The plate was placed in a custom live-cell imaging setup composed of a TiE Nikon inverted microscope equipped with a motorized stage, Nikon perfect focus system (PFS), CoolLED illumination, Nikon 40x apochromat objective and a 5 megapixel Neo Andor sCMOS camera. For each experiment, 40 imaging sites were selected manually. For each site, images were taken at 4 min. intervals for the initial 20 hours, which was later adjusted to 30 min. intervals. The imaging was stopped after 48 h. Exposure times were kept between 30-90 ms.

References

1. Pizarro-Cerda J, Moreno E, Sanguedolce V, Mege JL, Gorvel JP. Virulent *Brucella abortus* prevents lysosome fusion and is distributed within autophagosome-like compartments. Infect Immun. 1998;66(5):2387-92. PubMed PMID: 9573138; PubMed Central PMCID: PMC108212.
2. Celli J, de Chastellier C, Franchini DM, Pizarro-Cerda J, Moreno E, Gorvel JP. *Brucella* evades macrophage killing via VirB-dependent sustained interactions with the endoplasmic reticulum. J Exp Med. 2003;198(4):545-56. doi: 10.1084/jem.20030088. PubMed PMID: 12925673; PubMed Central PMCID: PMC2194179.
3. Smith EP, Miller CN, Child R, Cundiff JA, Celli J. Postreplication Roles of the *Brucella* VirB Type IV Secretion System Uncovered via Conditional Expression of the VirB11 ATPase. MBio. 2016;7(6). doi: 10.1128/mBio.01730-16. PubMed PMID: 27899503; PubMed Central PMCID: PMC5137499.
4. Miller CN, Smith EP, Cundiff JA, Knodler LA, Bailey Blackburn J, Lupashin V, et al. A *Brucella* Type IV Effector Targets the COG Tethering Complex to Remodel Host

Secretory Traffic and Promote Intracellular Replication. Cell Host Microbe. 2017. doi: 10.1016/j.chom.2017.07.017. PubMed PMID: 28844886.
5. Celli J, Salcedo SP, Gorvel JP. *Brucella* coopts the small GTPase Sar1 for intracellular replication. Proc Natl Acad Sci U S A. 2005;102(5):1673-8. doi: 10.1073/pnas.0406873102. PubMed PMID: 15632218; PubMed Central PMCID: PMC547823.
6. Deghelt M, Mullier C, Sternon JF, Francis N, Laloux G, Dotreppe D, et al. G1-arrested newborn cells are the predominant infectious form of the pathogen *Brucella abortus*. Nat Commun. 2014;5:4366. doi: 10.1038/ncomms5366. PubMed PMID: 25006695; PubMed Central PMCID: PMC4104442.
7. Hauri HP, Nufer O, Breuza L, Tekaya HB, Liang L. Lectins and protein traffic early in the secretory pathway. Biochem Soc Symp. 2002;(69):73-82. PubMed PMID: 12655775.
8. Wendler F, Tooze S. Syntaxin 6: the promiscuous behaviour of a SNARE protein. Traffic. 2001;2(9):606-11. PubMed PMID: 11555414.
9. Paz I, Sachse M, Dupont N, Mounier J, Cederfur C, Enninga J, et al. Galectin-3, a marker for vacuole lysis by invasive pathogens. Cell Microbiol. 2010;12(4):530-44. doi: 10.1111/j.1462-5822.2009.01415.x. PubMed PMID: 19951367.
10. Mellouk N, Weiner A, Aulner N, Schmitt C, Elbaum M, Shorte SL, et al. *Shigella* subverts the host recycling compartment to rupture its vacuole. Cell Host Microbe. 2014;16(4):517-30. doi: 10.1016/j.chom.2014.09.005. PubMed PMID: 25299335.
11. Fredlund J, Enninga J. Cytoplasmic access by intracellular bacterial pathogens. Trends Microbiol. 2014;22(3):128-37. doi: 10.1016/j.tim.2014.01.003. PubMed PMID: 24530174.
12. Wild P, Farhan H, McEwan DG, Wagner S, Rogov VV, Brady NR, et al. Phosphorylation of the autophagy receptor optineurin restricts *Salmonella* growth. Science. 2011;333(6039):228-33. doi: 10.1126/science.1205405. PubMed PMID: 21617041; PubMed Central PMCID: PMC3714538.
13. Cossart P, Helenius A. Endocytosis of viruses and bacteria. Cold Spring Harb Perspect Biol. 2014;6(8). doi: 10.1101/cshperspect.a016972. PubMed PMID: 25085912; PubMed Central PMCID: PMC4107984.
14. Simeone R, Bobard A, Lippmann J, Bitter W, Majlessi L, Brosch R, et al. Phagosomal rupture by *Mycobacterium tuberculosis* results in toxicity and host cell death. PLoS Pathog. 2012;8(2):e1002507. doi: 10.1371/journal.ppat.1002507. PubMed PMID: 22319448; PubMed Central PMCID: PMC3271072.
15. Smith GA, Marquis H, Jones S, Johnston NC, Portnoy DA, Goldfine H. The two distinct phospholipases C of *Listeria monocytogenes* have overlapping roles in escape from a vacuole and cell-to-cell spread. Infect Immun. 1995;63(11):4231-7. PubMed PMID: 7591052; PubMed Central PMCID: PMC173601.
16. Brodmann M, Dreier RF, Broz P, Basler M. *Francisella* requires dynamic type VI secretion system and ClpB to deliver effectors for phagosomal escape. Nat Commun. 2017;8:15853. doi: 10.1038/ncomms15853. PubMed PMID: 28621333; PubMed Central PMCID: PMC5481754.
17. Ke Y, Wang Y, Li W, Chen Z. Type IV secretion system of *Brucella* spp. and its effectors. Front Cell Infect Microbiol. 2015;5:72. doi: 10.3389/fcimb.2015.00072. PubMed PMID: 26528442; PubMed Central PMCID: PMC4602199.
18. Checroun C, Wehrly TD, Fischer ER, Hayes SF, Celli J. Autophagy-mediated reentry of *Francisella tularensis* into the endocytic compartment after cytoplasmic replication. Proc Natl Acad Sci U S A. 2006;103(39):14578-83. doi: 10.1073/pnas.0601838103. PubMed PMID: 16983090; PubMed Central PMCID: PMC1600002.
19. Boya P, Reggiori F, Codogno P. Emerging regulation and functions of autophagy. Nat Cell Biol. 2013;15(7):713-20. doi: 10.1038/ncb2788. PubMed PMID: 23817233.
20. Ackermann M, Stecher B, Freed NE, Songhet P, Hardt WD, Doebeli M. Self-destructive cooperation mediated by phenotypic noise. Nature. 2008;454(7207):987-90. doi: 10.1038/nature07067. PubMed PMID: 18719588.

21. Walton J. Lead aspartate, an en bloc contrast stain particularly useful for ultrastructural enzymology. J Histochem Cytochem. 1979;27(10):1337-42. doi: 10.1177/27.10.512319. PubMed PMID: 512319.
22. Starr T, Ng TW, Wehrly TD, Knodler LA, Celli J. *Brucella* intracellular replication requires trafficking through the late endosomal/lysosomal compartment. Traffic. 2008;9(5):678-94. doi: 10.1111/j.1600-0854.2008.00718.x. PubMed PMID: 18266913.
23. Richter B, Sliter DA, Herhaus L, Stolz A, Wang C, Beli P, et al. Phosphorylation of OPTN by TBK1 enhances its binding to Ub chains and promotes selective autophagy of damaged mitochondria. Proc Natl Acad Sci U S A. 2016;113(15):4039-44. doi: 10.1073/pnas.1523926113. PubMed PMID: 27035970; PubMed Central PMCID: PMC4839414.
24. Cardona A, Saalfeld S, Preibisch S, Schmid B, Cheng A, Pulokas J, et al. An integrated micro- and macroarchitectural analysis of the *Drosophila* brain by computer-assisted serial section electron microscopy. PLoS Biol. 2010;8(10). doi: 10.1371/journal.pbio.1000502. PubMed PMID: 20957184; PubMed Central PMCID: PMC2950124.
25. Kremer JR, Mastronarde DN, McIntosh JR. Computer visualization of three-dimensional image data using IMOD. J Struct Biol. 1996;116(1):71-6. doi: 10.1006/jsbi.1996.0013. PubMed PMID: 8742726.

4 Concluding remarks

4. CONCLUDING REMARKS

Bacteria from the genus *Brucella* are widespread facultative pathogens that are responsible for infections of humans and livestock, constituting a health risk and leading to large losses in agriculture. Brucellosis is difficult to diagnose and treat – antibiotic therapy is lengthy and often followed by relapses [1]. In order to tackle these problems it is essential to gain more insights into the processes that take place during *Brucella* infection. The pathogen's strategy of intracellular replication is the key element responsible for its ability to survive inside the host. Although we have some understanding of the nature of *Brucella*-host interaction, the exact mechanisms underlying it remain largely unknown. An improved description of the intracellular lifestyle of this pathogen may lead to the development of new methods for combating brucellosis. Moreover, the studies of *Brucella*, as well as other intracellular pathogens, go beyond microbiology and disease control. The analysis of pathogen interactions with different host organelles may shed light on yet unknown basic cellular processes, which would improve our understanding of life in general.

4.1. FIB/SEM tomography of the *Brucella* replicative niche reveals the level of integrity of the rBCV with the ER

We established a 3D correlative light and electron microscopy approach to study the intracellular lifestyle of *Brucella*. The goal was to employ high-end fluorescence microscopy with FIB/SEM in order to gain new insight into the structure of the replicative niche. The rBCV has been shown to be closely tied to the endoplasmic reticulum (ER) of the host cell in previous EM studies [2, 3]. However, these studies were limited in scope to 2D images of ultrathin sections of resin-embedded samples. The ER is, on the other hand, a complex structure spanning the entire volume of the cytoplasm. For this reason, we sought to visualize it using a 3D based approach that would at the same time provide information about different subcellular compartments. The recent development of block face SEM techniques [4] allows the imaging of thick samples at intermediate EM resolution. We were able to

use this advantage to reveal the true level of interaction between the rBCV and the ER.

We specifically targeted the replicative niche by combining the FIB/SEM approach with fluorescence microscopy of GFP-tagged ER markers. Stable HeLa cell lines expressing the markers GFP-calnexin and GFP-Sec61β were developed to overcome issues with low infectivity rates of *Brucella*. In order to improve the resolution of our light microscopy, we employed structured illumination microscopy (SIM), which proved to be useful for imaging of the complex ER meshwork.

Our initial experiments were performed using HeLa cells infected with *B. abortus.* Additionally, we confirmed our in vitro observations in a more relevant infection model. To do this, we performed FIB/SEM tomography of trophoblasts from murine placentas infected with *B. melitensis*.

We were able to show that the level of continuity between the rBCVs and the ER is higher than previously anticipated. Our results suggest that most of the rBCVs are not isolated vacuoles, but rather extensions of the ER that are stretched in order to accommodate the growing bacteria. This implies that *Brucella* manages to orchestrate fusion of the BCV with the entire ER meshwork and divide inside the organelle. The ER provides large membrane surface and has limited capacity to detect pathogens. The direct colonization of the ER has many potential consequences. Our results may allow us to better understand different observations about *Brucella* infection. We hypothesize that following the establishment of the rBCV, the bacteria enter a *passive*, growth oriented stage. There, instead of actively inducing membrane recruitment to the vacuole, the dividing bacteria simply grow into the already existing ER structure. It might explain why, as recent reports suggested, the VirB T4SS is active mainly during trafficking and seems to be of lower importance once the replicative niche is formed [5, 6].

The presence of bacteria in the ER lumen may explain why the activation of the unfolded protein response (UPR) is beneficial for the intracellular growth of *Brucella* [7]. The importance of UPR activation may be connected to the nutrient requirements of the growing microcolony. The UPR leads to an increase of the free amino acid pool, stimulates lipid biosynthesis and has been shown to encompass anti-apoptotic mechanisms [8]. ER stress also results in overall increase of ER surface [9], which would provide space for the growing bacteria. The structure of the rBCV may also provide some indications for the general biology of the ER. Apart from the

membranes directly surrounding the bacteria, the organelle preserves its structure, with limited lumen width. It seems that the volume of the organelle is kept at the minimum at the expense of greatly increasing the total surface of membranes. This indicates that the proteins responsible for the structural integrity manage to prevent the tubes and cisternae from expanding beyond the essential minimum.

Future experiments need to be done to provide better understanding of the rBCV. One of the potential follow up studies could involve different ER markers that would localize to more specific subcompartments of the organelle. This would potentially determine whether growing bacteria expand throughout the entire ER, or are limited to specific regions of the organelle. The CLEM approach can also be used to focus on more specific events related to late stages of *Brucella* replication. There are reports of re-emergence of late endosome markers, such as LAMP1, on the surface of rBCVs, a feature that has been linked to *Brucella* egress [10]. Additionally, it was reported that the process depends on early autophagy components. CLEM would allow specific targeting of those events, which in turn could indicate whether host cell egress is indeed related to autophagy factors.

4.2. Retromer components play a role in the establishment of the *Brucella abortus* replicative niche

During intracellular trafficking, *Brucella* follows a unique pathway that leads to the transition of the LE-like eBCV into an ER-like rBCV. The molecular mechanisms behind this remain largely unknown, with our knowledge limited mostly to T4SS-dependent interactions of the BCVs with ERES [6, 11]. At the same time, the establishment of the rBCV is the decisive factor for survival and spreading of *Brucella* inside the host and a better understanding of the process could provide us with means of fighting this pathogen. The siRNA screen presented in this study lead to the identification of 507 host factors that potentially play a role in *Brucella* infection. Additional analysis of the effects of this initial pool on bacteria entry into the host cell allowed the targeting of factors that play a role specifically in intermediate trafficking events.

Many of the host factors indicated by the screen have been previously identified as important for the life cycle of *Brucella* inside host cells. These include Rab7A [12], Rac1 and Cdc42 [13], or the COPB subunit of the COPI complex [14]. This provides additional validation of the screening approach and indicates that the results are a valuable resource for studying host proteins important in *Brucella* trafficking.

Some of the more interesting hits in the siRNA screen included components of the retromer machinery Vps35, Vps26a and Vps29 [15]. By validating the observations from the siRNA screen, we were able to show that Vps35 plays a role in successful transition from eBCV into rBCV. The importance of endosome-to-Golgi trafficking was additionally confirmed by showing that the chemical inhibitor Retro-2 [16] has a similar effect on BCV maturation.

We established an approach based on immunofluorescence and confocal microscopy that allowed us to quantify the percentage of LAMP1-positive bacteria inside each infected cell. We then employed it to specifically indicate that the knockdown of the protein leads to the retention of *Brucella* in the degradative pathway.

Several variants of the retromer complex have been identified, each involving different factors and responsible for transport of different cargos [17]. In the future, it will be important to determine the particular components that play a role in the establishment of the rBCV and the detailed mechanism behind this process. Future studies of colocalization of *Brucella* with different retromer components may provide some answers. Additionally, bacterial factors responsible for the interaction need to be identified. In this case it could be beneficial to look into the interactions of retromer components with *Brucella* proteins, including T4SS effectors. The scope of the future studies should, however, go beyond known effector proteins. Our understanding of *Brucella*-host interactions is still limited to few examples, and it is highly probable that some yet unknown factors play a role. In this case one solution could be to perform a yeast two-hybrid screen using the *Brucella* ORFeome, which would account for the whole proteome of the pathogen.

The identification of the retromer complex as a player in the intracellular trafficking of *Brucella* is a new contribution to the understanding of this pathogen. The study becomes even more significant when considering our limited understanding of the intracellular lifestyle of *Brucella* in general. Additionally, it

proves the value of genome-wide approaches in identifying previously unknown processes.

4.3. *Brucella abortus* escapes from the phagosome during intermediate trafficking stages in a VirB-dependent manner

We were able to successfully employ CLEM to target rare trafficking events at intermediate stages of *B. abortus* infection. Our EM data revealed that *Brucella* can reside directly in the cytosol. This initial observation prompted us to explore the possibility of phagosome escape during *Brucella* trafficking. We used live-cell imaging to indicate that at least a subpopulation of the bacteria may indeed escape into the cytosol. Additionally, we were able to show that this process depends on the presence of a functional T4SS. This suggests that the phagosome rapture is somehow connected to the introduction of effector proteins. Our data from live-cell imaging indicate that *Brucella* microcolonies successfully form following the escape. Unfortunately, due to technical limitations, we were unable to determine whether the cytosolic bacteria are the ones responsible to rBCV formation. Finally, we were able to show that the presence of *Brucella* directly in the cytosol triggers the recruitment of autophagy membranes, which may indicate a process of bacteria clearance previously reported for other pathogens [18].

At this point we do not have enough information to determine the role of phagosome rapture in *Brucella* trafficking. There are several possible explanations. The T4SS-dependence suggests that the process might be either a bona fide trafficking step on the way to the rBCV, or a side effect of effector injection that leads to off-pathway killing of the bacteria. A third explanation, which is a combination of both those alternatives, would state that there is a division of labor between bacteria inside the same cell, where one sacrifices itself in order to introduce effector proteins that later help the others to establish a replicative niche. In either case, the phenomenon of cytosolic escape is a new observation that could teach us many things about intracellular trafficking of pathogens and T4SS dynamics.

The importance of cytosolic *Brucella* needs to be further studied using different microscopy techniques. Improvement of live-cell imaging methodology for *Brucella* trafficking should allow us to determine the faith of the cytosolic bacteria in

regard to rBCV formation. These experiments would use already established markers such as GFP-Gal3, but should also explore interactions of *Brucella* with other cellular components. In this case the colocalization of markers such as optineurin, ATG9 and WIPI-1 with the bacteria should be studied using 3D CLEM. The ability of the 3D FIB/SEM approach to visualize membranous organelles has proven to be useful in providing the initial indications about phagosome escape of *Brucella*. It can certainly be used further in combination with fluorescence microscopy in order to fully resolve the interactions of cytosolic bacteria with specific organelles.

References

1. Pappas G, Akritidis N, Bosilkovski M, Tsianos E. Brucellosis. N Engl J Med. 2005;352(22):2325-36. doi: 10.1056/NEJMra050570. PubMed PMID: 15930423.
2. Celli J, de Chastellier C, Franchini DM, Pizarro-Cerda J, Moreno E, Gorvel JP. *Brucella* evades macrophage killing via VirB-dependent sustained interactions with the endoplasmic reticulum. J Exp Med. 2003;198(4):545-56. doi: 10.1084/jem.20030088. PubMed PMID: 12925673; PubMed Central PMCID: PMC2194179.
3. Detilleux PG, Deyoe BL, Cheville NF. Entry and intracellular localization of *Brucella* spp. in Vero cells: fluorescence and electron microscopy. Vet Pathol. 1990;27(5):317-28. doi: 10.1177/030098589002700503. PubMed PMID: 2122572.
4. Knott G, Marchman H, Wall D, Lich B. Serial section scanning electron microscopy of adult brain tissue using focused ion beam milling. J Neurosci. 2008;28(12):2959-64. doi: 10.1523/JNEUROSCI.3189-07.2008. PubMed PMID: 18353998.
5. Smith EP, Miller CN, Child R, Cundiff JA, Celli J. Postreplication Roles of the *Brucella* VirB Type IV Secretion System Uncovered via Conditional Expression of the VirB11 ATPase. MBio. 2016;7(6). doi: 10.1128/mBio.01730-16. PubMed PMID: 27899503; PubMed Central PMCID: PMC5137499.
6. Miller CN, Smith EP, Cundiff JA, Knodler LA, Bailey Blackburn J, Lupashin V, et al. A *Brucella* Type IV Effector Targets the COG Tethering Complex to Remodel Host Secretory Traffic and Promote Intracellular Replication. Cell Host Microbe. 2017. doi: 10.1016/j.chom.2017.07.017. PubMed PMID: 28844886.
7. Smith JA, Khan M, Magnani DD, Harms JS, Durward M, Radhakrishnan GK, et al. *Brucella* induces an unfolded protein response via TcpB that supports intracellular replication in macrophages. PLoS Pathog. 2013;9(12):e1003785. doi: 10.1371/journal.ppat.1003785. PubMed PMID: 24339776; PubMed Central PMCID: PMC3855547.
8. Pena J, Harris E. Dengue virus modulates the unfolded protein response in a time-dependent manner. J Biol Chem. 2011;286(16):14226-36. doi: 10.1074/jbc.M111.222703. PubMed PMID: 21385877; PubMed Central PMCID: PMC3077624.
9. Schuck S, Prinz WA, Thorn KS, Voss C, Walter P. Membrane expansion alleviates endoplasmic reticulum stress independently of the unfolded protein response. J Cell Biol. 2009;187(4):525-36. doi: 10.1083/jcb.200907074. PubMed PMID: 19948500; PubMed Central PMCID: PMC2779237.
10. Starr T, Child R, Wehrly TD, Hansen B, Hwang S, Lopez-Otin C, et al. Selective subversion of autophagy complexes facilitates completion of the *Brucella* intracellular

cycle. Cell Host Microbe. 2012;11(1):33-45. doi: 10.1016/j.chom.2011.12.002. PubMed PMID: 22264511; PubMed Central PMCID: PMC3266535.

11. Celli J, Salcedo SP, Gorvel JP. *Brucella* coopts the small GTPase Sar1 for intracellular replication. Proc Natl Acad Sci U S A. 2005;102(5):1673-8. doi: 10.1073/pnas.0406873102. PubMed PMID: 15632218; PubMed Central PMCID: PMC547823.
12. Starr T, Ng TW, Wehrly TD, Knodler LA, Celli J. *Brucella* intracellular replication requires trafficking through the late endosomal/lysosomal compartment. Traffic. 2008;9(5):678-94. doi: 10.1111/j.1600-0854.2008.00718.x. PubMed PMID: 18266913.
13. Guzman-Verri C, Chaves-Olarte E, von Eichel-Streiber C, Lopez-Goni I, Thelestam M, Arvidson S, et al. GTPases of the Rho subfamily are required for *Brucella abortus* internalization in nonprofessional phagocytes: direct activation of Cdc42. J Biol Chem. 2001;276(48):44435-43. doi: 10.1074/jbc.M105606200. PubMed PMID: 11579087.
14. Fugier E, Salcedo SP, de Chastellier C, Pophillat M, Muller A, Arce-Gorvel V, et al. The glyceraldehyde-3-phosphate dehydrogenase and the small GTPase Rab 2 are crucial for *Brucella* replication. PLoS pathogens. 2009;5(6):e1000487. doi: 10.1371/journal.ppat.1000487. PubMed PMID: 19557163; PubMed Central PMCID: PMC2695806.
15. Wassmer T, Attar N, Harterink M, van Weering JR, Traer CJ, Oakley J, et al. The retromer coat complex coordinates endosomal sorting and dynein-mediated transport, with carrier recognition by the trans-Golgi network. Dev Cell. 2009;17(1):110-22. doi: 10.1016/j.devcel.2009.04.016. PubMed PMID: 19619496; PubMed Central PMCID: PMC2714578.
16. Stechmann B, Bai SK, Gobbo E, Lopez R, Merer G, Pinchard S, et al. Inhibition of retrograde transport protects mice from lethal ricin challenge. Cell. 2010;141(2):231-42. doi: 10.1016/j.cell.2010.01.043. PubMed PMID: 20403321.
17. Bugarcic A, Zhe Y, Kerr MC, Griffin J, Collins BM, Teasdale RD. Vps26A and Vps26B Subunits Define Distinct Retromer Complexes. Traffic. 2011;12(12):1759-73. doi: 10.1111/j.1600-0854.2011.01284.x. PubMed PMID: WOS:000297573500009.
18. Wild P, Farhan H, McEwan DG, Wagner S, Rogov VV, Brady NR, et al. Phosphorylation of the autophagy receptor optineurin restricts *Salmonella* growth. Science. 2011;333(6039):228-33. doi: 10.1126/science.1205405. PubMed PMID: 21617041; PubMed Central PMCID: PMC3714538.

5 Acknowledgements

5. ACKNOWLEDGEMENTS

First and foremost I would like to thank my supervisors Prof. Christoph Dehio and Prof. Henning Stahlberg. I am very grateful for their constant support throughput the project and very much appreciate that they allowed me to explore my own ideas.

I would also like to thank Prof. Marek Basler for supporting me in my thesis committee. His insights and positive attitude have always been a valuable source of motivation.

I would like to thank Therese Tschon, Maxime Quebatte and Shyan Huey Low for their constant support regarding all aspects of my thesis. Without the effort that they have contributed to different aspects of my projects, I would not have been able to proceed with my work.

I am grateful to Kenneth Goldie, Christopher Bleck and Christel Genoud for sharing their expertise and providing me with tools that made my studies possible.

I would like to thank Isa and Claudia for their constant assistance regarding different aspects of laboratory work.

I am very grateful to Lena, Inay, Katja and Markus for providing me with opportunities to escape from everyday struggles in the lab.

I would like to thank Therese, Isabel, Katja, Kathrin and Alex for their great company during coffee breaks.

I am grateful to Maxime, Isa, Lena, Katja and Alex for careful reading of the thesis.

Furthermore, I would like to thank all the members of the Dehio Lab and C-CINA for a great working atmosphere, help and support.

Last but not least, I would like to thank Basia for always being there for me.

6 Curriculum vitae

6. CURRICULUM VITAE